MODELLING AND ANALYSIS OF AN ELECTRO HYDRAULIC ELEVON ACTUATION SYSTEM OF A MODERN FIGHTER AIRCRAFT

By

AMITABH MUKHERJEE

DEPARTMENT OF AEROSPACE ENGINEERING

INDIAN INSTITUTE OF TECHNOLOGY KANPUR

FEBRUARY, 1993

MODELLING AND ANALYSIS OF AN ELECTRO HYDRAULIC ELEVON ACTUATION SYSTEM OF A MODERN FIGHTER AIRCRAFT

A Thesis Submitted

in Partial Fulfilment of the Requirements

for the Degree of

MASTER OF TECHNOLOGY

in

AEROSPACE ENGINEERING

by

AMITABH MUKHERJEE

to the

DEPARTMENT OF AEROSPACE ENGINEERING

INDIAN INSTITUTE OF TECHNOLOGY KANPUR

FEBRUARY, 1993

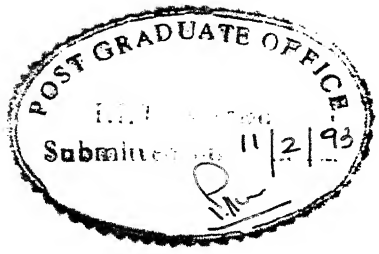

C E R T I F I C A T E

It is certified that the work contained in the thesis entitled **MODELLING AND ANALYSIS OF AN ELECTRO HYDRAULIC ELEVON ACTUATION SYSTEM OF A MODERN FIGHTER AIRCRAFT**, by **AMITABH MUKHERJEE**, has been carried out under my supervision and that this work has not been submitted elsewhere for a degree.

C V R MURTI

DEPARTMENT OF AEROSPACE ENGINEERING

I I T KANPUR

10th Feb.,1993

ABSTRACT

The elevon actuation system for a modern fighter airplane is modelled and analysed. Effect of various system parameters on the dynamic response of the electro hydraulic actuator is studied. Impedance characteristics of the system are determined and their relation to the overall transfer function of the elevon actuation system is obtained. The model developed is integrated into the longitudinal flight control loop to investigate its effect on the airplane short period dynamics.

The response of the E H actuator under load conditions is oscillatory and lowly damped. This is far from the ideal first-order-lag response. However, for an optimised actuator position feedback the airplane normal acceleration response is good, though the pitch rate response suffers in comparison.

TO MY MOTHER

SHE SHOWED ME THE WAY

ACKNOWLEDGEMENT

I wish to thank Prof. C V R Murti for his invaluable guidance and constant encouragement throughout the work. I shall always cherish the freedom he allowed me to work with.

I also wish to thank the following:

Dr. Prakash and Mr. K Panda ,ADA, Bangalore for suggesting the problem.

Dr. T K Sengupta and Dr. S Kamle for helping me with 'logistics' support whenever required.

Somakumar, K RaviramaChandran, Dixit, Dinesh, Phadke, Viji, Preethi, Bhanumati and Ashish Balaya for constantly urging me to perform well.

Dr. B S Reddy, Mr. D P Singh, HAL, Bangalore, and Dr. Rajeshwari,ADA, Bangalore for helping me out in official and personal matters.

Piyush, K C Navneeth Kumar, Parag, Babita, Atul, Amit, Anupama, Vandana, Nisha, Utpal and Sujit and a host of other friends for making my stay here an experience worth treasuring for ever.

CONTENTS

LIST OF FIGURES (contd.)

LIST OF FIGURES (concld.)

NOMENCLATURE

Upper case letters

A	system matrix (state space representation)
A_p	piston area (in^2)
B	input matrix (state space representation)
B_v	equivalent viscous friction coefficient (lb/in/s)
C	output matrix (state space representation)
D	output matrix (state space representation)
F_1	force due to 1^{st} actuator in the dual tandem system (lb)
F_2	force due to 2^{nd} actuator in the dual tandem system (lb)
F	$(=F_1+F_2)$
F_c	Coulomb friction (lb)
F_{cmax}	maximum level of Coulomb friction (lb)
H_m	dynamic pressure feedback circuit
H_s	static hinge moment (lb in)
I	moment of inertia of elevon about hinge line ($lb\ in^2$)
I_x, I_y, I_z, I_{xz}	moment of inertia and product of inertia of airplane ($lb\ in^2$)
K_F	describing function for Coulomb friction
L_s	location of normal acceleration sensor from the C.G of airplane (m)
M	pitching moment of airplane (positive pitch nose up) (N m)
M_α	dimensional variation of pitching moment with angle of attack (sec^{-2})
M_{δ_e}	dimensional variation of pitching moment with elevon angle (sec^{-2})

NOMENCLATURE (contd.)

M_q	dimensional variation of pitching moment with pitch rate (sec^{-1})
P_1	pressure in chamber 1 of actuator cylinder (psi)
P_2	pressure in chamber 2 of actuator cylinder (psi)
P_l	load pressure ($=P_1-P_2$) (psi)
P_{l1}	load pressure in 1st actuator in dual tandem system (psi)
P_{l2}	load pressure in 2nd actuator in dual tandem system (psi)
Q_1	flow rate into chamber 1 of actuator (in^3/s)
Q_2	flow rate out of chamber 2 of actuator (in^3/s)
Q_l	load flow ($=(Q_1+Q_2)/2$) (in^3/s)
T	torque (lb in)
U	input vector (state space representation)
V	total volume of actuator cylinder (in^3)
V_o	input command voltage (vdc)
X	state vector (state space representation)
X_F	force on airplane in X-axis (positive forward) (N)
Z_a	actuator hydraulic impedance (lb/in)
Z_α	dimensional variation of normal force with angle of attack (m/s^2)
Z_{eq}	equivalent impedance (lb/in)
Z_{δ_e}	dimensional variation in normal force with elevon angle (m/s^2)
Z_F	normal force on airplane in Z-axis (positive downwards) (N)
Z_q	dimensional variation of normal force with pitch rate (m/s)

NOMENCLATURE (contd.)

Lower case letters

a_{z_s}	normal acceleration at sensor station (m/s^2)
e	error signal
k1	DDV gain
k_a	actuator loop amplifier gain
k_α	hinge moment per unit angle of attack (lb in/rad)
k_b	mounting stiffness (lb/in)
k_c	valve flow pressure coefficient (in^3/s/psi)
k_δ	hinge moment per unit elevon deflection/ aerodynamic elevon stiffness (lb in /rad)
kda	lvdt gain
k_g	valve flow gain (in^3/s/in)
k_h	horn stiffness (lb/in)
kla	demodulator gain
k_p	dynamic pressure feedback gain
k_x	actuator position feedback gain (=kda*kla)
l	horn arm length (in)
m	mass of airplane (kg)
m_p	mass of piston (lb)
p	roll rate (rad/s)
q	pitch rate (rad/s)
r	yaw rate (rad/s)
rv	valve radius (in)
s	Laplace variable (sec^{-1})
u	perturbed forward velocity of airplane (m/s)

NOMENCLATURE (concld.)

v	perturbed side velocity (positive starboard) (m/s)
w	perturbed downward velocity (m/s)
x_a	displacement of the cylinder relative to the the airframe (in)
x_p	piston displacement relative to the cylinder of actuator (in)
x_v	valve opening (in)
y	output vector (state space representation)

Greek letters

α	angle of attack (rad)
β	bulk modulus of hydraulic oil (psi)
δ, δ_e	elevon deflection (rad)
θ	valve angular position (rad)
τ	DDV time constant (sec)
τ_p	dynamic pressure feedback circuit time constant (sec)
ω_h	hydraulic frequency of actuator (rad/s)
ω_n	natural frequency (rad/s)
ζ	damping ratio

Chapter 1. INTRODUCTION

1.1 INTRODUCTION

During the past decade, as the control power requirements increased and the control reaction time decreased, more and more reliance was placed on fully powered hydraulic actuators. Electro hydraulic servo mechanisms are used to provide power boost, stability augmentation control inputs, or primary control through main and auxiliary control surfaces of the aircraft. These servos are capable of performance superior to that of any other type of servo. Large inertia and torque loads can be handled with high accuracy and very rapid response [1].

A modern fighter airplane having a delta wing planform usually has a single set of control surface used for both pitch as well as roll control. These are known as elevons (elevator + aileron). In a typical airplane of this type, each elevon on either wing is split into two. Thus there are four elevons - two inboard and two outboard elevons. Each elevon is controlled by four servo actuators. In a fly by wire aircraft the conventional mechanical link between the pilot stick and the actuators is eliminated and replaced by a multiplex flight control computer. Pilot commands are translated into electrical voltages which are fed to the E H servos.

The present work deals with the modelling and analysis of an elevon actuation system. A typical working electro hydraulic actuator on a modern fighter aircraft is considered for illustration. The actuator is of a linear dual tandem type controlled by a direct drive valve.

1.2 LITERATURE SURVEY

Literature on electro hydraulic systems is extensive. Text books by Merritt [1] and Viersma [2] are excellent reference materials. Both these books present a rational and well balanced treatment of hydraulic components and systems. Hydraulic control is analysed by conventional linear analysis methods and general criteria applicable to "good" design of E H servos is evolved. In a nutshell, hydraulic servo design proceeds by first selecting the power element to meet the prime considerations of load and response capabilities. The remainder of the loop is then sized to obtain the best possible servo performance (i.e., accuracy and speed of response) under the limitations imposed by the power element dynamics. Noise rejection and stability always limit the system bandwidth. In fact, it is desirable to keep the bandwidth at a minimum consistent with the specifications. A reduced bandwidth usually simplifies compensation and, as peak power outputs are associated with high frequencies, it relaxes requirements on individual elements [1].

McRuer [3] has analysed the actuator response to a spectral input to determine the general requirements for such a system. He concludes that 'the actuator bandwidth should be

as low as possible, consistent with suppression of actuator loop disturbances, effective linearisation of non linearities and outer loop stability and dynamic performance' of the aircraft.

Flight control specialists are nowadays accepting high reliability in lieu of redundancy to increase the mean time between failures and decrease the complexity of the flight control system . Direct drive valves (DDV) are a natural choise. Their use is based on the premise that their reliability is so high that redundancy is unnecessary[4]. DDVs are being increasingly used instead of Electro Hydraulic Valves (EHV) in all modern fighter aircrafts. Not much literature is however available. Apart from some SAE papers [4], product information brochures of control system component manufacturers [5] are the only technical source available. Reference [4] and [5] briefly explain the working of the DDV and its advantages over the EHV. Reference [4] also discusses other advanced concepts, like variable displacement hydraulic control, electro mechanical servo systems, "smart" valves etc., which are yet in the experimental stage but nevertheless hold rich promise.

Edwards[6] in a NASA technical note has analysed an electro hydraulic aircraft rudder servo. The transfer functions are developed and their approximate literal factors are presented. Aerodynamic and horn stiffnesses are taken into account. However the actuator is assumed to be rigidly mounted in the airframe. A nonlinearity, such as Coulomb

friction, presents difficulty in linear analysis of a system. Edwards[6] has developed an equivalent linear model wherein an equivalent viscous friction coefficient has been considered instead of Coulomb friction and compared it with non linear test results. However, no criteria have been proffered to determine such an equivalent viscous friction coefficient.

Aeroservoelastic studies are now carried out during the design stage of all modern fighter aircraft to explore the possibility of active flutter suppression. A "real" actuation system is a necessary part of an Aeroservoelastic model. An actuator with finite impedance characteristics instead of an infinite impedance actuator is therefore considered for such analysis [7]. Benun [8] has analysed a simplistic actuator model (no masses; no dampers) to illustrate the frequency dependant characteristics of the hydraulic actuator.

1.3 PREVIEW OF THE WORK

Chapter 2 describes the various elements of the electro hydraulic actuator - elevon system. The equations of motion, the transfer function and the block diagrams are presented. Effect of change in values of the parameters of E H actuator on the system response is investigated. The instability of the load resonance poles due to elevon inertia is brought out and the dynamic pressure feedback is designed.

Chapter 3 presents the importance of the impedance characteristics of the actuator - elevon system. A physical explanation is attempted for the actuator hydraulic

stiffness. The system impedance is derived and its relation with the transfer function between elevon deflection and command input) of the elevon actuation system brought out.

Chapter 4 describes the effect of putting the servo system in the overall flight control loop. The aim is not to design a control law, rather to see how the realistic model of the actuator developed interacts with the control law.

Chapter 5 presents the conclusions drawn from the study and suggests possible extension of the present work..

CHAPTER 2 ELEVON ACTUATION SYSTEM

For the purpose of analysis the dynamics of the actuator-elevon servo system may be subdivided into:

i) The direct drive valve dynamics

ii) The hydraulic actuator dynamics

iii) The actuator load dynamics

A block diagram of a typical actuator - elevon servo system used in the flight control system of a modern fighter aircraft is shown in Figure 2.1 [1].

2.1 DIRECT DRIVE VALVE

2.1.1 INTRODUCTION

Conventional 2 - stage electro-hydraulic servovalves (EHV) are now being increasingly replaced by Direct Drive Valves(DDV). EHVs achieve high power gain through hydraulic amplification of a small electrically generated torque. The operation of the torque motor and hydraulic amplifier involves small forces and displacements that makes the system vulnerable to jamming by possible contamination of hydraulic fluid. Redundancy by multiplexing is therefore introduced which results in somewhat bulky and mechanically complex servo actuator systems. In addition, hydraulic system pressures are limited to around 4-5000 psi as the EHVs are subject to leakage beyond this pressure . Development of the DDV seeks to overcome these limitations by means of increased mechanical reliability and conservative redundant coil

configuration [4,5]. The DDV has facilitated configurations having simplified control surface actuation systems and specification of higher hydraulic pressures (8000 psi) as the construction of DDV tolerates pressures of this magnitude without leakage.

The DDV, which is shown in Figure 2.2 , consists of a small high output electromagnetic torque motor which is directly coupled to a hydraulic metering arrangement (the main control valve). A variable gap torque motor consists of two RECO (Rare Earth CObalt) magnets which set up a polarizing flux in the two air gaps. At null the flux in each air gap is balanced and there is no output. Control is effected by applying a command signal to the coil(s) (usually there is one coil per multiplex channel) wound around the outside of the motor. This current creates a control flux imbalance between the air gap and consequently a net torque on the motor armature. The motor is spring centered and therefore the opening of the valve is proportional to the command signal [4,5].

2.1.2 TRANSFER FUNCTION OF THE DDV

The block diagram and associated transfer functions of a typical DDV used in Flight Control systems is given in Figure 2.3. The rotary torque from the motor is coupled to a rotary control valve. For optimum performance a position loop is closed around the valve. This is also used to detect a jam if it occurs and to generate additional voltages to chip away the jamming particle [4]. This is a distinguishing feature of

the DDV. The 5^{th} order transfer function which results from the block diagram is given in Appendix A (A1). It may be seen from the values of the coefficients of higher order terms of s in the denominator of the transfer function that the transfer function may be approximated to a first order lag thus:

$$\frac{\theta(s)}{V_o(s)} = \frac{K1}{\tau s + 1} \qquad (2.1)$$

where, K1 = 0.0254 rad/volt

τ = 0.0042 s

A plot of the frequency response of the 5^{th} order system and the 1^{st} order approximation of the DDV is shown in Figure 2.4 The figure shows a good match between the 1^{st} order and the 5^{th} order system up to 400 rad/s. The range of characteristic frequencies of the elevon servo system is usually up to 10 Hz (65 rad/s). The 1^{st} order system is therefore used to represent the DDV for further analysis. It may be noted from the frequency response curves in Figure 2.4 that the bandwidth of the DDV is 240 rad/s.

2.2 HYDRAULIC ACTUATOR

2.2.1 ACTUATOR DYNAMICS

The hydraulic actuator considered is a dual - tandem - actuator. Figure 2.5 shows the schematic diagram of a typical valve actuator combination. Hydraulic fluids , such as oil, even though far less compressible than gas, when compressed

in a cylinder compartment act like a spring and introduce a second order mass - spring system whose natural frequency limits the bandwidth of any hydraulic servo system abruptly.

At no load the equations of motion of the piston may be written as follows:

$$Q_1 = A_p \frac{d x_p}{d t} + \frac{V}{4 \beta} \frac{d P_1}{d t} \qquad (2.2a)$$

$$Q_1 = \frac{Q_1 + Q_2}{2} \qquad (2.2b)$$

$$P_1 = \frac{P_1 + P_2}{2} \qquad (2.2c)$$

$$A_p P_1 = m_p \frac{d^2 x_p}{d t^2} \qquad (2.3)$$

where, x_p = piston displacement

β = bulk modulus of the fluid = $- \frac{dP}{dV/V}$

Q_1 = load flow

Q_1 = flow rate into chamber 1

Q_2 = flow rate out of chamber 2

P_1 = pressure in chamber 1

P_2 = pressure in chamber 2

m_p = mass of the piston

A_p = area of the piston

V = total volume of the cylinder

The first term on the RHS of Equation 2.2a is the rate of change of the volume of the two chambers of the hydraulic

cylinder, while the second term represents the rate of change of volume of the hydraulic fluid due to finite compressibility of the hydraulic fluid.

2.2.2 VALVE DYNAMICS

Constant supply pressure and sump pressure are assumed. The load flow Q_l through the valve may be expressed[1] as a function of valve position x_v and the load pressure P_l.

$$Q_l = f (x_v , P_l)$$

The above relation may be linearised to yield an expression for incremental value ΔQ_l for load flow Q_l

$$\Delta Q_l = \frac{\partial Q_l}{\partial x_v} \Delta x_v + \frac{\partial Q_l}{\partial P_l} \Delta P_l \qquad (2.4)$$

The required partial derivatives are obtained by differentiation of the equation for the load flow characteristics or graphically from a plot of load flow curves.

Defining,

$$\text{valve flow gain } k_g = \frac{\partial Q_l}{\partial x_v} \qquad (2.5)$$

$$\text{valve flow pressure coefficient } k_c = - \frac{\partial Q_l}{\partial P_l} \qquad (2.6)$$

From Equations (2.4), (2.5) and (2.6) , neglecting the higher order terms , we get

$$\Delta Q_l = k_g \Delta x_v - k_c \Delta P_l \qquad (2.7)$$

$(\partial Q_1 / \partial P_1)$ is negative for any valve configuration which makes the flow pressure coefficient k_c always a positive number. The valve flow gain k_g indicates the increment in load flow due to incremental displacement of valve, at a given load pressure P_1. k_g is always positive for the definition of x_v and Q_1. The valve pressure coefficient k_c indicates the sum of decrease in inflow into chamber 1 from supply, due to increase in pressure P_1 in chamber 1 and decrease in outflow from chamber 2 to the sump due to decrease in the pressure P_2 in chamber 2. This also accounts for decrease in flow rate Q_1 and increase in Q_2 due to leakage across the piston due to P_1, the difference in chamber pressures[1].

2.3 LINEAR ANALYSIS OF ELECTRO - HYDRAULIC ACTUATOR (NO LOAD)

Considering Equations (2.2), (2.3) and (2.7) we obtain an expression for the transfer function between the displacement of the valve and the displacement of the piston of the hydraulic actuator

$$\frac{X_p(s)}{X_v(s)} = \frac{k_g / A_p}{s\left(s^2/\omega_h^2 + 2\zeta/\omega_h s + 1\right)} \qquad (2.8)$$

where $$\omega_h^2 = \frac{4\beta A_p^2}{m_p V}$$

$$2\zeta/\omega_h = \frac{k_c m_p}{A_p^2}$$

For the typical actuator considered ω_h the hydraulic frequency is 659.25 rad/s and ζ the damping coefficient is 0.01287 for the nominal values of the parameters of the hydraulic actuator.

The nominal values of all the parameters of the system considered for illustration of the analysis as given in Appendix B are based on the product information brochure of an E H actuator manufacturer.

The frequency response corresponding to the open loop transfer function of the hydraulic actuator is shown in Figure 2.6 . It may be seen from the figure that at low frequencies, the amplitude ratio has an attenuation at the rate of 20 db/decade; has a sharp resonance at around 650 rad/s and an attenuation of 60 db/decade at high frequencies.

The frequency response of the electro hydraulic actuator (configuration : DDV + actuator) to input voltage at no load, is given in Figure 2.7. The bandwidth of the system is 80 rad/s. For an elevon actuator the frequency range of interest is usually up to 10 Hz (65rad/s). The bandwidth of the E H actuator system is therefore adequate for the purpose of actuation of the elevons. The corresponding transfer function is given in Appendix A(A3). It is of considerable interest to study the changes in the dynamics of the E H actuator as some important parameters are varied.

2.3.1 EFFECT OF VALVE COEFFICIENTS

In the above analysis the valve flow dynamics was linearized about a nominal operating condition.(vide Section

coefficients may be at variance with the nominal values. It therefore seems important to study the effect of the valve coefficients. From Equation (2.8) it may be seen that the valve flow gain k_g directly affects the gain of the hydraulic actuator. It therefore affects the stability of the closed loop E H actuator system. Figure 2.8a shows the root locus of the E H actuator for variation in the value of k_g . The roots move towards the unstable half of the s-plane as k_g increases. Figure 2.8b shows the frequency response of the E H actuator for three values (half, nominal and double) of k_g. It may be seen from the figure that the resonance frequency does not change with the variation in the valve flow gain k_g. The damping reduces with the increase of k_g.

The valve flow pressure coefficient directly affects the damping coefficient. This may be seen from Equation (2.8) as well as from Figure 2.9. For half the nominal value of k_c the roots are almost on the imaginary axis indicating a very low value of damping. However the increase in damping is not substantial as the value of valve flow pressure coefficient k_c is increased to double the nominal value. The resonance frequency again remains unaffected by change in k_c.

2.3.2 EFFECT OF BULK MODULUS

The effect of bulk modulus of the hydraulic fluid on E H actuator is studied. The variation of the eigenvalues as the bulk modulus β is varied from half the nominal value to double the nominal value is shown in Figure 2.10a. It may be noted that the system is unstable for low values of bulk

modulus. The usual value of bulk modulus for hydraulic fluids used in actuators are of the order of 250000 psi. However, the nominal value of 100000 psi has been arrived at to take into account the flexibility of the cylinder walls and the pipe lines which supply the fluid from the source[1].It may be seen that both the resonance frequency and the damping ratio increase with increase in β. This may also be seen from Figure 2.10b (frequency response plots for varying values of β).

2.4 COULOMB FRICTION [1 , 2]

The factors affecting the damping of the motion of the hydraulic actuator are viscous friction, intersurface friction between the piston and cylinder, which has the nature of Coulomb friction, and leakage flow. A difficulty here is the non-linear behaviour of Coulomb friction, making conventional linear analysis impossible. It has been demonstrated by Edwards [6] that a valid model may be assumed by setting Coulomb friction equal to zero and introducing (or increasing) viscous friction to provide the required damping for a frequency range. A similar model is chosen in the present work for linear analysis purposes.

To justify such a model a digital simulation is carried out. Coulomb friction F_c is simulated as follows (Figure 2.11)

$$F_c = F_{cmax} \frac{\dot{x}_p}{|\dot{x}_p|} \quad ; \quad \dot{x}_p \neq 0$$

$$= 0 \quad ; \quad \dot{x}_p = 0$$

F_{cmax} is the maximum value of Coulomb friction between the

actuator piston and the actuator chamber.

In physical reality, Coulomb friction at $\dot{x}_p = 0$ is determined by the fact that it will take whatever value is necessary to keep the velocity zero. As long as the net force, F (barring Coulomb friction) acting on a stationary piston is $-F_{cmax} < F < F_{cmax}$, the speed will remain zero. As soon as F exceeds F_{cmax} the piston starts moving.

Figure 2.12a shows a simulated time response to unit step input of voltage to the actuator system with and without Coulomb friction. A fourth order Runge-Kutta method is used to solve the associated differential equations. Viscous friction coefficient is now chosen by trial and error method to achieve a time response as close to that of the system with coulomb friction as possible. The two time responses are compared in Figure 2.12b. The figure shows a very good match. The two responses are indistinguishable after 0.03 seconds. This appears to justify further analysis of the system using equivalent viscous friction for the model.

An analysis of the system by Describing Function (D F) method throws a different light on how the coulomb friction operates.

In the method of the Describing Function all signals are assumed to be harmonic. Assuming the velocity input signal to be sinusoidal, the Coulomb friction output function may be written as:

input : $\dot{x}_p = \bar{\dot{x}}_p \sin \omega t$

output : $F_c = \frac{4}{\pi} F_{cmax} (\sin \omega t + \frac{1}{3} \sin 3 \omega t + \ldots)$

It is important to note that in writing the above expression, it has been assumed that the nonlinearity does not generate sub harmonics. As the Coulomb friction function is an odd function of $\dot{x}_p$ the even harmonics terms do not appear in the output. The absence of a phase shift is due to the memory-less nature of the Coulomb friction function [9].

In the DF - method one takes the first harmonic only, ignoring the higher harmonics. So, the DF - method gives a linearized relation between the input and the output through an equivalent transfer function.

$$K_F(x_p, \omega) = \frac{F_c(\omega)}{\dot{x}_p(\omega)} = \frac{4}{\pi} \frac{F_{cmax}}{\dot{x}_p} = \frac{4}{\pi} \frac{F_{cmax}}{\omega \bar{x}_p} \qquad (2.9)$$

Putting the above linearized transfer function in the loop and taking the root locus by varying K_F it is clearly seen from Figure 2.13 that as K_F varies from 0 to ∞, the damping factor of the dominant root increases. From the above one may infer the following:

i) Coulomb friction contributes positively to the damping of a hydraulic actuator.

ii) Let F_{cmax} be of a constant value. In that case as $\bar{x}_p$ varies from 0 to ∞, K_F varies from ∞ to 0. Thus at a given frequency, as displacement of the piston of a hydraulic actuator reduces, the coulomb friction contributes

more towards the damping of the system.

The above inferences made from the describing function study of the Coulomb friction function are proven correct by actual simulation of the electro hydraulic actuator system in which the Coulomb friction function is directly incorporated. Figure 2.14 shows the time response of the actuator to step inputs of varying magnitudes viz. 1 vdc, 5 vdc and 10 vdc. The nominal level of Coulomb friction F_{cmax} is 80 lbs. Compared to the response of the system with no Coulomb friction, which is lowly damped, high frequency oscillatory, as shown in Figure 2.12, Coulomb friction uniformly damps these oscillations.

Furthermore, it may be observed from Figure 2.14 that the damping due to Coulomb friction reduces as the magnitude of the response (displacement) increases.

In addition, a study is made of the effect of the level of Coulomb friction on the response of E H actuator which is shown in Figure 2.15. It may be seen that as Coulomb friction is increased from 80 lbs. to 8000 lbs, the damping increases, resulting in increased settling time.

2.5 MOUNTING STIFFNESS

The actuator so far , has been assumed to be rigidly mounted on the airframe. A flexible mounting is now considered. The pressure developed in the cylinder chambers now not only accelerates the piston but also moves the cylinder in the opposite direction.

The Equation (2.2a) now gets modified as follows:

$$Q_l = A_p \frac{d(x_p - x_a)}{d t} + \frac{V}{4 \beta} \frac{d P_l}{d t} \qquad (2.10)$$

where x_a is the displacement of the cylinder and is given by

$$x_a = - \frac{P_l A_p}{k_b} \qquad (2.11)$$

where k_b is the mounting stiffness expressed as an equivalent spring stiffness. It should be mentioned here that the value of cylinder mass for the actuator considered for illustration is not available. However, simple calculations show that at the operating frequencies the inertial force associated with possible values of this mass will be insignificant compared to the force due to the mounting stiffness at its nominal value for the system considered, and therefore the mass of cylinder may be ignored.

The transfer function between the voltage input to the DDV and the actuator displacement and the corresponding eigenvalues are given in Appendix A (A4).

Figure 2.16a shows the root locus for the variation of the mounting stiffness from 10% of the nominal value to double the nominal value. The roots which are nearer to the imaginary axis show an increase in natural frequency as well as an increase in damping when the stiffness is increased from 0.1*(nominal value) to 1.2*(nominal value). Beyond that the damping decreases and the natural frequency increases. On

the other hand the roots farther from the imaginary axis show a different trend. The natural frequency decreases as the stiffness is increased. The damping first increases, reaches a peak for a stiffness value of 0.7 times the nominal value and then decreases.

Figure 2.16b compares the frequency response of a flexibly mounted E H actuator at the nominal value of stiffness with that for rigidly mounted actuator. The bandwidth of the E H actuator with flexible mounting is 140 rad/s (compared to 80 rad/s for the rigidly mounted actuator). However, at higher frequencies the attenuation is greater for the E H actuator with flexible mounting.

The step response of the E H actuator is shown in Figure 2.16c for a finite (nominal value) and infinite value of the mounting stiffness. It may be seen from the figure that the damping has reduced and there is an overshoot of about 11% when the mounting stiffness is finite. The rise time has however reduced as is also indicated by Figure 2.16b.

A frequency response study is carried out for variation in mounting stiffness to understand this phenomenon, and shown in Figure 2.16d. The bandwidth is seen to be increasing as the mounting stiffness is reduced from infinity. The maximum is reached at the nominal value of the mounting stiffness. Any further reduction in the mounting stiffness results in a reduced bandwidth. The explanation may be as follows:

eigenvalues of E H actuator (rigid mounting) :

$$-109.87 \pm 641.52\ i \quad (\omega_n = 650.86;\ \zeta = 0.1688)$$
$$-119.36 \pm 14.58\ i \quad (\omega_n = 120.24;\ \zeta = 0.9926)$$

eigenvalues of E H actuator (flexible mounting) :
(for nominal values of the mounting stiffness)

$$-66.58 \pm 122.66\ i \quad (\omega_n = 135.56;\ \zeta = 0.477)$$
$$-154.98 \pm 80.09\ i \quad (\omega_n = 174.45;\ \zeta = 0.888)$$

From the above values it may be seen that the value of the undamped natural frequency of the lower frequency mode the E H actuator on flexible mounting is greater than the corresponding value for rigidly mounted E H actuator. Similarly the damping factor for the E H actuator with flexible mounting is lower than that of the rigidly mounted E H actuator. Both these factors contribute to a larger bandwidth.

As the stiffness is further decreased to half the nominal value, the eigenvalues of the system are as follows:

$$-29.07 \pm 82.19\ i \quad (\omega_n = 87.18;\ \zeta = 0.3334)$$
$$-192.11 \pm 63.69\ i \quad (\omega_n = 202.39;\ \zeta = 0.9492)$$

It may be seen that the lower end natural frequency value is now less than that for the nominal value of the mounting stiffness. Besides, the damping ratio is more. Hence a smaller bandwidth may be expected.

2.6 ACTUATOR - LOAD DYNAMICS [6]

Figure 2.17 shows schematically the actuator - elevon servo system. The elements included for the analysis of this system apart from the DDV, hydraulic actuator, and the

mounting stiffness are:

i) Inertia of the elevon (I)

ii) Horn stiffness (k_h)

iii) Aerodynamic Hinge Moment (H_s)

It is assumed that the elevons are rigid. The flexibility of the linkages (piston rod and elevon horn) is represented by a linear spring at the horn coaxial to the piston rod.

Since the mass of the cylinder is not accounted for, the whole system is represented as a two mass system, whereas, strictly it is a three mass system. Figure 2.18 shows the sign convention of the displacements, linear and rotary, of the actuator - elevon system.

The equations of motion are as follows:

$$m_p(\ddot{x}_p + \ddot{x}_a) + B_v \dot{x}_p + k_h (x_p - \delta l) = A_p P_l \qquad (2.12)$$

$$k_h (x_p - \delta l) l = I \ddot{\delta} + k_\delta \delta + k_\alpha \alpha \qquad (2.13)$$

where l = horn length

δ = elevon deflection

α = angle of attack (AOA)

k_δ = hinge moment per unit elevon deflection

k_α = hinge moment per unit AOA

The angle of attack inputs may be considered as disturbances for the present and the transfer function between the piston displacement and the elevon deflection follows from Equation (2.13)

$$\frac{\delta(s)}{x_p(s)} = \frac{k_h l}{I s^2 + (K_h l^2 + k_\delta)} \qquad (2.14)$$

Equation 2.12 is shown in Figure 2.1 (categorized as load dynamics).

The overall transfer function of the actuator - elevon servo system obtained from Figure 2.1 is given in Appendix A (A5). The eigenvalues are :

-100.72 ± 854.41 i
-234.21
-28.35
+10.44 ± 28.63 i

The load resonance poles have positive real part. The system is therefore unstable for the nominal position feedback gain. It is instructive to study the root locus of the E H actuator for varying mass. Figure 2.19 shows the dominant roots moving towards the right half of the s - plane with increasing mass (the mass considered is the mass of the piston and the equivalent mass of the elevon due to its moment of inertia. The two masses are assumed to ba rigidly connected to each other). The roots become unstable for an equivalent mass greater than 3.0 lbs.

The instability may be due to the overcorrection of the position feedback. The feedback gain may have been determined for a no - load case and hence the instability appears due to elevon inertia. A possible solution is the damping of the load poles by suitable means.

2.6.1 DAMPING BY DYNAMIC PRESSURE FEEDBACK

Quite a few methods exists for damping of hydraulic servos[2]. Prominent among them being:

a) Damping through increased leakage (disadvantage :

high pumping requirements)

b) Damping through pressure feedback (disadvantage : increased load sensitivity)

c) Damping through acceleration feedback (disadvantage : increased hardware complexity)

c) Damping through Dynamic pressure feedback (DPF) :

Dynamic (or derivative) pressure feedback is usually preferred because this does not change the load stiffness.

It is represented in the transfer function form associated with what is known as a washout circuit.

$$H_m = k_p \frac{\tau_p s}{\tau_p s + 1} \qquad (2.15)$$

At low frequencies $H_m = 0$ and the load stiffness therefore remains unchanged. At higher frequencies, $H_m = k_p$ will provide adequate damping if $\omega \tau \gg 1$. The block diagram of the actuator - elevon servo system with Dynamic Pressure Feedback is given in Figure 2.20.

τ is determined such that it satisfies the condition $\omega\tau \gg 1$ Thus $\tau = 3$ is taken (determined by trial and error). Root locus is then drawn, as shown in Figure 2.21, to determine the value of k_p. k_p is varied from 0.0002 to 0.001. Best results are obtained for $k_p = 0.0005$. The transfer function of the actuator - elevon servo system with dynamic pressure feedback is given in Appendix A(A6). Figure 2.22 shows the unit step response of the actuator - elevon servo system for

τ = 3 and k_p = 0.0005. It may be seen from the Figure that the transient response is oscillatory with an overshoot of about 66%. The settling time is about two seconds.

As may be seen from Appendix A(A6), the damping ratio of the dominant load resonance poles is 0.113. Evidently the dynamic characteristics of the elevon actuation system are poor although those of the E H actuator under no load conditions were satisfactory, as shown in Figure 2.12b. It may be noted that the above characteristics of the elevon actuation system were the best (in terms of rise time and settling time) that could be achieved by adjustment of the two parameters k_p and τ_p of the dynamic pressure feedback loop, the rest of the parameters of the system considered for illustration being preserved. The E H actuator appears to have a mismatch with the impedance characteristics of the elevon system.

While one may attempt at changing the structure of the system by introducing more feedback loops, or changing the controller of the dynamic pressure feedback loop, which has presently the form of a washout circuit having two parameters, it may be worthwhile to see how the system performs, when placed as it is in the longitudinal flight control system of the aircraft.

2.6.2 EFFECT OF VARIATION OF HORN STIFFNESS

A study is made to show the effect of variation of the horn stiffness on the elevon actuation system. Figure 2.23a shows the root locus of the dominant poles when the horn

stiffness is varied from 10% of the nominal value to double the nominal value. It may be seen from the Figure that the sensitivity of the roots to variation in horn stiffness is very little above stiffness value of 0.7 times the nominal value. The system natural frequency and the damping factor reduce for smaller values of the horn stiffness. The same inferences may be drawn from the frequency response curves which are shown in Figure 2.23b.

CHAPTER 3 IMPEDANCE OF THE ELEVON ACTUATION SYSTEM

3.1 INTRODUCTION

The restraint to displacement of a control surface which is provided by its control system may be termed as its 'impedance'[8]. The stiffness of the actuator loop must consider all elements including stiffness of the horn on the control surface, bending of bolts, internal stiffness of bearings, free play and friction in bolted connections, actuator structural stiffness, actuator hydraulic stiffness and spring rate of the tie down structure etc. [4].

3.2 IMPORTANCE OF IMPEDANCE CHARACTERISTICS STUDIES

Impedance characteristics of the elevon actuation system are usually determined to carry out aeroservoelasticity studies. Though aeroservoelasticity is beyond the scope of the present work, it may be worthwhile to determine the impedance characteristics of the elevon actuation system as an input to further studies on flutter control of the wing, the control surfaces etc.

Table 3.1 reveals the importance of impedance studies [4]. It summarizes potential solutions for the different types of control surface flutter (different from wing flutter and characterized by higher frequency of 40-50 Hz) with comments regarding relative effectiveness of each solution. Manipulation of the control system stiffness appears to be the most efficient means of flutter supression.

TABLE 3.1

SOLUTIONS TO WING FLUTTER CONTROL

FLUTTER TYPE	CANDIDATE SOLUTIONS			
	MASS BALANCE	HYDRAULIC DAMPER	RESTRAINT VIA STIFFNESS	HINGE LINE LOCATION
Type 1 classical coupling	very effective	use is rare	ALMOST ALWAYS THE MOST	balanced surfaces present less problem
Type 2 all movable surfaces	limited success at times	use is rare	EFFICIENT SOLUTION IN TERMS	effect difficult to generalize
Type 3 transonic/ supersonic "buzz"	not effective	very effective	OF LBS/KNOT IMPROVEMENT	not a major variable

The dynamic effect of actuator impedance is illustrated in Figure 3.1. Here $Z(\bar{Q}_1, i\omega)$ is the mechanical impedance of the actuator on a flexible mounting, expressed as equivalent hinge moment per unit elevon rotation. $\bar{Q}_1$ is the steady aerodynamic hinge moment appropriate to the flight condition under consideration. If feed back control is not employed (i.e. the open loop case) to suppress flutter we have [7]

$$Z\, q_1 = Q_1$$

where q_1 is the amplitude of elevator deflection and $Q_1 \exp(i\omega t)$ is the total dynamic elevon hinge moment viewed as a loading action.

Thus from Figure 3.1 we get

$$q_1 = T(\bar{Q}_1, i\omega)\, d + \frac{Q_1}{Z}$$

where T is the transfer function of the actuator elevon servo system under steady loading $\bar{Q}_1$ and d is the demand signal.

The above two cases illustrate the need for determining the impedance of the actuator elevon servo system. Linearized results from actuator impedance tests are sometimes used. But the impedance may also be estimated by mathematical modelling of the actuator.

3.3 ACTUATOR HYDRAULIC STIFFNESS

Impedance of a mechanical system depends on clearly defined physical entities viz. spring stiffness, dampers,

masses and their combinations. Hydraulic actuator stiffness however depends on factors like piston area, bulk modulus, servo action provided by feedbacks etc. to provide the necessary impedance. A simplified hydraulic actuator (single cylinder; rigid mounting; Figure 2.5) is analysed to understand the actuator hydraulic stiffness.

Let the direct drive valve be represented by a unit gain.

Then the equations of motion are:

$$Q_l = k_g x_v - k_c P_l \qquad (3.1a)$$

$$Q_l = A_p \dot{x}_p + \frac{V}{4\beta} \frac{d P_l}{d t} \qquad (3.1b)$$

$$x_v = V_o - k_x x_p - k_p \frac{d P_l}{d t} \qquad (3.1c)$$

$$P_l A_p = F \qquad (3.1d)$$

where k_x = position feedback gain

k_p = dynamic pressure feedback gain

V_o = command voltage

The other terms are the same as used in Chapter 2.

For $V_o = 0$, from Equation 3.1a - 3.1d we get,

$$\frac{F(s)}{x_p(s)} = \frac{(A_p s + k_g k_x)(4\beta A_p / Vs)}{(1 + (4\beta k_c / Vs) + (4\beta k_g k_p s / Vs))} \qquad (3.2)$$

3.3.1 CASE A: No feedback to the valve ($k_p = 0$; $k_x = 0$)

Equation 3.2 reduces to

$$\frac{F(s)}{x_p(s)} = \frac{A_p^2 s}{\frac{V}{4\beta} s + k_c} \qquad (3.3)$$

If we assume for the present that the hydraulic oil to be incompressible ($\beta=\infty$), Equation 3.3 reduces to

$$\frac{F(s)}{s x_p(s)} = \frac{A_p^2}{k_c} \qquad (3.4)$$

Physically Equation 3.4 may be explained as follows: The motion of the actuator piston induces load flow which is resisted by the finite opening of the valves and possible leakage across the piston, as reflected in the inverse of k_c, the valve flow pressure coefficient at Equation 2.6 .

Now let the hydraulic oil be considered to be compressible.

Defining effective oil spring k_o[8] as

$$k_o \equiv \frac{4 \beta A_p^2}{V}$$

we obtain from Equation 3.3

$$\frac{F(s)}{X_p(s)} = \frac{k_o s}{s + k_o k_c / A_p^2} \qquad (3.5)$$

For high values of input frequency this reduces to

$$\frac{F(s=j\omega)}{X_p(s=j\omega)} = k_o$$

From the above equation it may be seen that at high frequencies the displacement of the actuator piston is essentially resisted by the effective oil spring. An increase in the bulk modulus increases the stiffness of the hydraulic actuator. For low frequencies the expression for impedance reduces to Equation 3.4 which indicates resistance to motion, not to displacement.

Alternatively equation 3.5 may be viewed as follows: If flow pressure coefficient k_c is very small such that the term $k_o k_c / A_p^2$ may be neglected (i.e. the load flow is negligible) the resistance to motion of the piston is provided by the effective oil spring. For high values of k_c, the load flow alone determines the amount of resistance which is provided by the actuator.

3.3.2 CASE B: $k_p = 0$; $k_x \neq 0$; $\beta = \infty$

In this case the effect of position feedback is investigated. Equation 3.2 reduces to

$$\frac{F(s)}{X_p(s)} = \frac{k_g k_x A_p}{k_c} + \frac{A_p^2 s}{k_c} \qquad (3.6)$$

The second term has been already investigated. For lower values of frequency the impedance value tends to be

$$\frac{F(s=j\omega)}{X_p(s=j\omega)} = \frac{k_g k_x A_p}{k_c}$$

Reference [8] defines $(k_g A_p / k_c)$ as effective actuator servo stiffness. Thus, for lower values of frequency

Actuator hydraulic stiffness = position gain feedback * effective actuator servo stiffness

Physically, what happens is as follows:

Without loss of generality it may be assumed that initially the valves are closed. A change in the piston position causes the servovalve to move in the opposite direction due to the position feedback and the consequent reversal of flow of hydraulic oil resists the displacement.

3.3.3 CASE C: $k_p \neq 0$; $k_x = 0$; $k_c = 0$

In this case the effect of dynamic pressure feedback is investigated. Equation 3.2 reduces to

$$\frac{s\,F(s)}{s\,X_p(s)} = \frac{A_p^2}{(k_g k_p V + V/4\beta)} \qquad (3.6)$$

Equation 3.6 may be interpreted as follows:
A motion of the piston in positive direction (Figure 2.5) results in outflow of hydraulic oil from chamber 2 along with the compression of the oil in the chamber and associated rise in pressure. In chamber 1 there is an inflow along with drop in the chamber pressure and expansion of the oil. Thus a

constant velocity input results in a rate of change of load pressure $P_l (\equiv P_1 - P_2)$ which is fed back to the valve through the dynamic pressure feedback which results in a change in valve position so that the outflow from chamber 2 and the inflow to chamber 1 reduces thus providing resistance to the the motion of the piston.

3.4 DETERMINATION OF IMPEDANCE OF THE ELEVON ACTUATION SYSTEM

Initially the mass is not considered. This enables us to determine the actuator hydraulic stiffness. From Figure 2.1 we get,

$$e(s) = V_o - kda*kla*X_p(s) - k_p \frac{\tau_p s}{\tau_p s+1} (P_{l1}(s)+P_{l2}(s)) \quad (3.7)$$

$$\left(\frac{e(s)\ KT}{\tau s + 1} - s A_p X_p(s) - s A_p \frac{F_1(s)}{k_b} \right) \frac{4\beta A_p}{Vs + 4\beta k_c} = F_1(s) \quad (3.8)$$

$$\left(\frac{e(s)\ KT}{\tau s + 1} - s A_p X_p(s) - s A_p \frac{F_2(s)}{k_b} \right) \frac{4\beta A_p}{Vs + 4\beta k_c} = F_2(s) \quad (3.9)$$

where $KT = ka * k1 * rv * k_g$

$$\begin{aligned} P_{l1}(s)\ A_p &= F_1(s) \\ P_{l2}(s)\ A_p &= F_2(s) \\ F_1(s) &= F_2(s) \end{aligned} \quad (3.10)$$

NOTE: 1) In the above equations e(s) is the Laplace transform

of the error signal to the system.

2) The subscript 1 & 2 refer to the two cylinders of the dual - tandem- actuator.

3) It is assumed that the force generated by the two actuators is identical.

From Equation (3.8), (3.9) & (3.10) we get, taking $V_o = 0$

$$\frac{F(s)}{X_p(s)} = \frac{[s(\tau s+1)8\beta A_p^2 + 8KT\ kda\ kla\ \beta A_p](\tau_p s + 1)}{(\tau s+1)(\tau_p s+1)(Vs+4\beta k_c)+8\beta\frac{A_p^2}{k_b}s(\tau s+1)(\tau_p s+1)+(KT\ 8\beta\ k_p\ \tau_p)s} \quad (3.11)$$

Now considering the mass and equivalent damping we get

$$\bar{F}(s) = F(s) + (m_p s^2 + B_v s)\, X_p(s)$$

$$\therefore \quad Z_a = \frac{\bar{F}(s)}{X_p(s)} = \frac{F(s)}{X_p(s)} + (m_p s^2 + B_v s) \quad (3.12)$$

Actuator impedance (Z_a) and the horn stiffness may now be considered as two springs in series.

Hence, the equivalent impedance Z_{eq} is

$$Z_{eq} = \frac{Z_a\ k_h}{Z_a + k_h} \quad (3.13)$$

Impedance is usually expressed in terms of required torque per unit deflection of the control surface

Therefore,

$$\frac{T}{\delta} = l^2 Z_{eq} \qquad (3.14)$$

The elevon may now be considered to be restrained by a torsional spring. The torque required to deflect the elevon has to overcome the torsional force due to this spring, the hinge moment for a given flight condition and the inertial force of the elevon.

Hence,

$$\bar{T} = T + I \ddot{\delta} + H_s \qquad (3.15)$$

where, $H_s = k_\alpha \alpha + k_\delta \delta$

For a given flight condition considering the hinge moment due to elevon deflection only we get the following closed form solution:

$$\frac{\bar{T}(s)}{\delta(s)} = \frac{T(s)}{\delta(s)} + (I s^2 + k_\delta)$$

$$= l^2 Z_{eq} + (I s^2 + k_\delta) \qquad (3.16)$$

Figure 3.2 shows the impedance characteristics of the actuator elevon servo system versus frequency for the following flight conditions:

i) altitude = 5 km ; Mach No = 0.3
k_δ = 47.58 N m / deg

ii) altitude = sea level ; Mach No = 1.2
k_δ = 4827.85 N m / deg

iii) Aircraft at rest $k_\delta = 0$

The following observations may be made from Figure 3.2.

a) The dip in the impedance curves is at the load

resonance frequency (i.e. 15.9 rad/s for flight condition (i) and 32.6 rad/s for flight condition (ii). The impedance curve for aircraft at rest overlaps the curve for flight condition (i). This is because of the small difference in the aerodynamic elevon stiffness k_δ values.

b) For low values of frequency, an increase in aerodynamic elevon stiffness predictably causes an increase in impedance of the elevon actuation servo. However for higher values of frequency the trend reverses.

c) For $\omega \rightarrow \infty$, the impedance of the elevon actuation servo system does not change much with the change in flight condition. This is due to the fact that at higher values of frequency the coefficients of s and higher powers of s in Equation 3.16 predominates and impedance of the elevon actuation system is thus no longer sensitive to the variation in k_δ.

Figure 3.3 shows the phase plot for the impedance of the elevon actuation system. It may be seen from the figure that for lower values of frequency the elevon deflection is almost in phase with the external loading. As the frequency increases the phase difference tends towards 180°. However, for intermediate frequency values (16 to 32 rad/s approximately) the phase difference between the external loading and the elevon deflection is greater for low values of aerodynamic stiffness compared to that for higher values. The relative phases of applied torque and elevon deflection have a strong bearing on the flutter characteristics of the

control surface.

3.5 RELATION BETWEEN IMPEDANCE AND THE TRANSFER FUNCTION OF THE ELEVON ACTUATION SERVO

To determine the relation between the impedance and the transfer function (≡ control surface deflection / command signal) of the elevon actuation system, it is necessary to consider the inverse of impedance, i.e. compliance. Compliance may also be defined as the transfer function between the control surface deflection and the external load (compliance = control surface displacement / external torque). Figure 3.4a (derived from Figure 2.1) shows the relation between the transfer function and the compliance of the elevon actuation servo. If the command voltage is considered to be zero, Figure 3.4a gives the expression for compliance. If the external load is considered zero, the figure gives the expression for transfer function between the command signal and the elevon deflection.

Thus,

$$\text{compliance} = \frac{X_p(s)}{F(s)} = \frac{G2\ G3}{1 + G1\ G2\ H2 + G2\ G3\ H1}$$

$$\text{transfer function} = \frac{X_p(s)}{V_o(s)} = \frac{G1\ G2\ G3}{1 + G1\ G2\ H2 + G2\ G3\ H1}$$

The simplified block diagram representation of the elevon actuation system is shown in Figure 3.4b. It may be seen from the Figure that

$$\text{compliance} = \frac{G2}{1 + G1G2H1}$$

$$\text{transfer function} = \frac{G1\ G2}{1 + G1G2\ H1},$$

Figure 3.5 compares the frequency response of the transfer function and the compliance for flight condition (i). The two curves show similar behaviour. The response is uniform up to 10 rad/s, with a resonance peak at around 16 rad/s.

Figure 3.6 shows the difference between the transfer function and the compliance in decibels. The transfer function G1*1 is also plotted. G1 may also be seen as the transfer function between the force in the piston rod and the command voltage input as the piston position x_p is held constant. Opening the valve through input command voltage results in changes in P_l and consequently in the force developed in the piston rod of the actuator. The position feedback to the DDV will be ineffective when the actuator position is held constant. P_l eventually reaches the value $P_{supply} - P_{sump}$, for a constant command voltage .

Compliance indicates the effect of disturbances, including the aerodynamic forces due to gusts, wake or flutter, vibration of the aircraft and control surface, on the response of the control surface, as the command signal is given to the actuator system. Thus compliance viewed as the sensitivity of the control surface deflection to forces considered as noise/disturbances, should be as small as possible, i.e. impedance should be high.

It may be noted from Figure 3.4b that the forward path

associated with compliance is $G2'$, while that associated with the transfer function between V_o and δ is $G1G2'$. G1 and $G2'$ are closely related in the sense that changing parameters of $G2'$ to effect the compliance is not possible in most cases without simultaneously changing G1. G1 and $G2'$ are not independent physical entities.

Figure 3.4c shows the simplified block diagram representation of the impedance of the elevon actuation system. From the figure it may be seen that a deflection of the control surface is resisted by the control system through the following two forward paths:

a) $G1H1'$; which represents the transfer function between the resistance offered by the actuator due to its servo action through the elevon position feedback and the elevon deflection.

b) $1/G2'$; which represents the transfer function between the resistance offered by the inertia (mass of piston and control surface), Coulomb friction, aerodynamic and horn stiffness etc. to the elevon deflection and the elevon deflection. This includes the resistance offered to motion by the hydraulic fluid.

The impedance may be thus represented as

$$\frac{\text{resisting load}}{\text{elevon deflection}} = \frac{T(s)}{\delta(s)}\Bigg|_{V_o=0} = \frac{1 + G1G2'H1'}{G2'}$$

CHAPTER 4 ACTUATOR AIRCRAFT INTEGRATION

4.1 INTRODUCTION

Electro hydraulic servo mechanisms are used to provide power boost, stability augmentation control inputs, or primary control of the airplane. The present generation airplanes are control configured vehicles wherein the static stability requirement is relaxed at the design stage in order to increase maneuverability. In such airplanes the actuator forms an integral part of the overall control law scheme.

4.2 AIRPLANE MODEL [3, 10]

The airplane considered here for illustration is a fighter aircraft of relaxed static stability. The primary control loop of the longitudinal control system consists of pitch rate and normal acceleration as feedback variables to the longitudinal control surface actuators as shown schematically in Figure 4.1 .

Since the system is a Single Input Multi Output (SIMO) system, the airplane is represented in State Space form :

$$\dot{X} = A X + B U$$

$$Y = C X + D U$$

Where X = state of the system
A = State Matrix
U = Input vector
Y = Output vector

The linearised small perturbation equations of longitudinal motion of the airplane are:

$$m [\dot{u} + q w - r v] = d X_F \qquad (4.1)$$

$$m [\dot{w} + p v - q u] = d Z_F \qquad (4.2)$$

$$\dot{q} I_y + p r (I_x - I_z) - r^2 I_{xz} + p^2 I_{xz} = d M \qquad (4.3)$$

$$\left.\begin{aligned} X_F &= X_F(\alpha, q, \delta_e) \\ Z_F &= Z_F(\alpha, q, \delta_e) \\ M &= M (\alpha, q, \delta_e) \end{aligned}\right\} \qquad (4.4)$$

For simplicity, making the short period approximation of the dynamics of the airplane, we set u=0 and ignore the equation for X_F.

Equations 4.1 - 4.3 reduce to

$$\frac{\dot{w}}{u} = \dot{\alpha} = \frac{1}{m} \left[\frac{\partial Z}{\partial \alpha} \alpha + \frac{\partial Z}{\partial q} q + \frac{\partial Z}{\partial \delta_e} \delta_e \right] \qquad (4.5a)$$

$$\dot{q} = \frac{1}{I_y} \left[\frac{\partial M}{\partial \alpha} \alpha + \frac{\partial M}{\partial q} q + \frac{\partial M}{\partial \delta_e} \delta_e \right] \qquad (4.5b)$$

Defining,

$$Z_\alpha = \frac{1}{m} \left(\frac{\partial Z}{\partial \alpha} \right) \quad ; \quad M_\alpha = \frac{1}{I_y} \left(\frac{\partial M}{\partial \alpha} \right)$$

$$Z_q = \frac{1}{m} \left(\frac{\partial Z}{\partial q} \right) \quad ; \quad M_q = \frac{1}{I_y} \left(\frac{\partial M}{\partial q} \right)$$

$$Z_{\delta_e} = \frac{1}{m} \left(\frac{\partial Z}{\partial \delta_e} \right) \quad ; \quad M_{\delta_e} = \frac{1}{I_y} \left(\frac{\partial M}{\partial \delta_e} \right)$$

we have

$$\begin{Bmatrix} \dot{\alpha} \\ \dot{q} \end{Bmatrix} = \begin{bmatrix} Z_\alpha/U & Z_q/U \\ M_\alpha & M_q \end{bmatrix} \begin{Bmatrix} \alpha \\ q \end{Bmatrix} + \begin{Bmatrix} Z_{\delta_e}/U \\ M_{\delta_e} \end{Bmatrix} \delta_e \qquad (4.6)$$

Noting that

normal accn. at station distant L_s aft of c.g. of the airplane

$$a_{z_s} = u(\dot{\alpha} - q) + \dot{q} L_s \qquad (4.7)$$

From Equations (4.5) and (4.7) we get

$$a_{z_s} = (uZ_\alpha + M_\alpha L_s)\alpha + (uZ_q - u + M_q L_s)q + (uZ_{\delta_e} + M_{\delta_e} L_s)\delta_e \qquad (4.8)$$

Using the airplane data available for the flight condition Altitude = 5 km ; Mach No = 0.3 we may write the equations of motion (the state equation) and the equation for output variables as

$$\begin{Bmatrix} \dot{\alpha} \\ \dot{q} \end{Bmatrix} = \begin{bmatrix} -0.6333 & 1.0 \\ 1.701 & -0.6174 \end{bmatrix} \begin{Bmatrix} \alpha \\ q \end{Bmatrix} + \begin{Bmatrix} -0.2710 \\ -7.1030 \end{Bmatrix} \delta_e$$

$$\begin{Bmatrix} q \\ a_{z_s} \end{Bmatrix} = \begin{bmatrix} 0.0 & 1.0 \\ -68.66 & 1.723 \end{bmatrix} \begin{Bmatrix} \alpha \\ q \end{Bmatrix} + \begin{Bmatrix} 0.0 \\ -8.219 \end{Bmatrix} \delta_e$$

The open loop eigenvalues for the system are:

-1.9296

0.6789

The airplane is thus inherently unstable. The primary control loop consists of pitch rate and normal acceleration as feedback variables fed to the elevon actuator through a filter network and a gain. .The filter constants are:

i) Pitch rate feedback filter:

$$qfil = \frac{0.31\ s + 2.25}{0.25\ s + 1.0}$$

$$q\ gain = GB = 0.3721$$

ii) normal acceleration feedback filter:

$$a_{z_s}\ fil = \frac{1}{0.35\ s + 1}$$

$$a_{z_s}\ gain = GA = 0.014$$

The resultant closed loop eigenvalues are :

$$-1.9238 \pm 1.4999\ i$$

$$-3.6044 \pm 2.4465\ i$$

which are stable.

4.3 ACTUATOR IN THE LOOP

The actuator model, as developed in Chapter 2, is put in the primary control loop as shown in Figure 4.1 using the appropriate hinge moment derivatives for the given flight condition.

The eigenvalues with the actuator in the loop are:

-100.77 ± 855.28 i
-118.99 ± 102.73 i
-1.76 ± 15.90 i
-1.94
-3.15
-0.24
-3.79
+0.57

The eigenvalue shows marginal instability. Thus it may be seen that the system needs some tuning. A tuning gain is provided in the feedback loop so that a good response is provided. A root locus is plotted for the dominant poles for the tuning gain varying from 1 to 15 in Figure 4.2 . The figure shows that a tuning gain above 12 may give desirable response. Step response of the airplane is shown in Figure 4.3a (normal acceleration vs time) and 4.3b (pitch rate vs time) to a unit command voltage for various values of tuning gain. It may be seen from the figures that the airplane response with a tuning gain of 14 is the smoothest. A tuning gain above 14 gives a wavy response while a tuning gain less than 14 is comparatively sluggish. Thus a tuning gain of 14 is chosen.

The eigenvalues for the actuator - aircraft system with realistic actuator with a tuning gain of 14 are :

-100.77 ± 855.28 i
-118.98 ± 102.73 i
-0.93 ± 15.57 i
-3.57 ± 1.62 i
-1.37 ± 1.42 i

The step response of the airplane with the realistic actuator with a tuning gain of 14 is now compared with the response of the airplane with an ideal actuator in Figure 4.4a and 4.4b .It may be seen from Figure 4.4a that airplane response with the realistic actuator model is sluggish compared to the airplane response with the ideal actuator. This may also be seen from the fact that the short period frequency of the aircraft with realistic actuator model is lower, 3.92 rad/s compared to the corresponding frequency of 4.36 rad/s for the aircraft with ideal actuator. The aircraft with realistic actuator has a higher short period damping ratio of 0.9106 compared to 0.8274 for the aircraft with the ideal actuator.

The overshoot of the normal acceleration has increased to 5.25 % from 2% for the ideal case and the rise time is higher, 1.0733 seconds compared to 0.875 seconds for the ideal case.

From Figure 4.4b it may be seen that the pitch rate response for the realistic model is less smooth, though the overshoot has been reduced to 72.92% compared to 91.91% for the ideal case. The rise time is nearly the same - 0.24 seconds compared to 0.23 seconds for the ideal case.

The settling time for both the responses (i.e. normal acceleration response as well as the pitch rate response) is seen to have increased for the realistic actuator from 3 seconds (for the ideal case) to 4 seconds.

A study is now carried out to determine if a better performance may be obtained by having an elevon position feedback instead of actuator position feedback. Figure 4.5a shows the root locus of the airplane (only short period roots shown) for variation in elevon feedback gain from the nominal value to 5.5 times the nominal value of position feedback gain. It may be seen from the figure that for lower values of elevon feedback gain the short period damped frequency is higher and the damping is less. However as the feedback gain value increases the damped frequency reduces and the damping increases. it is found that for an elevon feedback gain of 3.5 times the nominal value of position feedback gain k_x) the short period roots are the nearest to that with the ideal actuator.

The eigenvalues of the airplane with realistic actuator model for the optimum elevon feedback gain ($= 3.5 * k_x$) are:

$$\begin{aligned} &-100.79 \pm 855.75\,i \\ &-118.36 \pm 98.34\,i \\ &-1.04 \pm 12.73\,i \\ &-3.68 \pm 2.29\,i \\ &-1.75 \pm 1.49\,i \end{aligned}$$

The time response of the airplane with the realistic actuator model with optimal elevon position feedback gain compared with that with the nominal value of actuator position feedback and the ideal actuator is shown in Figure 4.5b and 4.5c. It may be seen from the figures that there seems to be an improvement in the response with optimal elevon feedback compared to that with the nominal position

feedback. Compared to the response with the ideal actuator the elevon feedback response is wavy. However, the settling time is the same.

It may be erroneous to claim in general that elevon feedback is better than the position feedback based on the above results which compare the eigenvalues for optimal elevon position feedback with those for nominal, non optimal value of actuator position feedback. A study is therefore made to find out the optimum value of actuator position feedback gain k_x. The optimum k_x is found to be 0.65*(nominal value). The eigenvalues of the airplane with the realistic actuator model with optimum actuator position feedback gain are:

$$\begin{array}{l} -100.77 \pm 855.43\ i \\ -118.41 \pm 101.17\ i \\ -1.0 \pm 12.59\ i \\ -3.69 \pm 2.28\ i \\ -1.75 \pm 1.49\ i \end{array}$$

Comparing the above eigenvalues with that for optimal elevon position feedback shows that the values are very close. The response is therefore expected to be the same as there is no difference in the short period roots of the airplane (i.e. $-3.69 \pm 2.28\ i$). This may also be seen from Figure 4.6a and 4.6b.

The above values of optimum feedback gains are determined for a rigid airplane. It may be of interest to study the response of a flexible airplane with the realistic actuator with optimum elevon deflection feedback gain as

determined above. Since the model of the flexible airplane is not available for carrying out such a study, it was decided to reduce arbitrarily the efficiency of the elevon by 20% (as though effected by the chordwise flexure of the control surface) without changing the state matrices. Figure 4.7a and 4.7b show the airplane response with a reduced efficiency elevon. The normal acceleration response of the "flexible" airplane shows slight waviness, though the settling time compared to the response of the airplane with ideal actuator remains the same (i.e. 3 seconds). However, the pitch rate response (Figure 4.7b) shows reduction in damping and the response is oscillatory. This is evident for the optimal elevon position feedback gain was determined on the basis of normal acceleration response.

A study is made to observe the effect of the actuator velocity feedback on the airplane response. As is seen from Figure 2.22b the actuator response showed marked improvement when the velocity feedback was introduced. However, no significant improvement is observed in the airplane response as may be seen from Figure 4.8a and 4.8b. The overshoot of the normal acceleration as well as the pitch rate of the airplane with an additional actuator velocity feedback loop increases compared to that without the velocity feedback. The settling time is however the same.

CHAPTER 5 CONCLUSIONS

Based on the study carried out on the electro hydraulic elevon actuation system for the fighter aircraft, the following conclusions may be arrived at:

The direct drive valve may be represented by a first order lag transfer function for linear analysis purposes.

Increasing the valve flow gain about the nominal value tends to destabilise the E H actuator. The damped frequency remains more or less the same. The bandwidth increases.

Changes in valve flow pressure coefficient do not show marked effect on any dynamical characteristics of the E H actuator. There is a very small increase in damping ratio as the value increases.

E H actuator displays instability at low values ($\leq$ 65% of nominal value) of effective bulk modulus of the hydraulic fluid. Increasing the value of bulk modulus increases the natural frequency and the damping ratio of the system.

Coulomb friction between the piston and the cylinder surface displays a distinct damping effect on the otherwise lightly damped system, totally suppressing the oscillations at the nominal value of the level of the friction. The effect of the Coulomb friction is more pronounced for smaller oscillations of the actuator piston. For smaller command input values, equivalent viscous friction may be used to represent the Coulomb friction to facilitate linear analysis.

A rigidly mounted E H actuator with no load has a first order lag response. The bandwidth is 80 rad/s. However, for finite nominal value of the mounting stiffness, the response has an overshoot and the rise time is shorter.

Effect of variation of horn stiffness about the nominal value is visible only for very low values (10% of nominal value). Damping reduces for low values of horn stiffness.

The inertia of the control surface as a load on the E H actuator system brings about instability. Introducing dynamic pressure feedback through a washout circuit stabilises the system, and yet the best step response of the system obtainable in this configuration is very lightly damped (damping ratio of 0.113) which is far from the first-order-lag response expected from a well designed actuator.

Introduction of actuator velocity feedback improves the poor dynamical characteristics of the elevon actuator system markedly, suppressing the lightly damped oscillations. However, its contribution to improvement of the overall dynamical characteristics of the airplane, as the elevon actuation system is integrated into the flight control loop, is insignificant.

In order that the sensitivity of the deflection of the control surface to applied loads (externally applied or internally generated) is minimised, the impedance of the elevon actuation system should be as large as possible.

The transfer function (between command input voltage and

the elevon deflection) of the elevon actuation system, and its compliance are related through a transfer function between the force developed by the actuator for a command input voltage when the piston rod of the actuator is locked.

The normal acceleration response of the airplane with the realistic actuator matches quite well with that of the airplane with an ideal actuator when the position feedback gain is optimised. The pitch rate response of the airplane is not satisfactory even for the ideal actuator. Actuator with the optimised position feedback gain achieves nearly equally good performance although the gain value has been obtained to achieve a good normal acceleration feedback match.

Replacing actuator position feedback with elevon position feedback in the flight control loop does not show any significant improvement in the dynamical characteristics of the aircraft.

Reducing the effectiveness of the control surface due to possible aeroelastic effects results in some deterioration of the response characteristics of the airplane, but apparently not significantly.

Within the limitations of the present study (confined to the short period dynamics of the aircraft considered), the proposed E H elevon actuation system appears to result in overall dynamical characteristics of the airplane not significantly different from those when an ideal actuator (pure gain) is installed.

RECOMMENDATIONS FOR FURTHER WORK:

The present work may be extended further as follows:

The inertia of the hydraulic fluid introduces a time delay in the system. The E H actuator may be investigated further taking into account such time delay.

Effect of Coulomb friction and saturation limits (brought about by mechanical stops to the valve and actuator piston displacement) on the elevon actuation system may be studied by nonlinear simulation.

The effect of elevon damping coefficients $C_{h_{\dot{\alpha}}}$ and $C_{h_{\dot{\delta}}}$ on the dynamical characteristics of the elevon actuation system have not been included in the present study for want of data. Their effects may be investigated.

The dynamic pressure feedback circuit parameters and the tuning gain have been determined by trial and error in the present work. A systematic optimisation may be carried out to determine these values. A controller different from the one chosen for dynamic pressure feedback loop may be considered for a more refined study of the system. Similarly the tuning gain may be replaced by a controller other than a proportional controller used in the present study.

To study the full impact of incorporating a realistic actuator in the flight control loop, the total airplane model (including both the longitudinal and the lateral dynamics) may be simulated. An "elastic" airplane may also be considered.

The present study confines itself to unit step input to study the short period response of the airplane. Airplane response to various other inputs, such as ramp inputs or spectral inputs, may also be investigated.

REFERENCES

[1] Merritt, H.E. Hydraulic Control system, John Wiley & Sons Inc., 1967

[2] Viersma, T.J. Analysis, Synthesis and Design of Hydraulic Servosystems and pipelines,Elsevier Scientific Publishing Company, Amsterdam, 1980.

[3] McRuer D., Ashkenas I., and Graham D., Aircraft Dynamics and Automatic Control, Princeton, New Jersey, 1973, pp 522-528.

[4] Lyle B.S., Advanced Actuation, Controls and Integration for Aerospace Vehicle, SAE P-170 A-6 symposium papers, Feb 1986 Chapter 1.

[5] McCallum J., Direct Drive Valves : A background into design principles and recent technological developments. MOOG CONTROLS Ltd. Handout.

[6] Edwards, John W. Analysis of an Electro Hydraulic Aircraft Control Surface servo and comparison with test results. NASA Technical Note NASA TN D-6928, August 1972.

[7] Simpson A. Real Actuator effects and the Aerodynamic Energy Method, Aeronautical Journal. Feb 1988.

[8] Benun D., Manual on Aeroelasticity, AGARD,AAADL-TR-7213, October,1968, Chapter 5.

[9] Nagrath I.J., Gopal M., Control System Engineering, Wiley Eastern Limited, New Delhi, 1982.

[10] Friedland B, Control System Design, McGraw-Hill International, 1987.

APPENDIX A

A1. 5^{th} order DDV Transfer Function

$$\frac{37.87s^2 + 1.3\times10^5 s + 1.08\times10^8}{8.52\times10^9 s^5 + 1.785\times10^{-3} s^4 + 6.53s^3 + 1.94\times10^4 s^2 + 2.06\times10^7 s + 4.25\times10^9}$$

ROOTS of Denominator:

$$-2.055\times10^5$$
$$-1.008\times10^3 \pm 2.525\times10^3\, i$$
$$-1.4232\times10^3$$
$$-2.3053\times10^2$$

A2. Transfer Function of Electro Hydraulic Actuator (at no load; no equivalent viscocity)

$$\frac{1.4211\times10^{-13} s^3 + 3.4925\times10^{-10} s^2 + 1.3411\times10^{-7} s + 1.3865\times10^9}{s^4 + 2.55\times10^2 s^3 + 4.3865\times10^5 s^2 + 6.125\times10^9}$$

EIGENVALUES : $-5.0068 \pm 649.34\, i$
-144.61
-100.45

APPENDIX A

A3. Transfer Function of Electro Hydraulic Actuator (no load; with equivalent viscocity)

$$\frac{5.6843*10^{-14}s^3 + 1.4901*10^{-8}\,s + 1.3862*10^{9}}{s^4 + 4.5846*10^{2}s^3 + 4.9053*10^{5}s^2 + 1.043*10^{8}s + 6.125*10^{9}}$$

EIGENVALUES: $-109.87 \pm 641.52\ i$
$-119.36 \pm 14.58\ i$

A4. Transfer Function of Electro Hydraulic actuator with flexibl mounting (no load ; with equivalent viscosity)

$$\frac{1.1369*10^{-13}s^3 + 1.455*10^{-11}s^2 + 1.341*10^{8}}{s^4 + 4.43*10^{2}s^3 + 9.1166*10^{4}s^2 + 1.0087*10^{7}s + 5.9286*10^{8}}$$

EIGENVALUES: $-66.58 \pm 122.66\ i$
$-154.98 \pm 80.09\ i$

A5 Transfer Function of the Actuator Elevon Servo System (without dynamic pressure feedback)

$$\frac{2.395\ s^2 + 4.3675\ s + 1.984*10^{11}}{s^6 + 443.13\ s^5 + 7.9099*10^{5}s^4 + 1.9742*10^{8}s^3 + 1.5713*10^{9}s^2 + 1.5713*10^{9}s + 4.566*10^{12}}$$

EIGENVALUES: $-100.72 \pm 854.44\ i$
-234.21
-28.35
$+10.44 \pm 28.63\ i$

APPENDIX A

A6 Transfer Function of the Actuator Elevon Servo System (with dynamic pressure feedback)

$$\frac{4.0\times10^{-11}s^6 + 4.09\times10^{-6}s^5 + 8.3038\times10^{-4}s^4 + 2.84s^3 + 3.21s^2 + 1.98\times10^{11}s + 6.6134\times10^{10}}{s^7 + 4.43\times10^{2}s^6 + 8.16\times10^{5}s^5 + 1.85\times10^{8}s^4 + 1.93\times10^{10}s^3 + 1.19\times10^{11}s^2 + 4.74\times10^{12}s + 1.522\times10^{12}}$$

EIGENVALUES:

$-100.77 \pm 855.28\ i$
$-118.99 \pm 102.72\ i$
-0.32
$-1.81 \pm 15.92\ i$

APPENDIX B
SYSTEM CONSTANTS

SYMBOL	DESCRIPTION	UNIT	VALUE
A_p	Actuator Area	in^2	3.142
β	Fluid Bulk Modulus	lb/in^2	100000
F_{cmax}	Maximum value of Coulomb friction	lb	80
I	Elevon Inertia	$kg\ m^2$	3.36
Ka	Actuator Loop Amplifier Gain	vdc/vdc	12.5
kb	Mounting stiffness	kg/cm	4.91×10^4
k_c	Valve flow pressure coefficient	$\frac{in^3/s}{psi}$	0.0006535
kla	demodulator gain	vdc/vac	3.09
kh	Horn stiffness	kg/cm	14.60×10^4
k_α	Hinge moment per unit Angle of Attack	Nm/deg	83.26
k_δ	Hinge moment per unit elevon deflection	Nm/deg	47.58
kda	lvdt gain	vac/in	1.43
k_g	Valve flow gain	$\frac{in^3/s}{in}$	704
l	Horn Arm Length	m	0.136
m_p	Piston mass	$\frac{lb}{in/s^2}$	1.18
rv	Valve spool radius	in	0.1883
V	Total Cylinder Volume	in^3	15.4

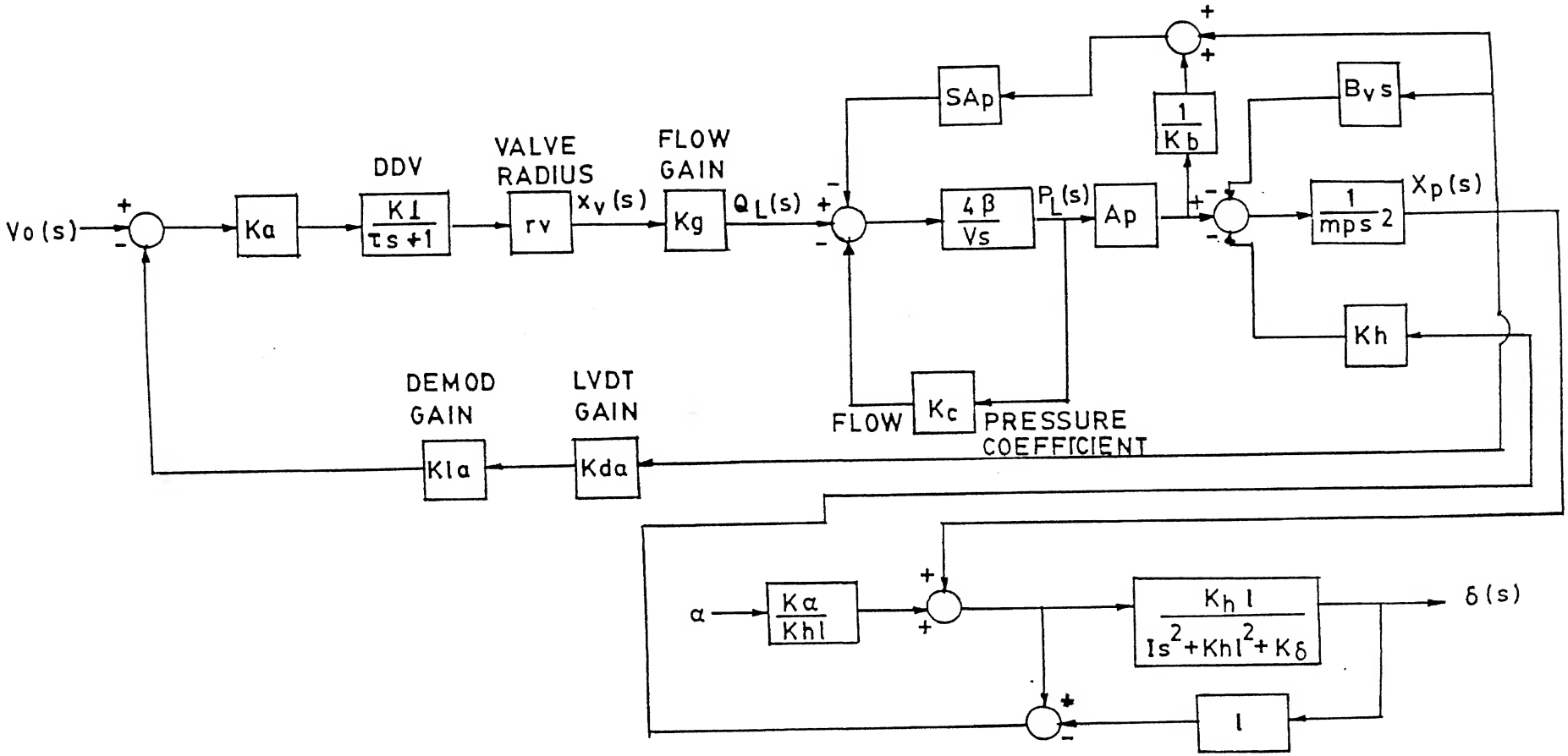

FIG. 2.1 ACTUATOR - ELEVON SERVO

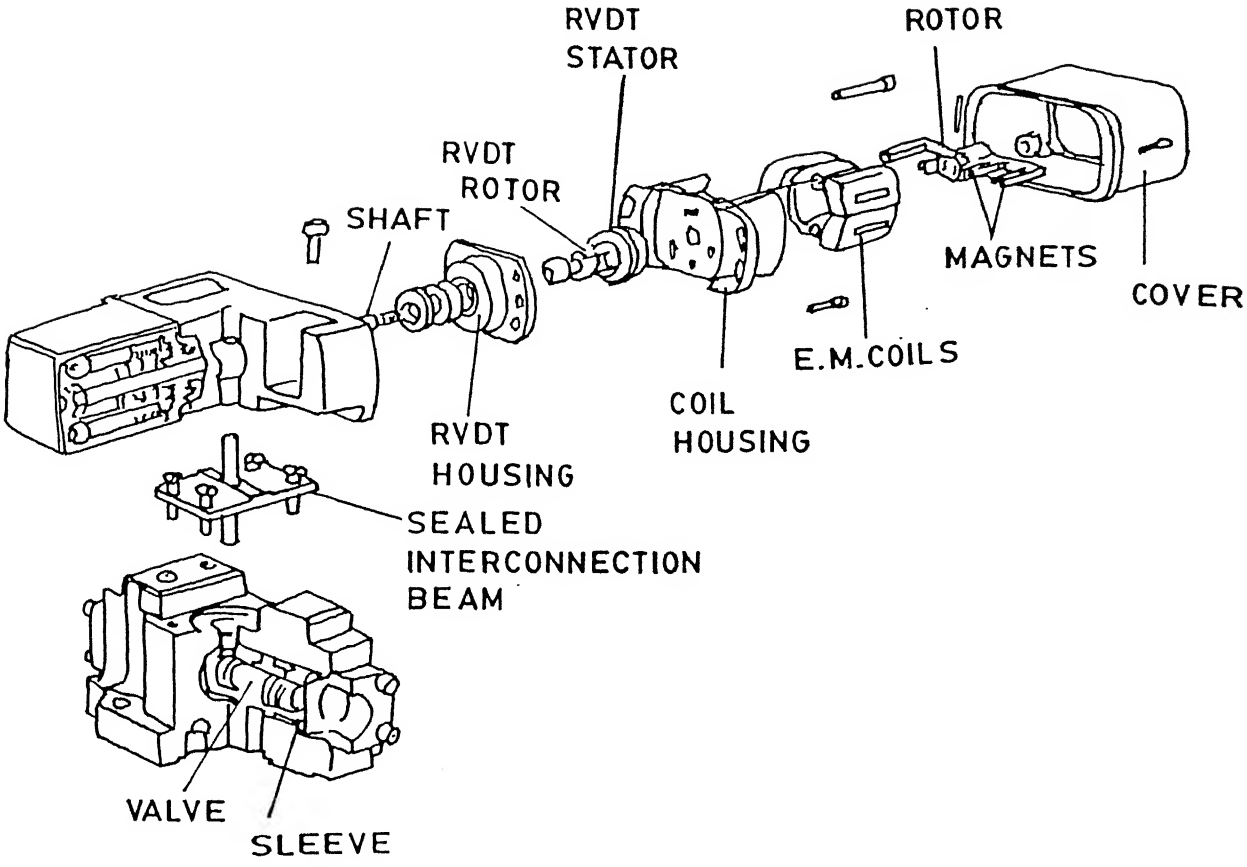

FIG. 2-2 DIRECT DRIVE VALVE

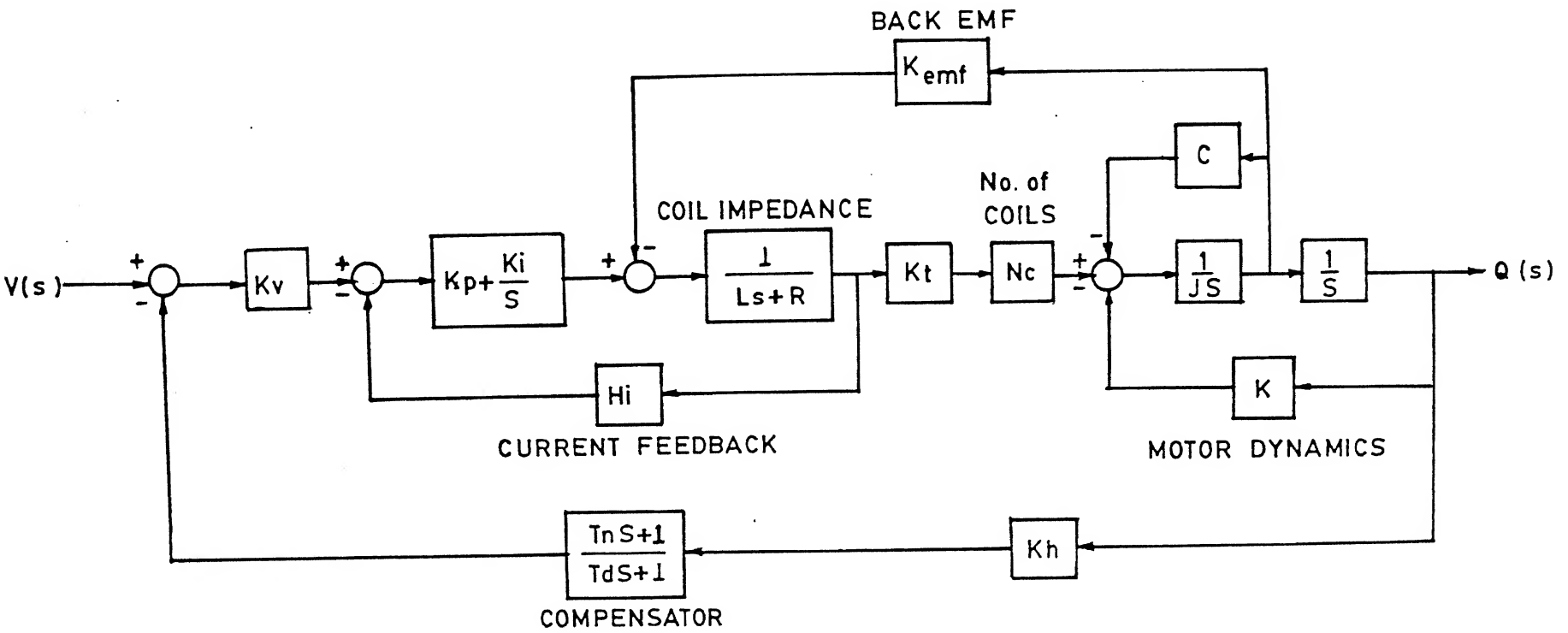

FIG. 2·3 DIRECT DRIVE VALVE

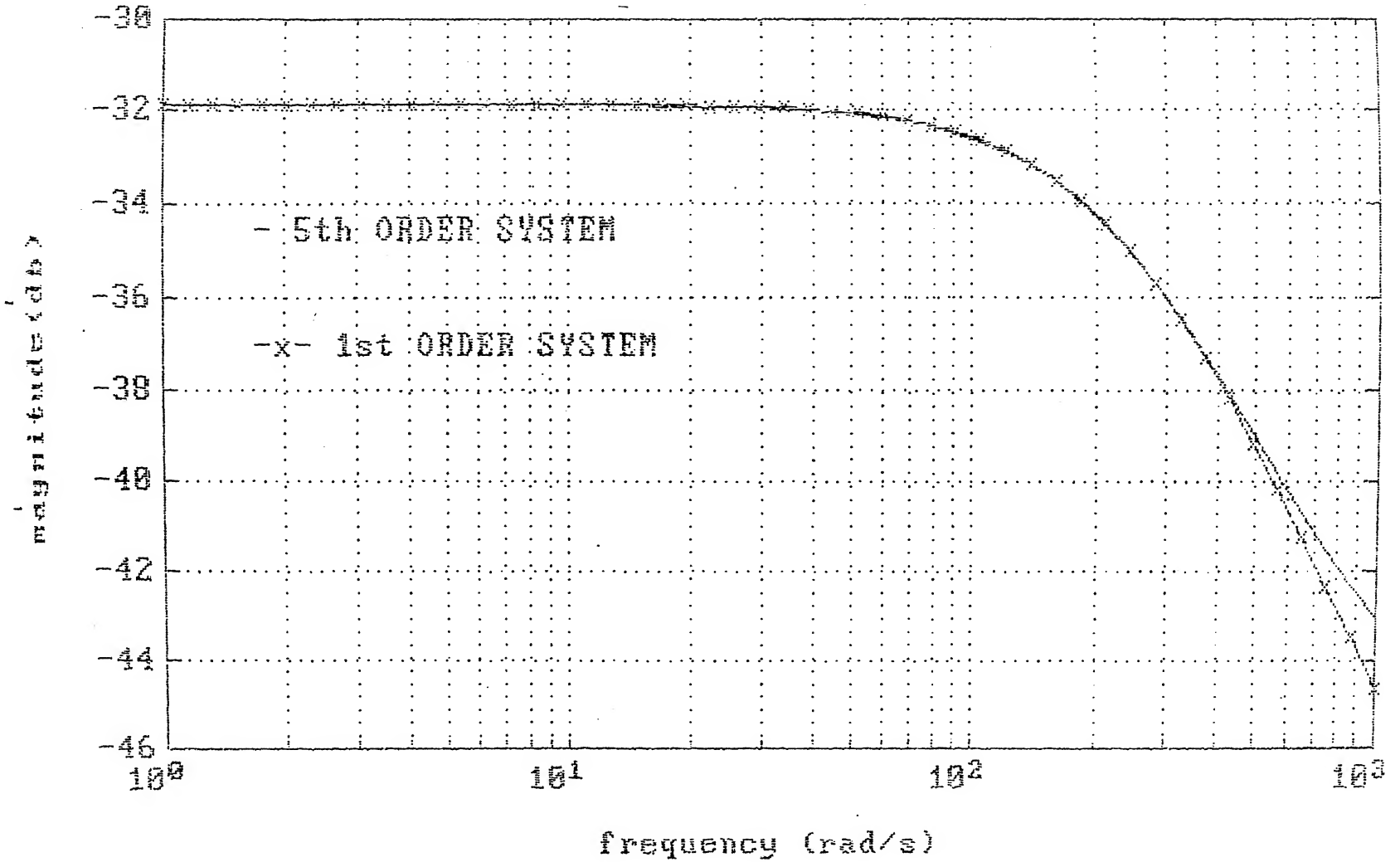

FIG. 2.4 FREQUENCY RESPONSE OF DDV

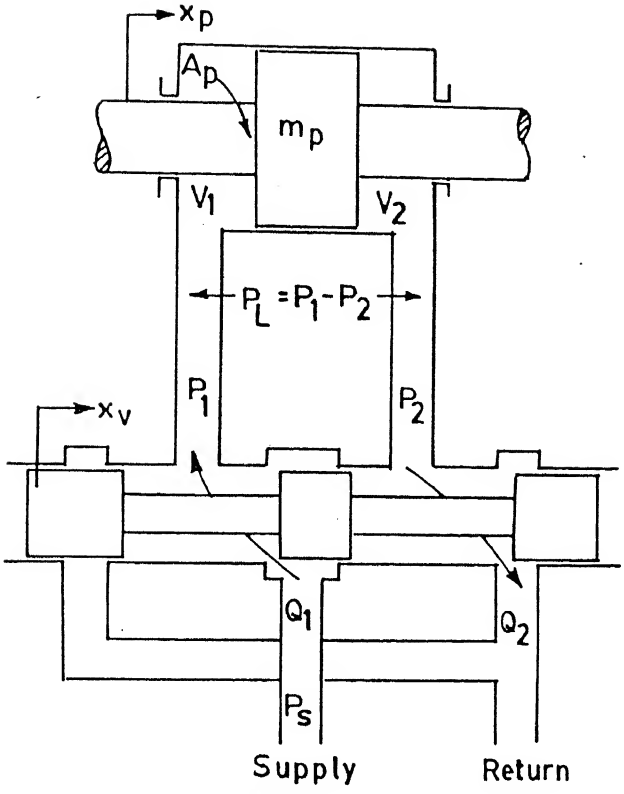

FIG. 2.5 VALVE-PISTON COMBINATION

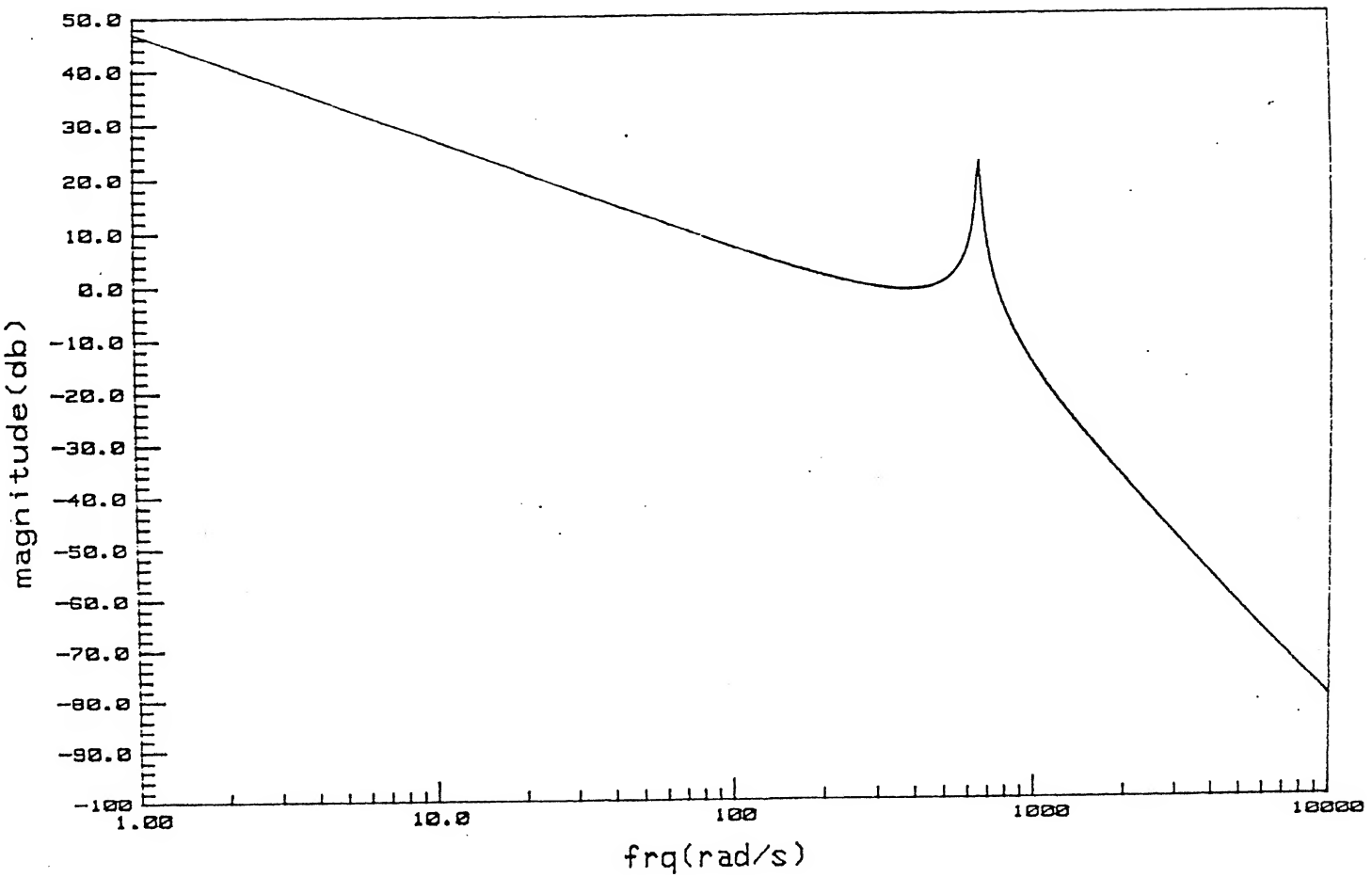

FIG. 2.6 FREQUENCY RESPONSE OF OLTF OF HYDRAULIC ACTUATOR

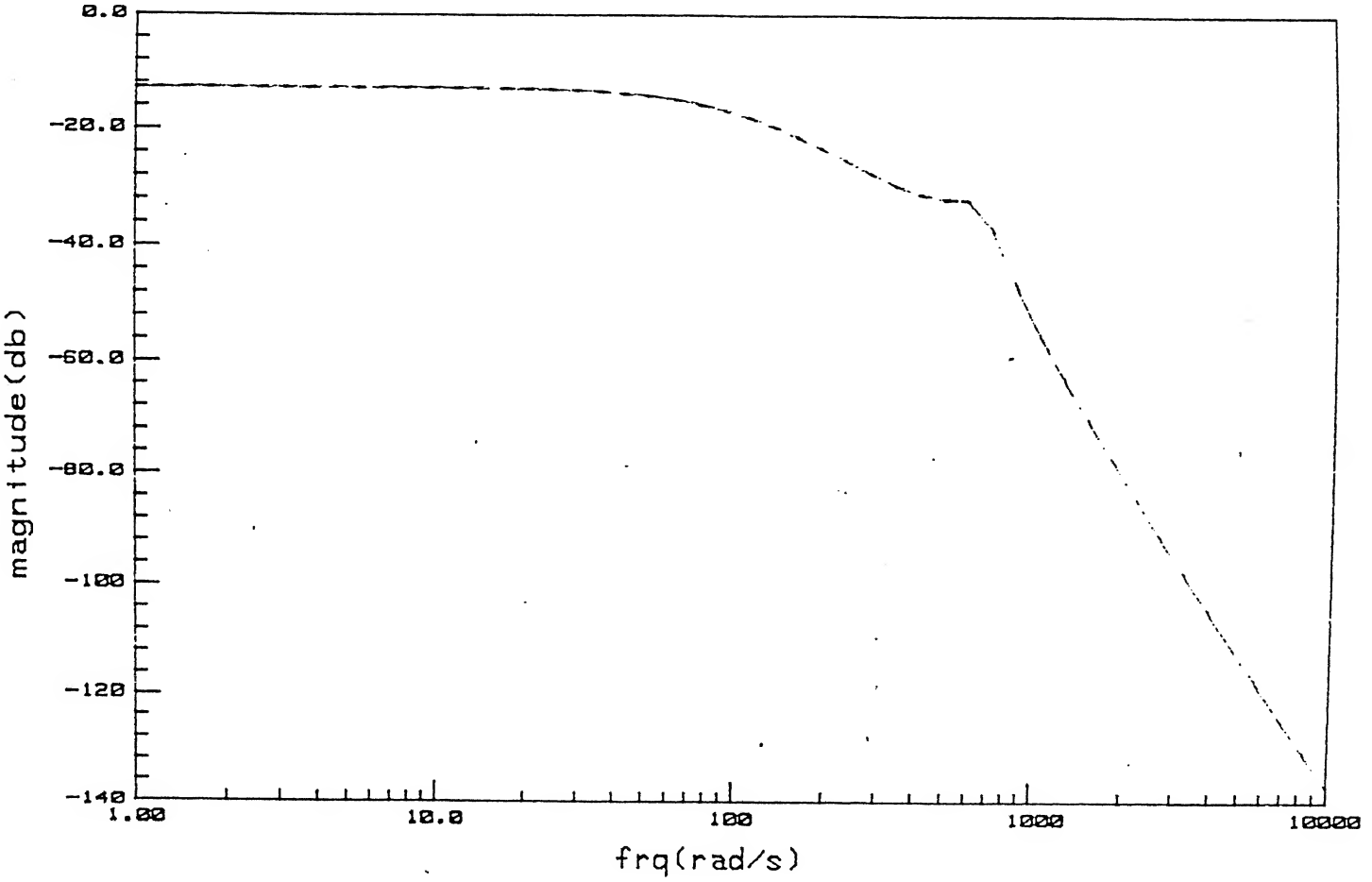

FIG. 2.7 FREQUENCY RESPONSE OF E H ACTUATOR

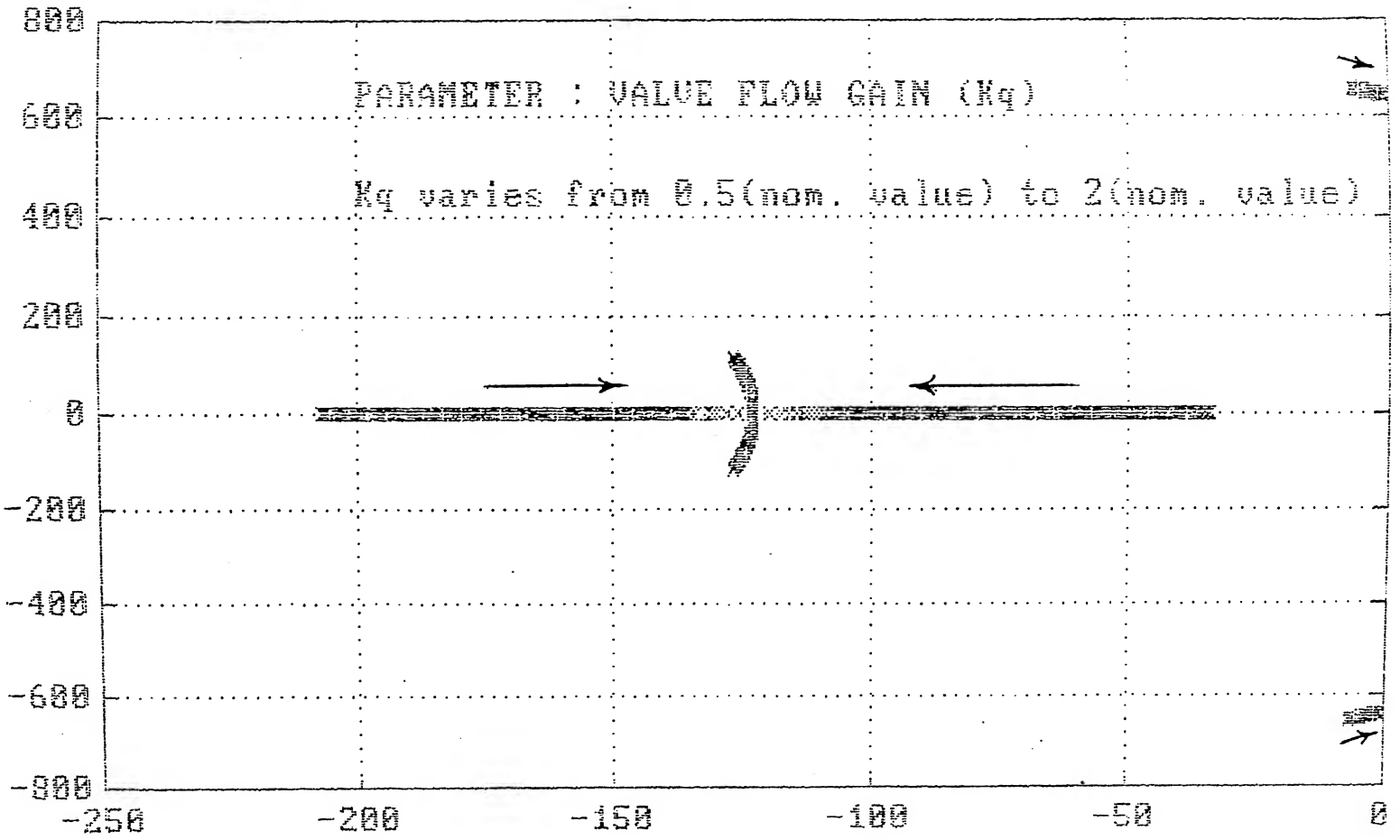

FIG. 2.8A ROOT LOCUS OF E H ACTUATOR; PARAMETER : VALVE FLOW GAIN

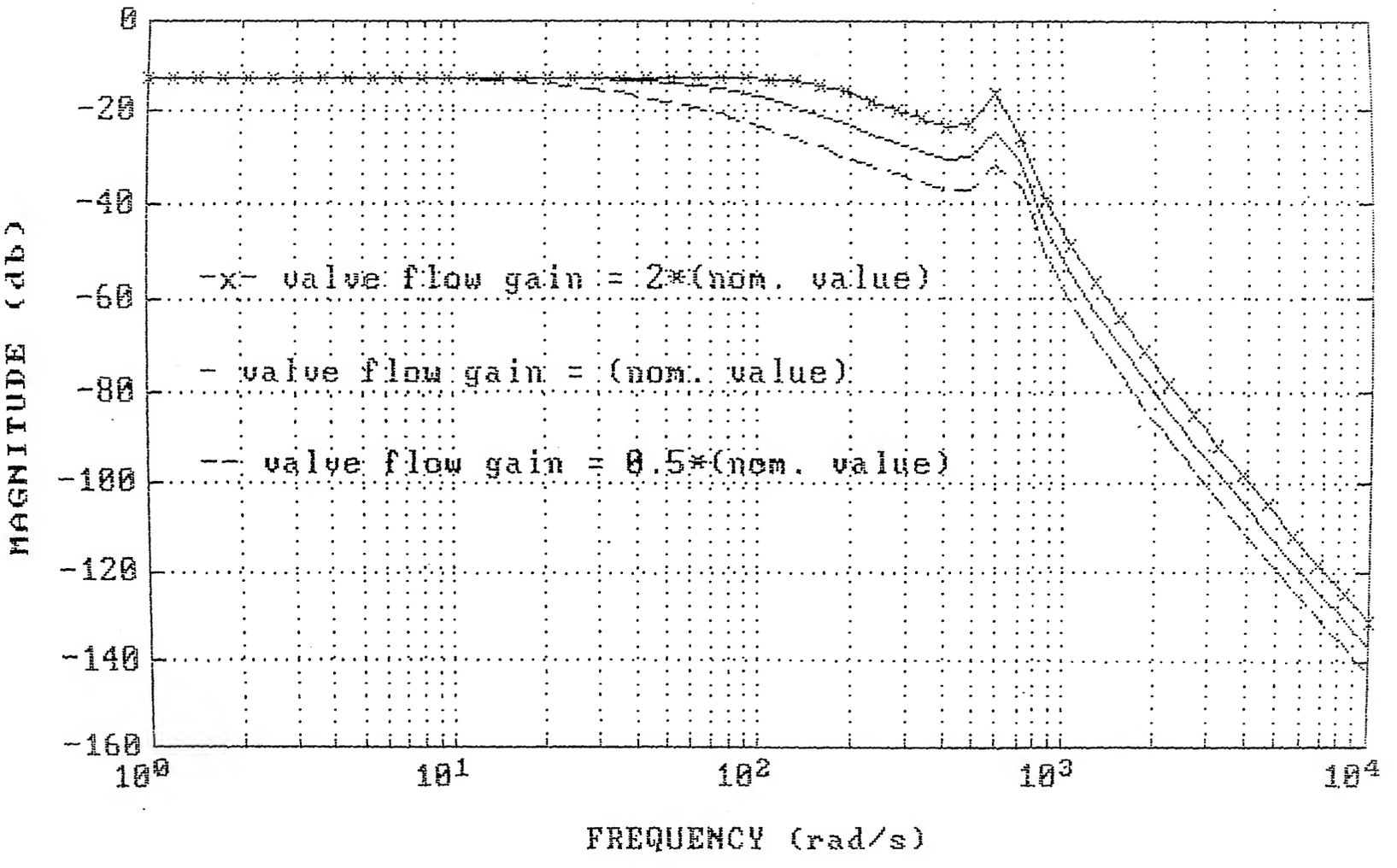

FIG. 2.8B FREQUENCY RESPONSE OF E H ACTUATOR; PARAMETER : VALVE FLOW GAIN

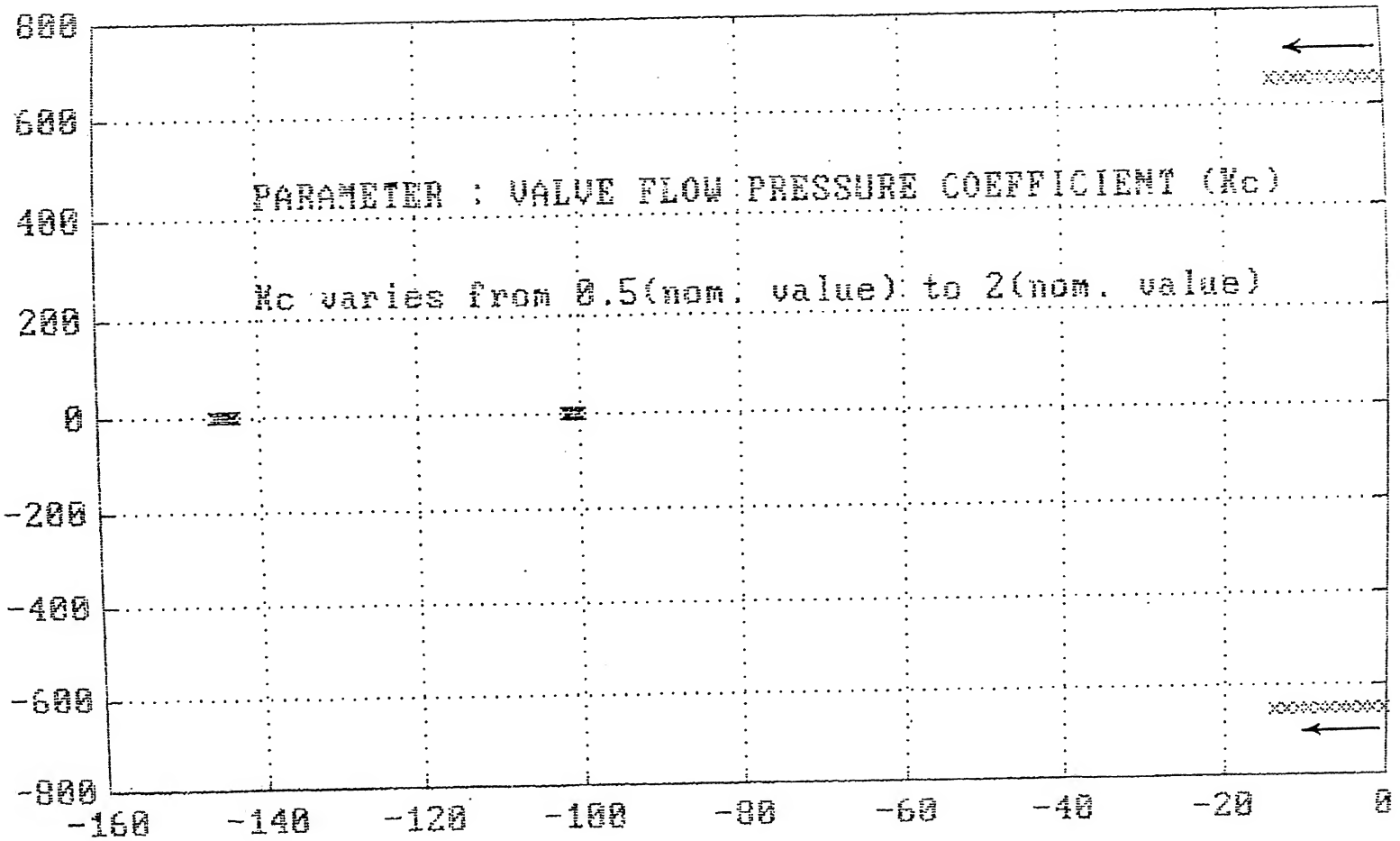

FIG. 2.9 ROOT LOCUS OF E H ACTUATOR; PARAMETER: VALVE FLOW PRESSURE COEFFICIENT

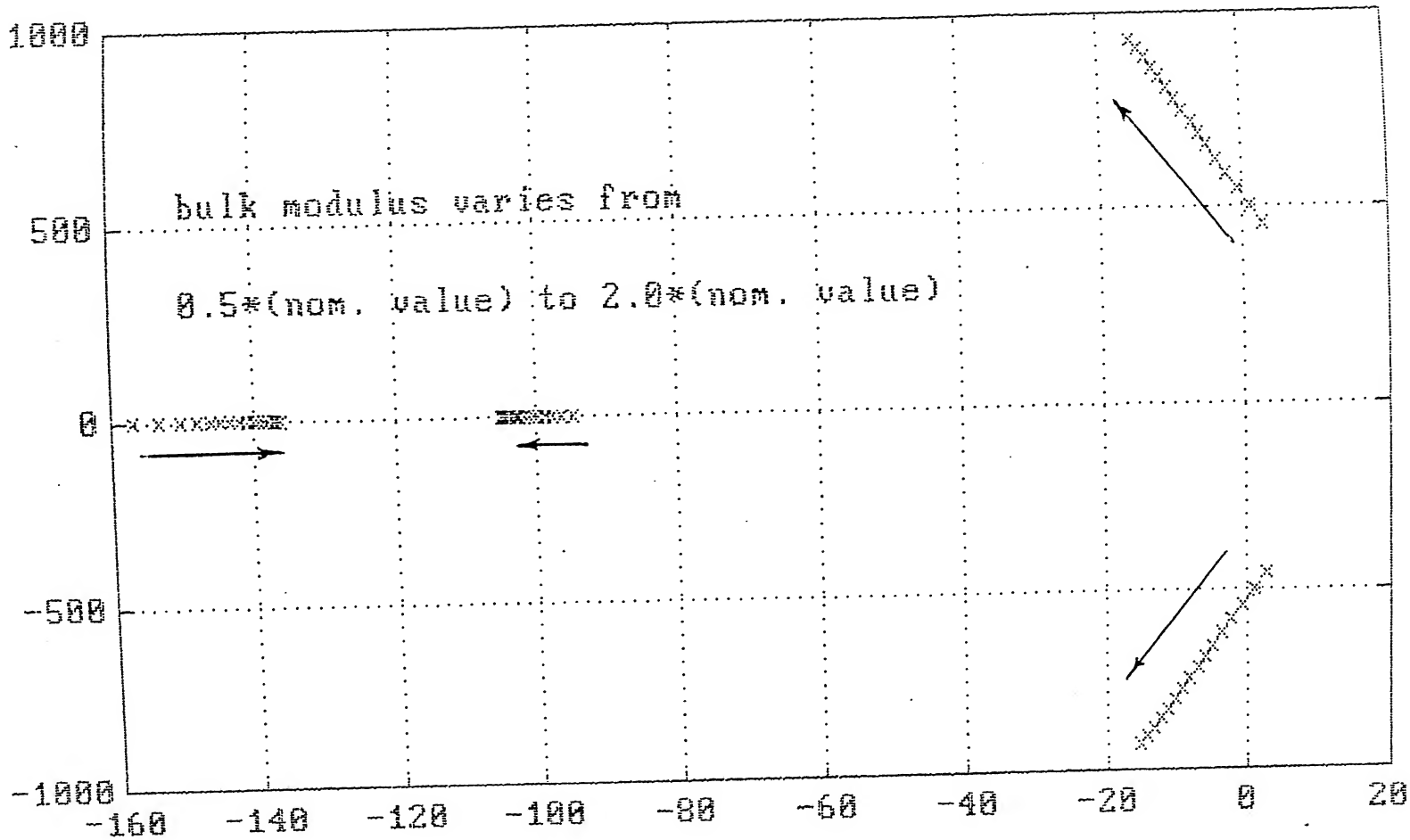

FIG. 2.10A ROOT LOCUS OF E H ACTUATOR; PARAMETER: BULK MODULUS

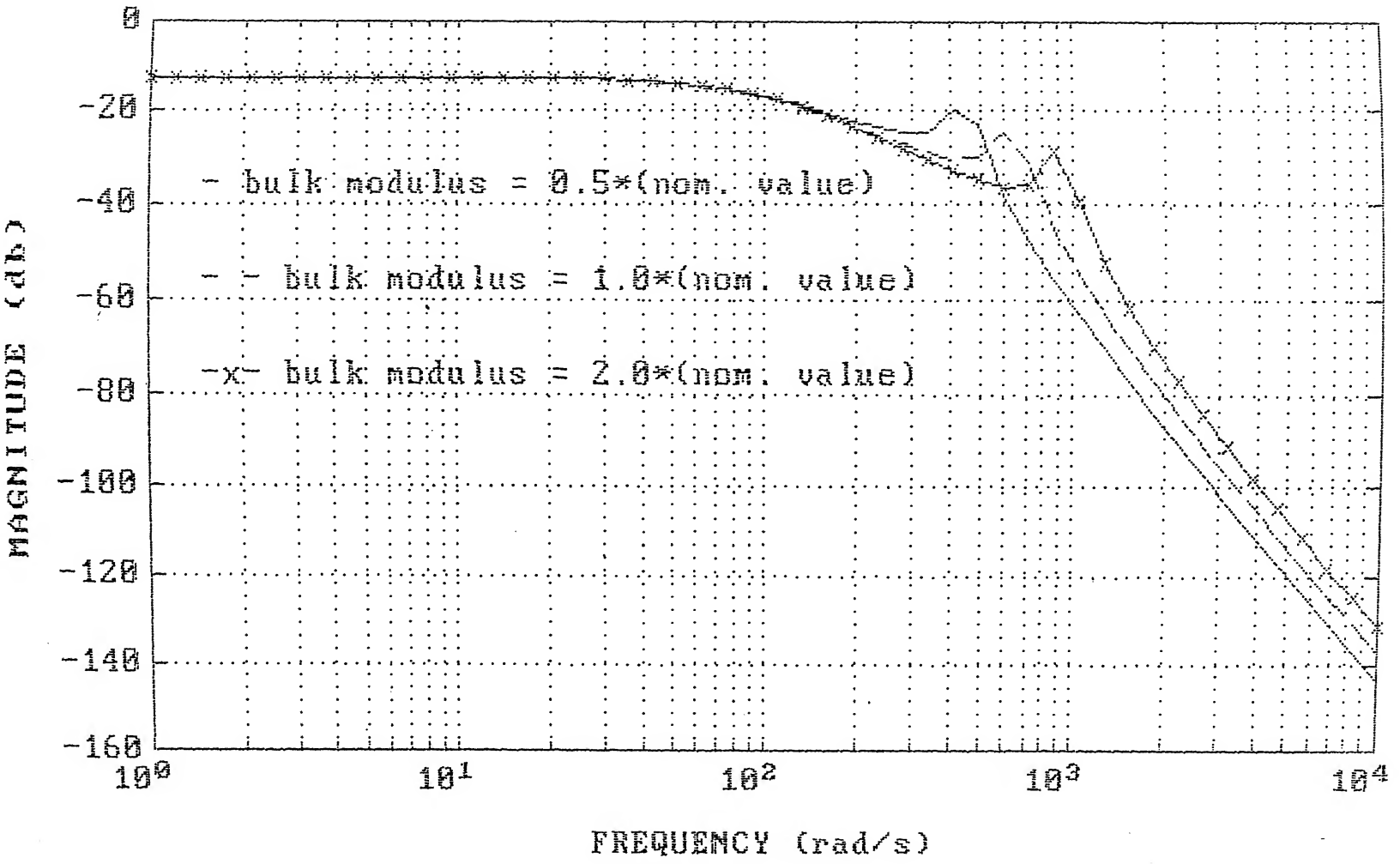

FIG. 2.10B FREQUENCY RESPONSE OF E H ACTUATOR; PARAMETER: BULK MODULUS

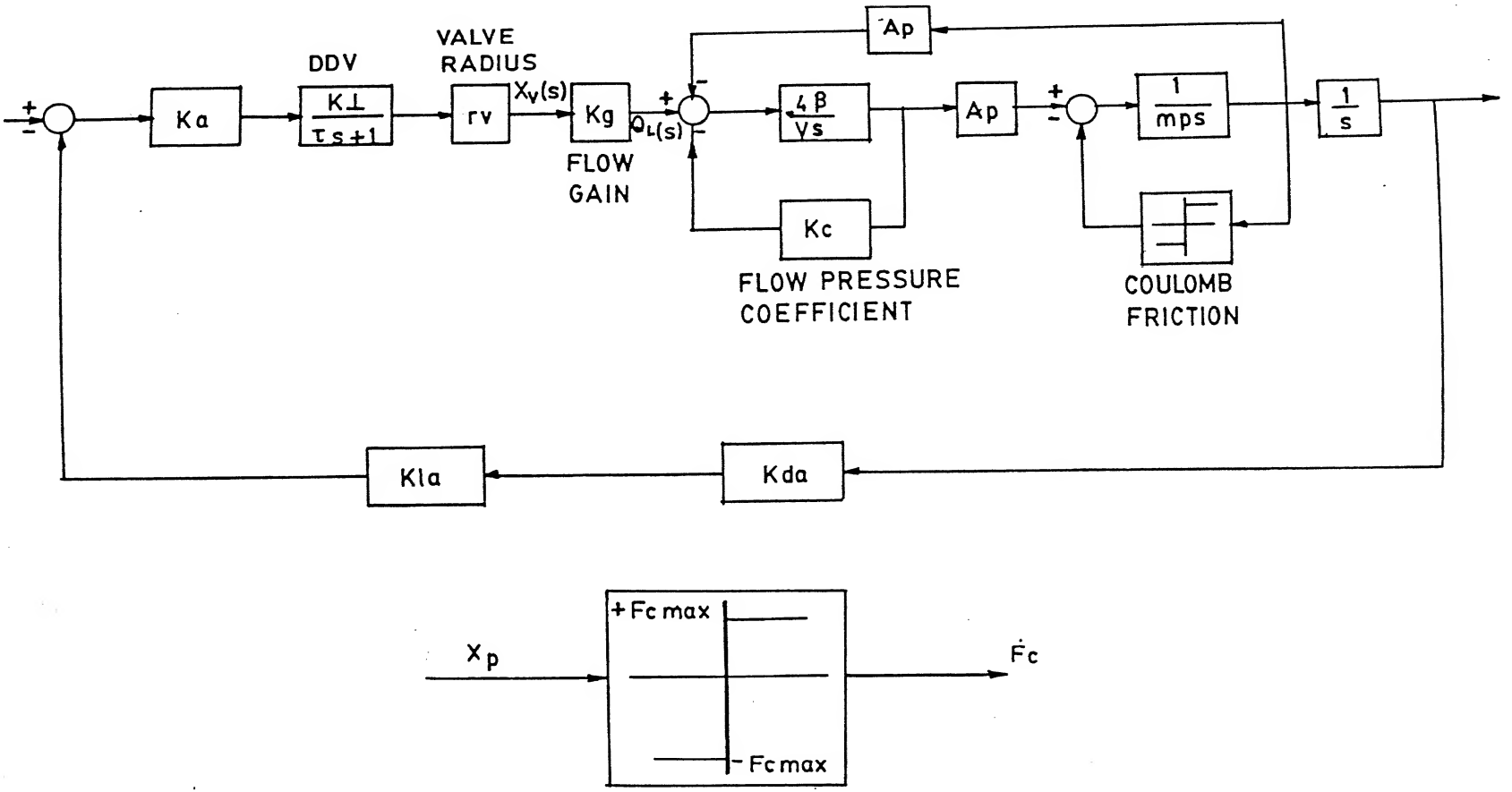

FIG. 2·11 ELECTRO HYDRAULIC ACTUATOR (with coulomb friction)

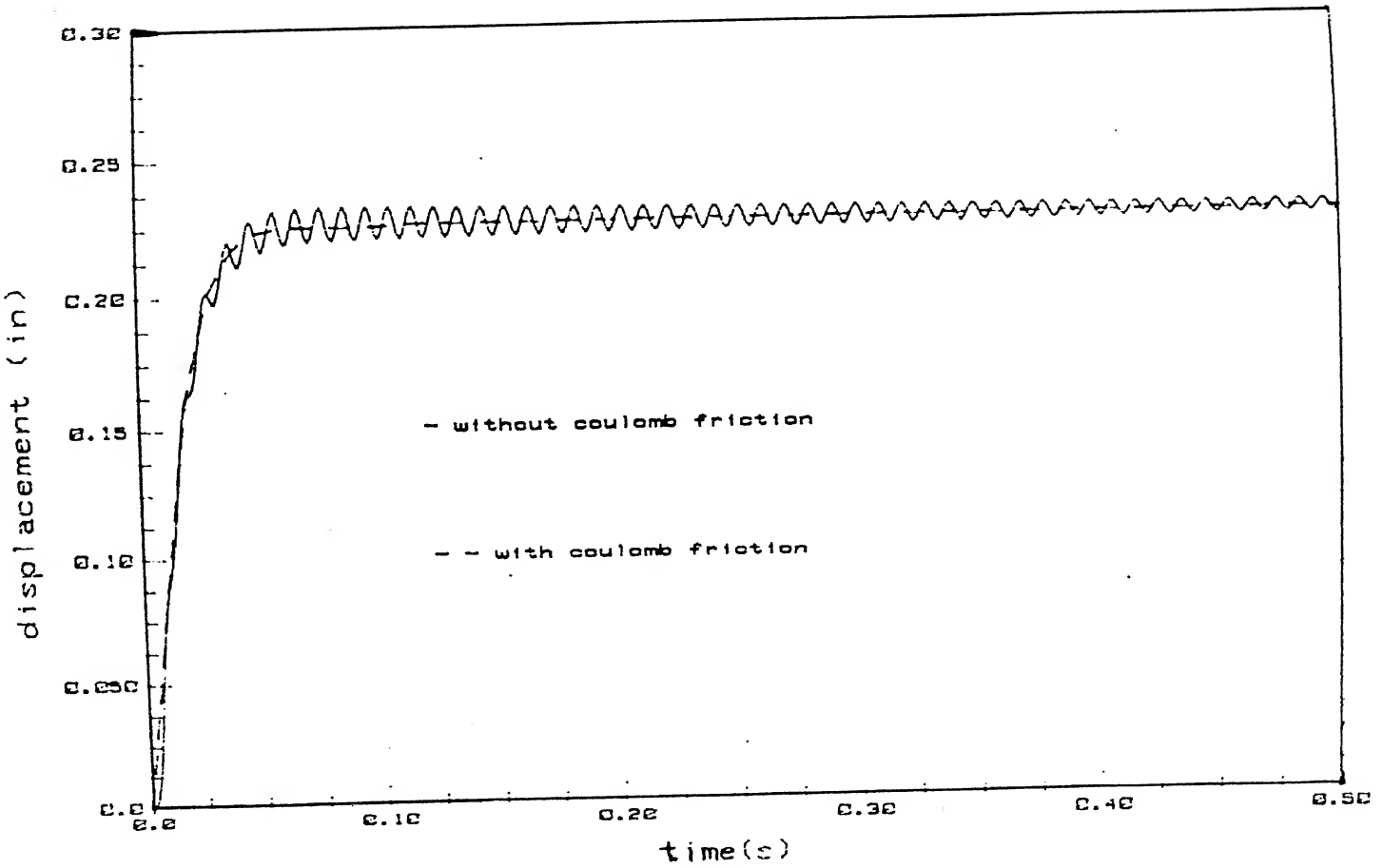

FIG. 2.12A STEP RESPONSE OF E H ACTUATOR (WITH & WITHOUT COULOMB FRICTION

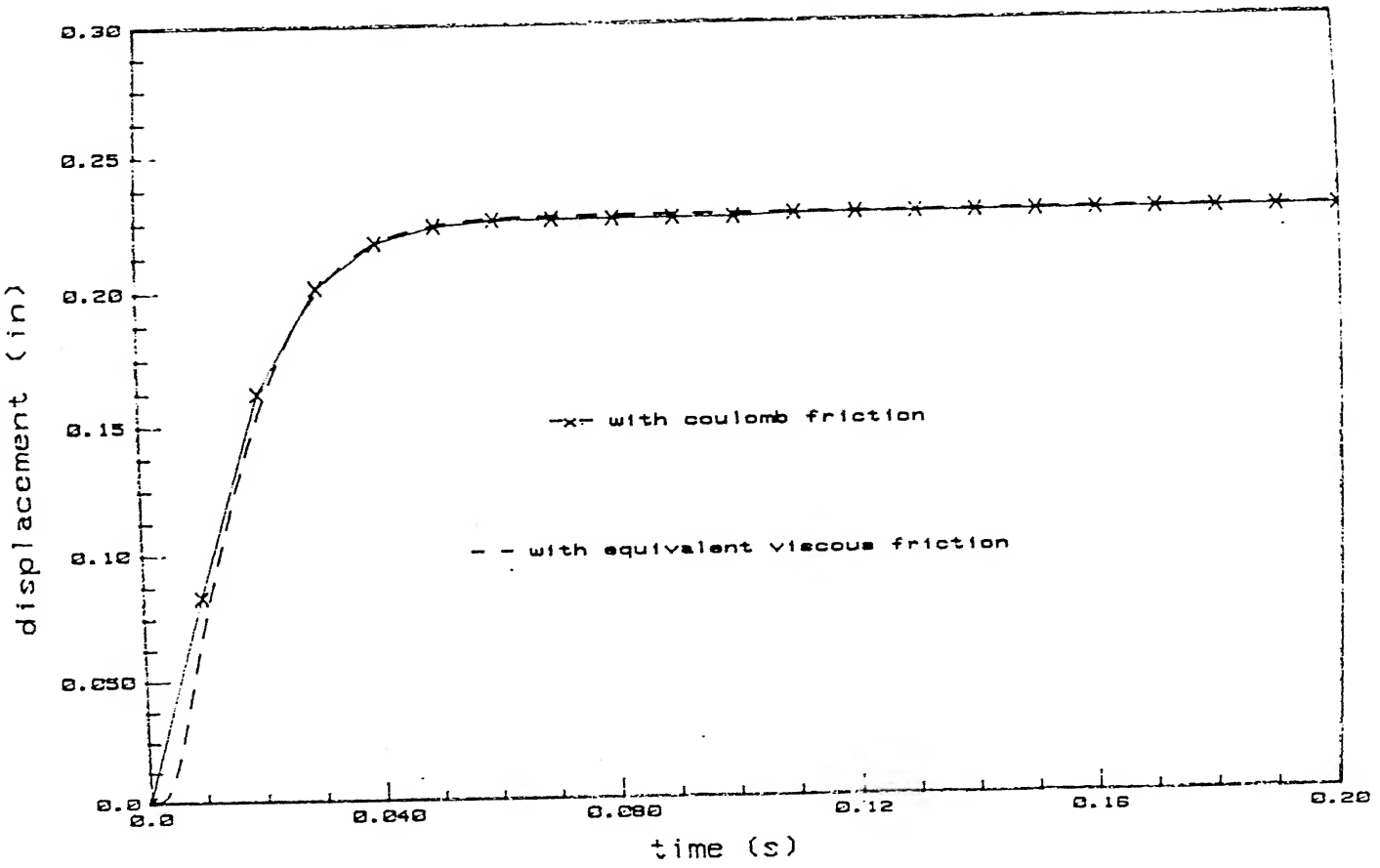

FIG. 2.12B COMPARATIVE STUDY OF STEP RESPONSE OF E H ACTUATOR

(COULOMB FRICTION VS EQUIVALENT VISCOUS FRICTION)

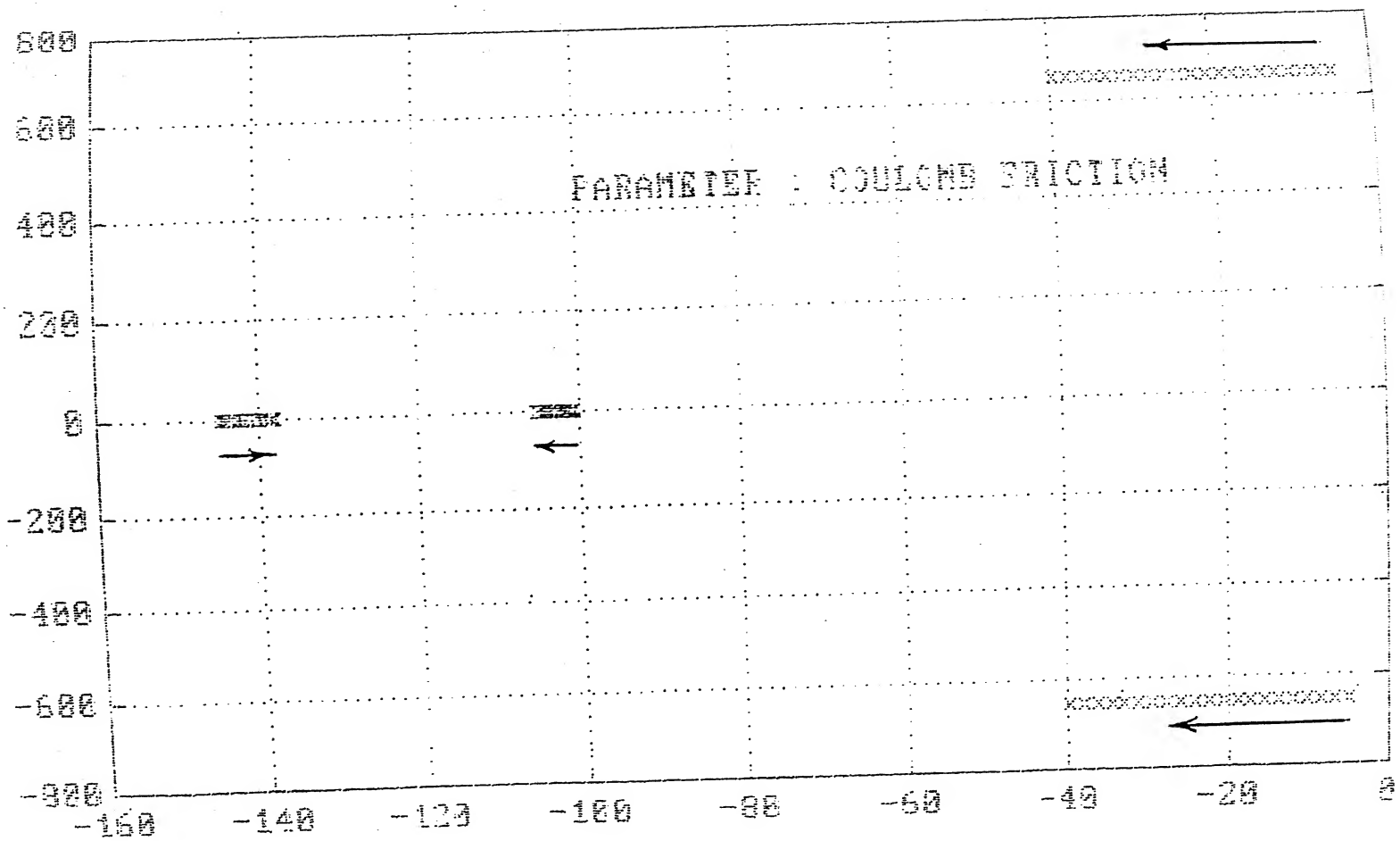

FIG. 2.13 ROOT LOCUS OF E H ACTUATOR;

DESCRIBING FUNCTION ANALYSIS OF COULOMB FRICTION

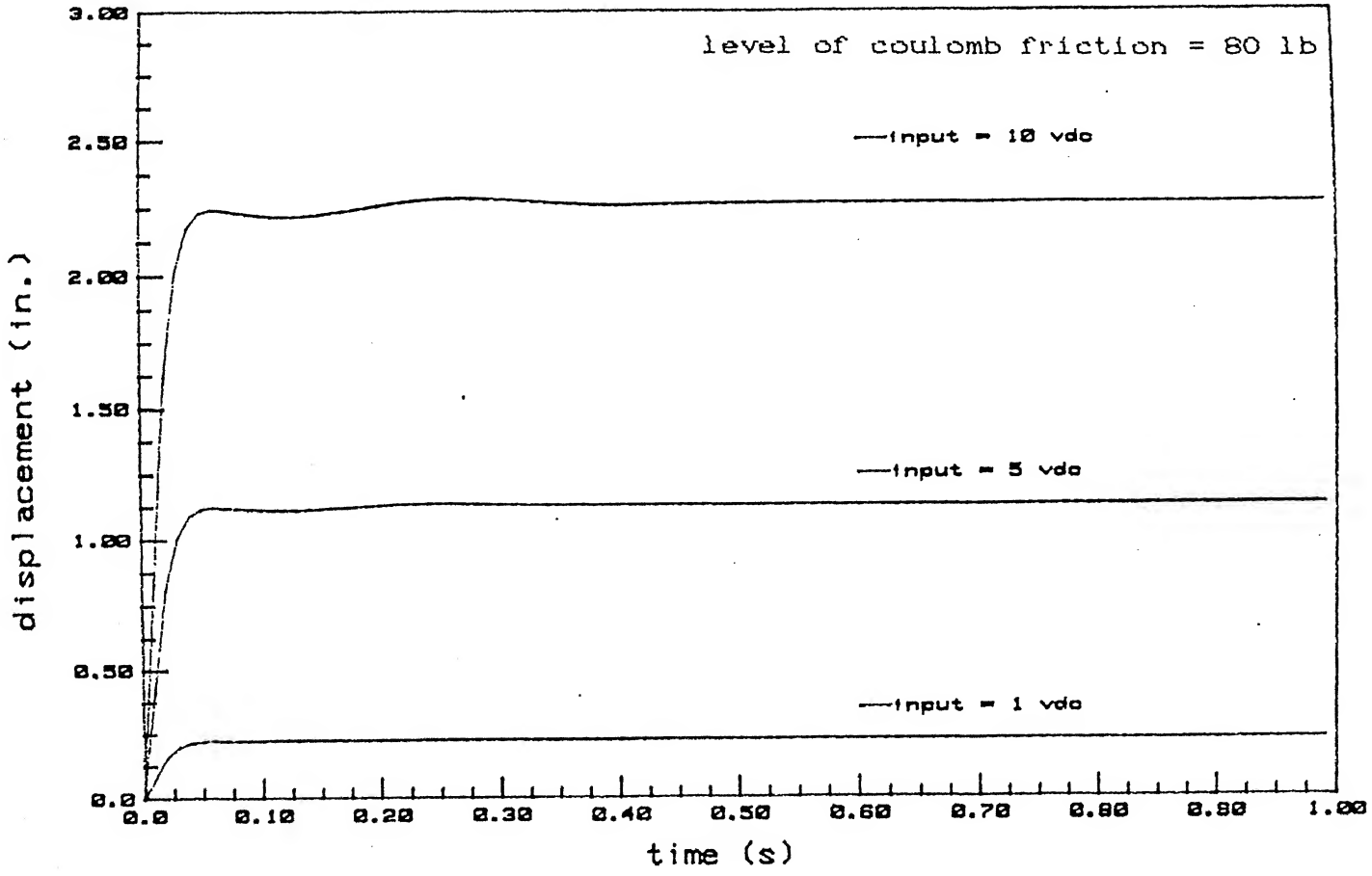

FIG. 2.14 TIME RESPONSE OF E H ACTUATOR: VARYING STEP VOLTAGE INPUTS

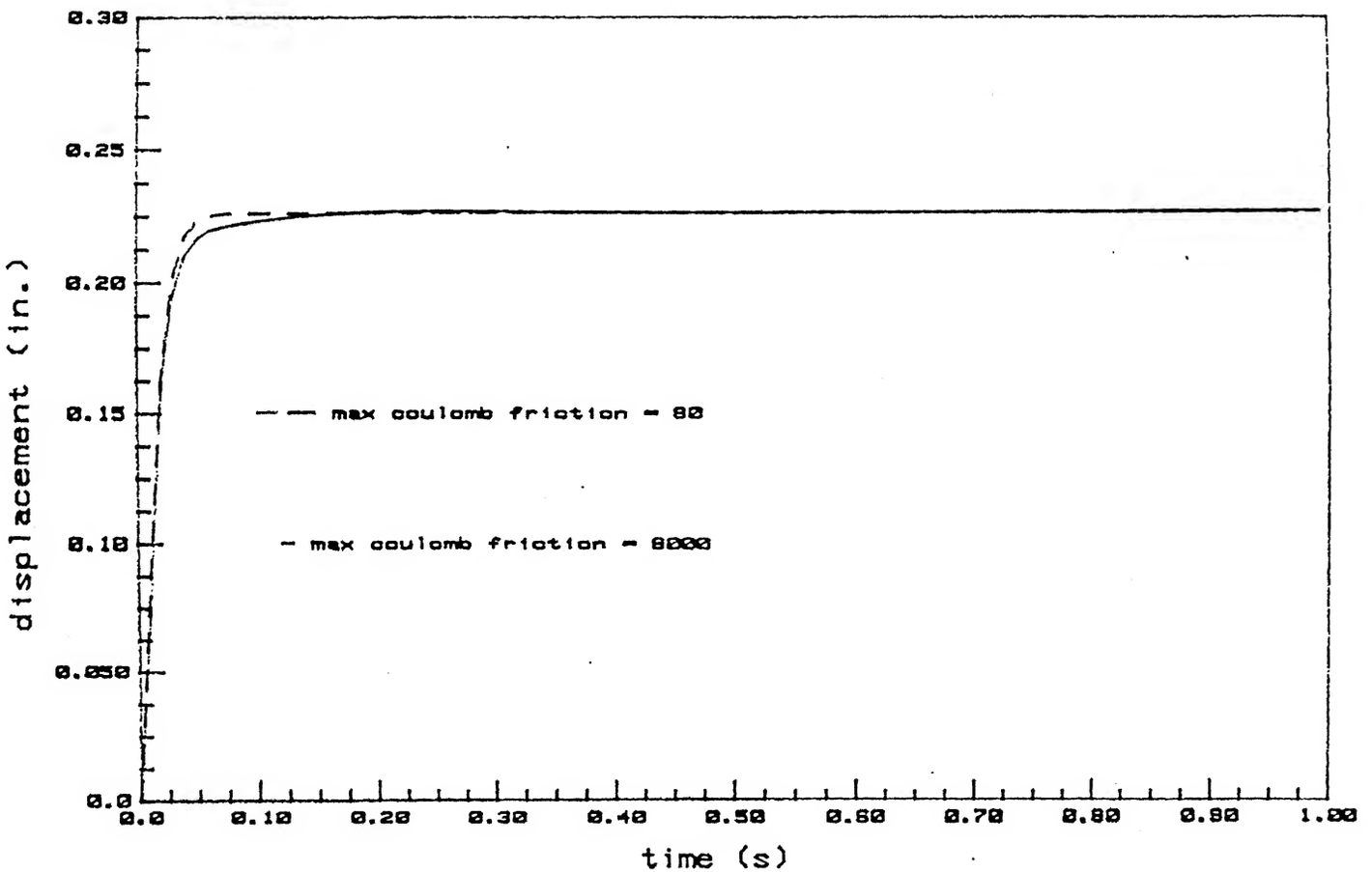

FIG. 2.15 TIME RESPONSE OF E H ACTUATOR: VARYING COULOMB FRICTION MAGNITUDE

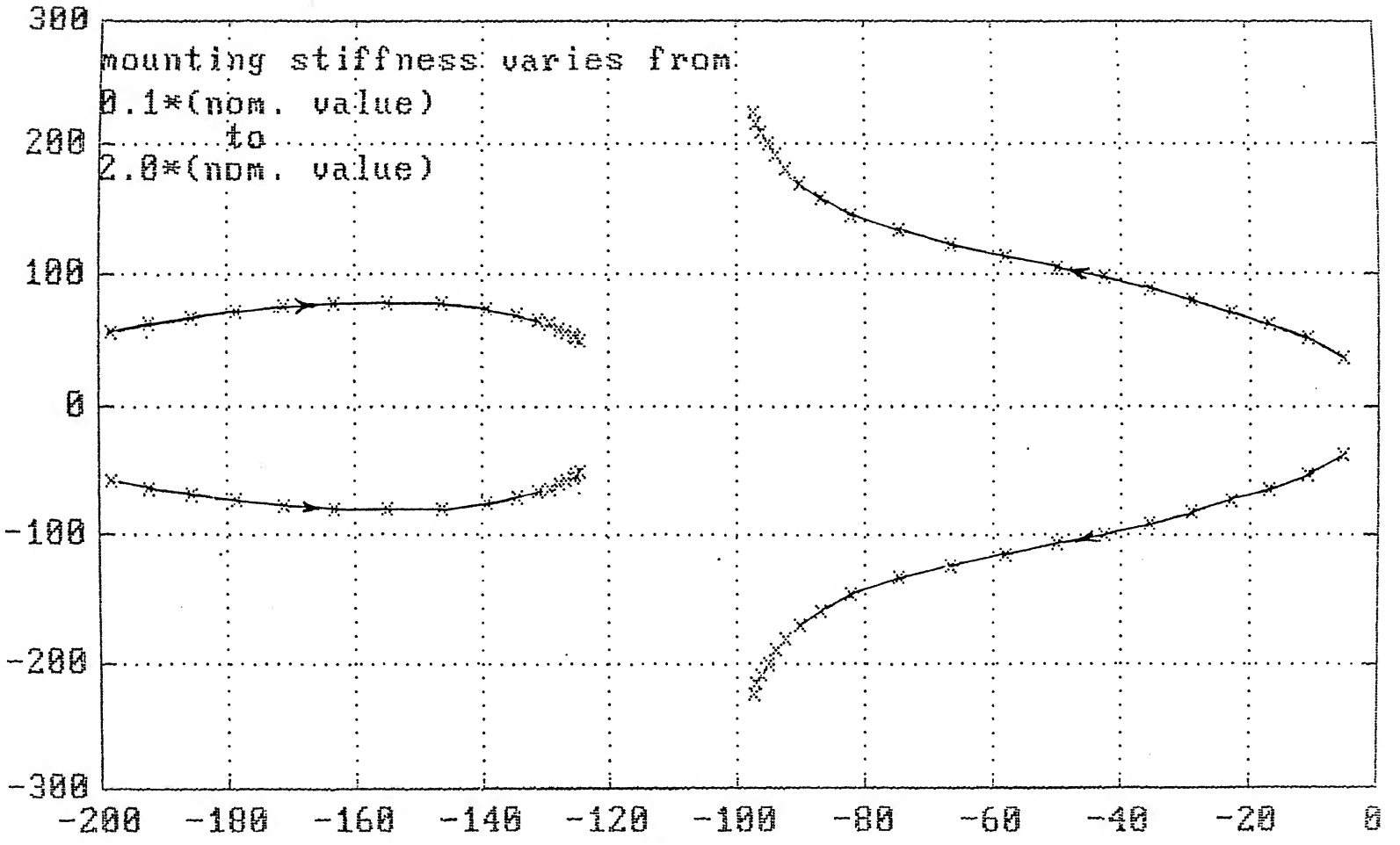

FIG. 2.16A ROOT LOCUS OF E H ACTUATOR; PARAMETER: MOUNTING STIFFNESS

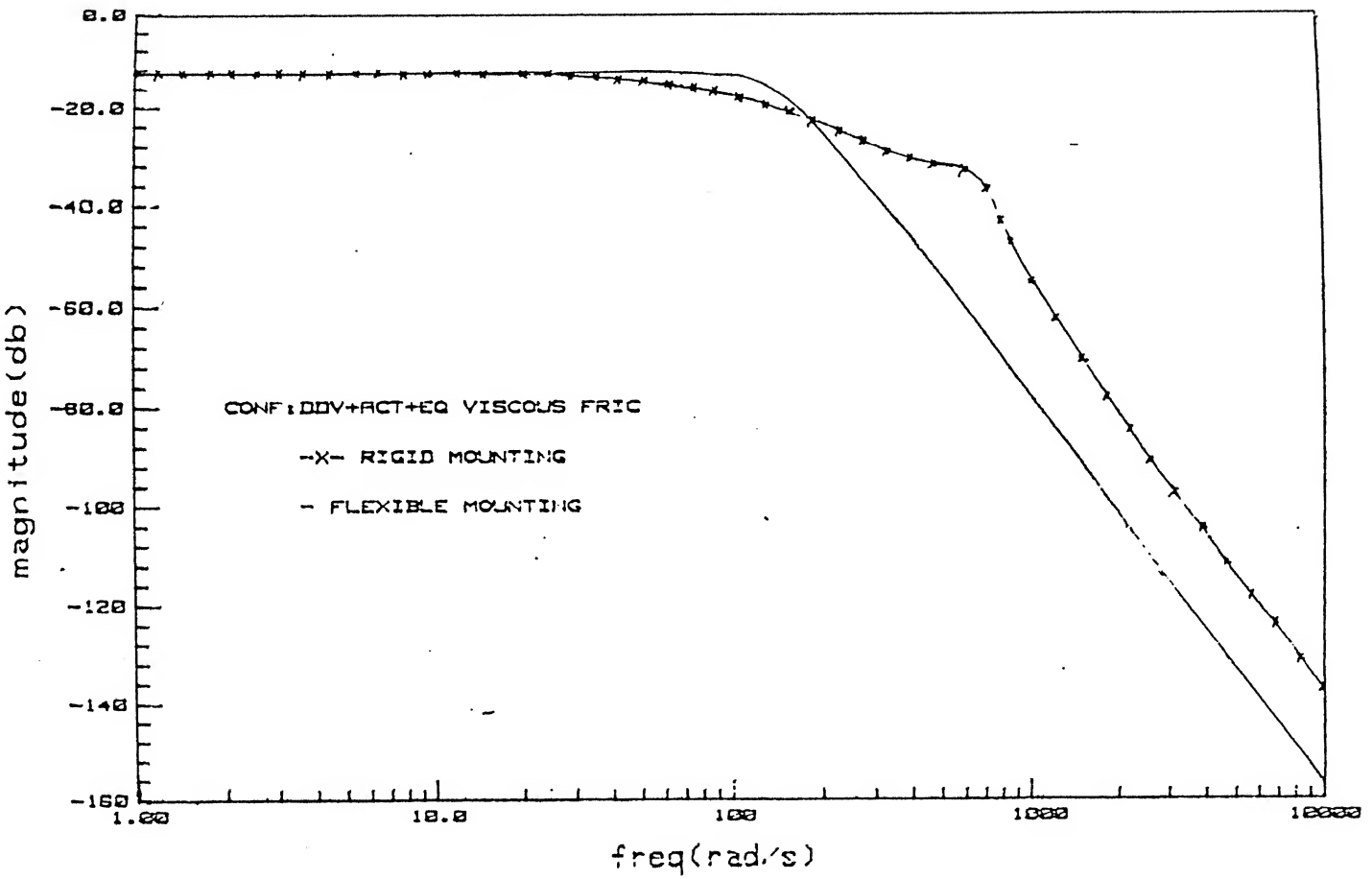

FIG. 2.16B COMPARATIVE STUDY OF RIGID AND FLEXIBLY MOUNTED E H ACTUATOR

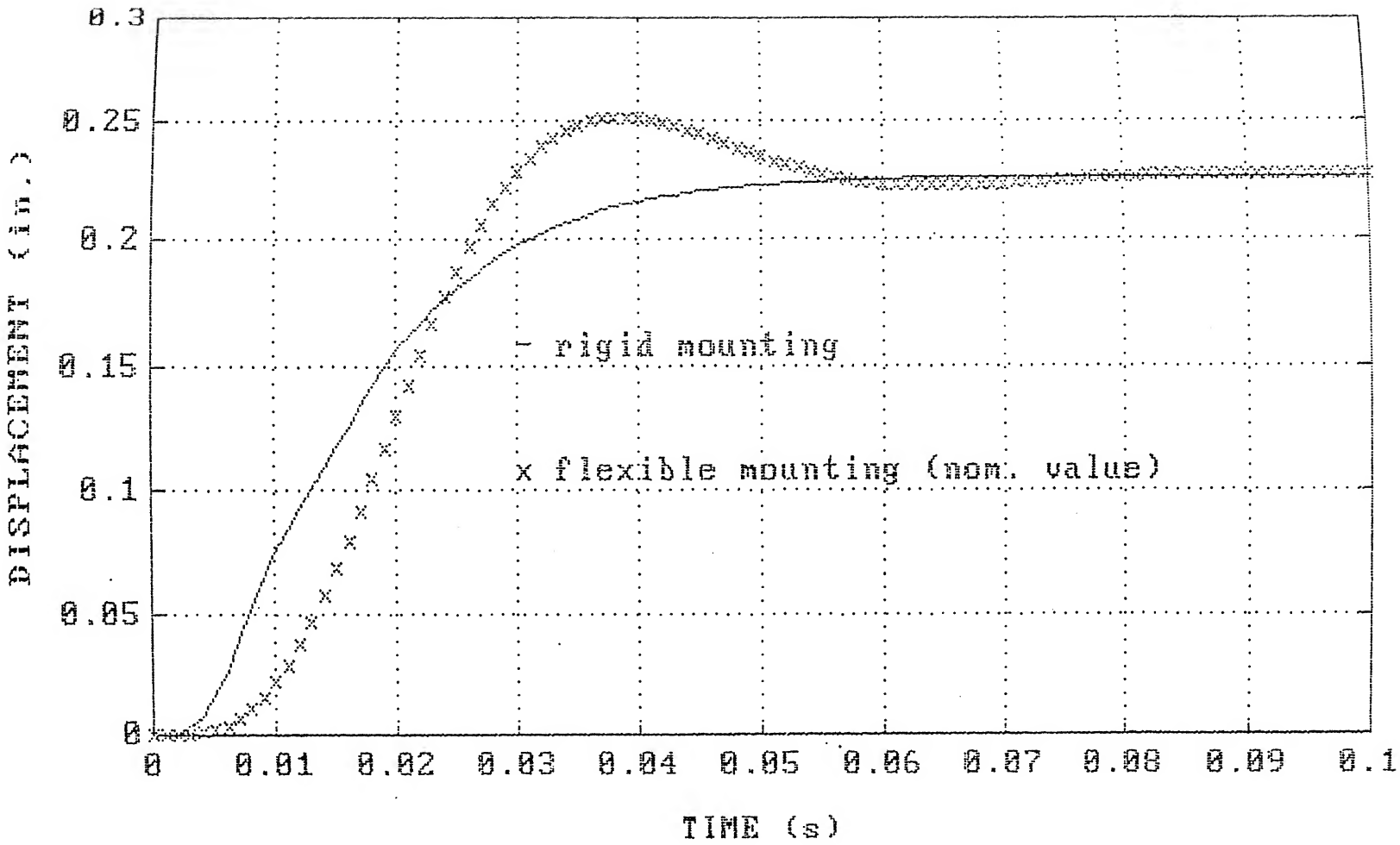

FIG. 2.18C STEP RESPONSE OF E H ACTUATOR; PARAMETER: MOUNTING STIFFNESS

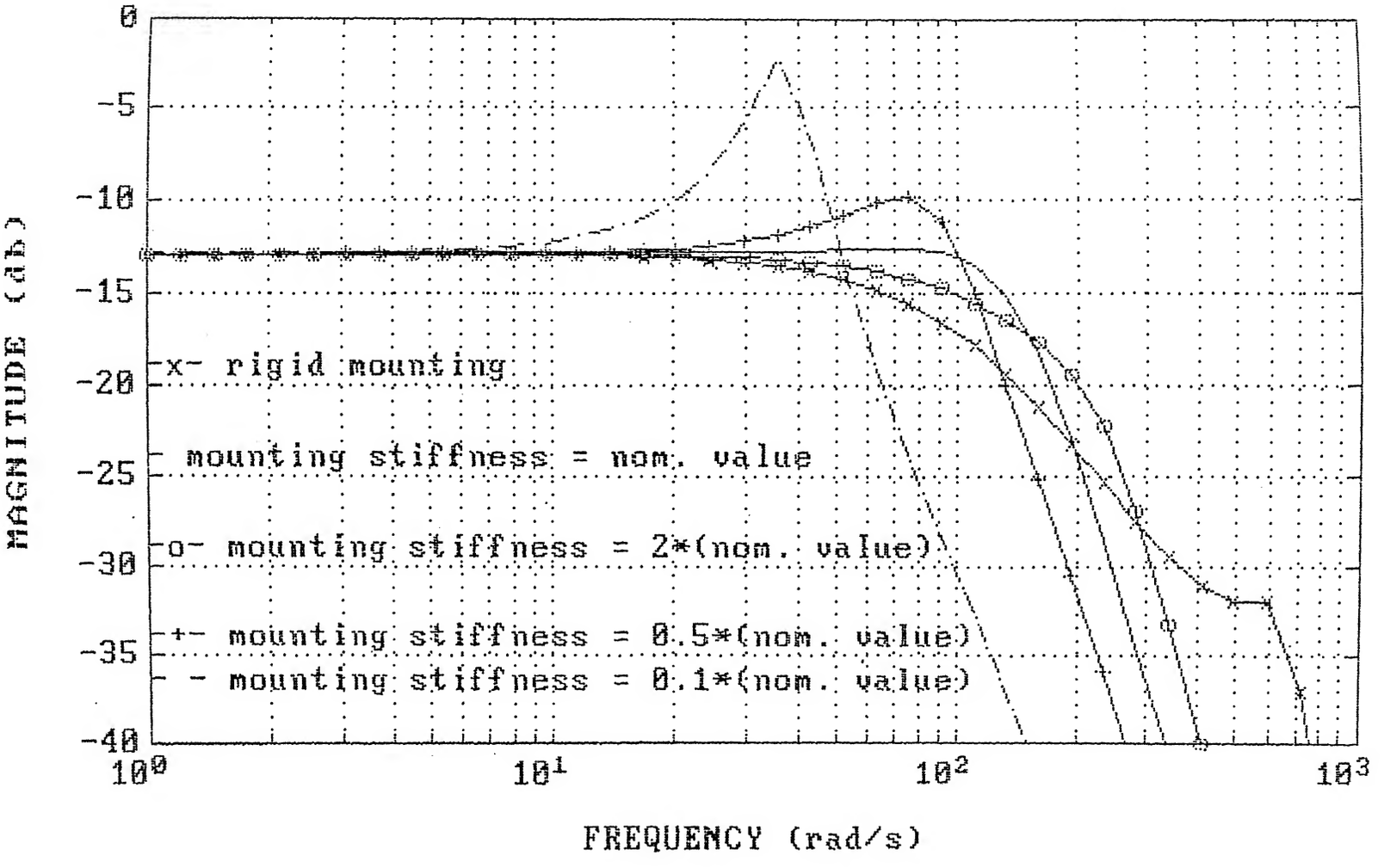

FIG. 2.16D FREQUENCY RESPONSE OF E H ACTUATOR; PARAMETER: MOUNTING STIFFNESS

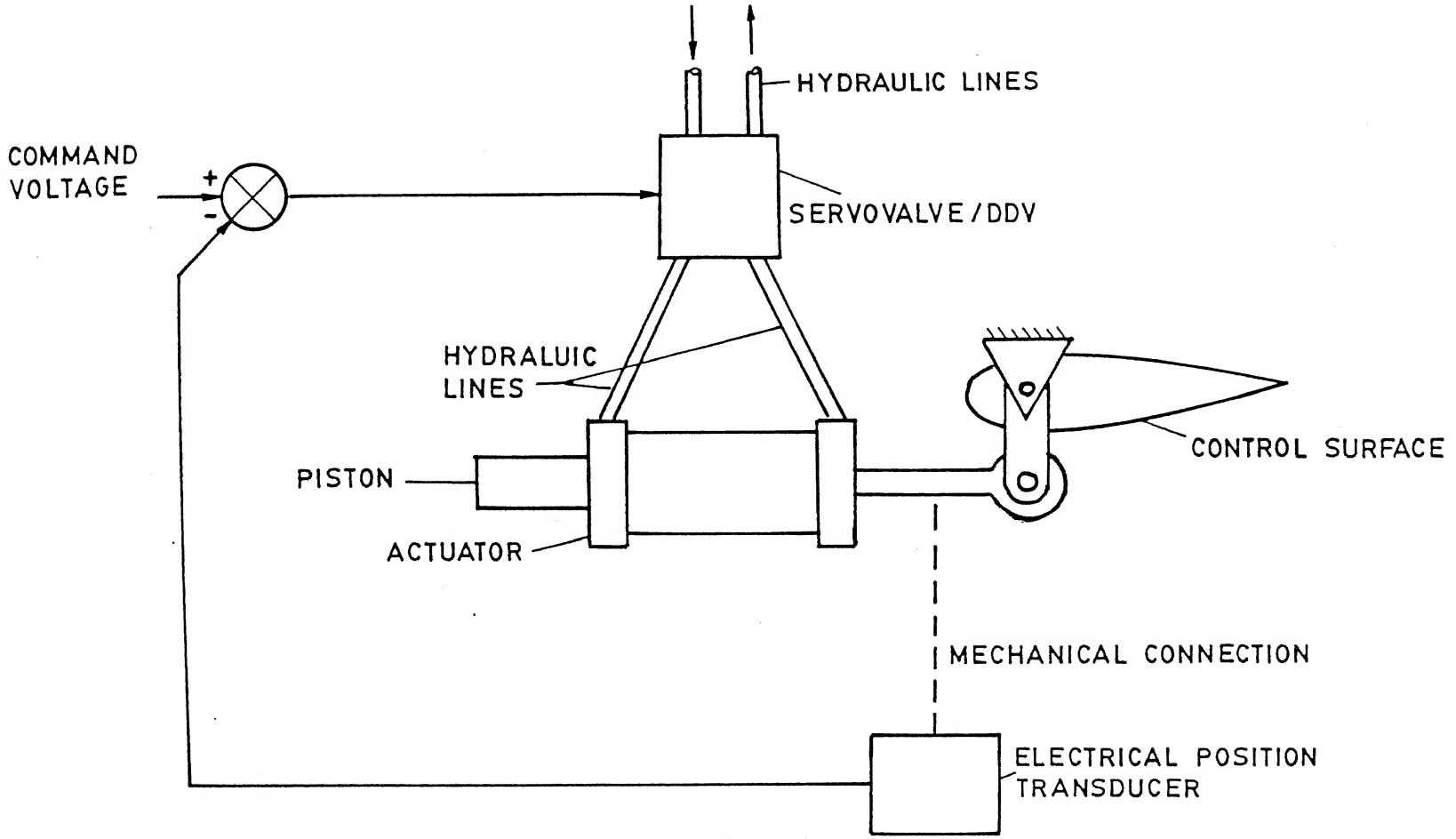

FIG. 2·17 AIRCRAFT CONTROL SURFACE-SERVO MODEL

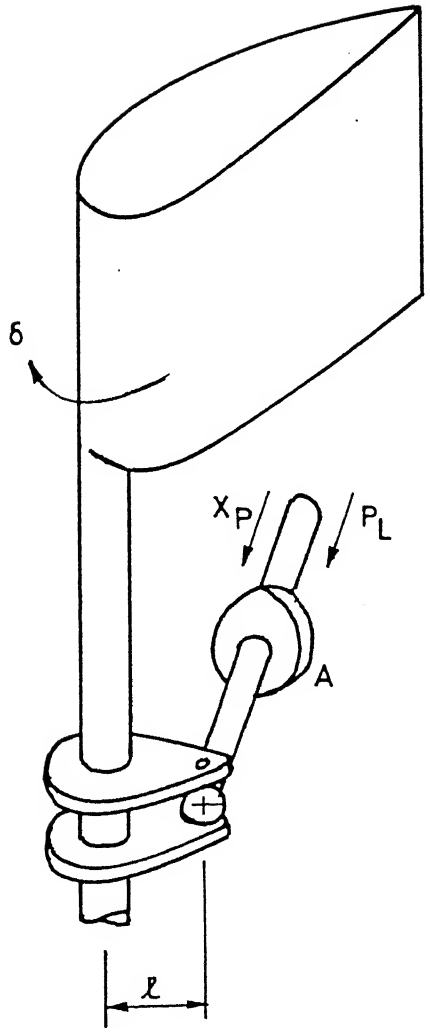

FIG.2.18 SIGN CONVENTION

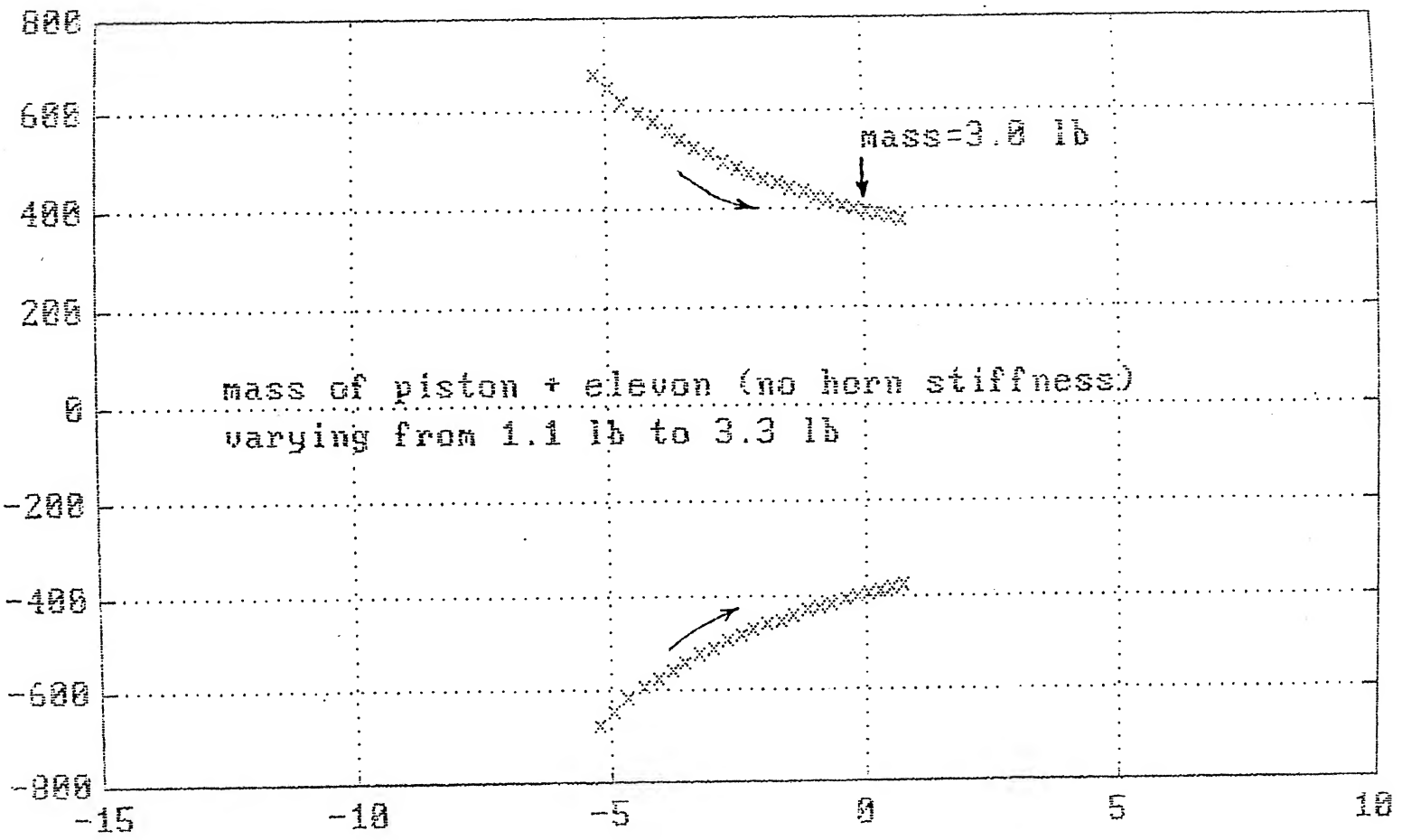

FIG. 2.19 ROOT LOCUS OF E H ACTUATOR; PARAMETER : MASS OF PISTON AND ELEVON

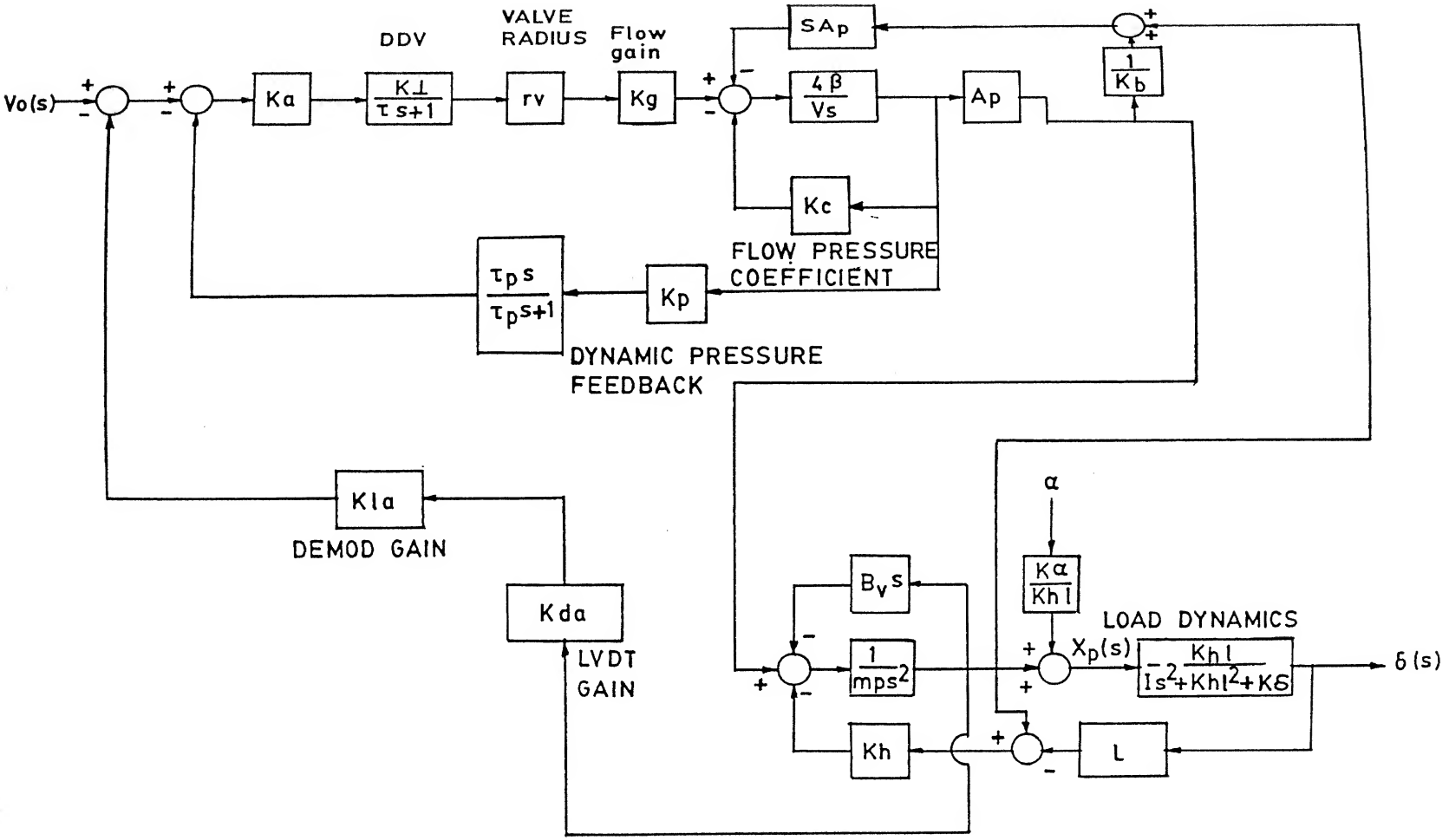

FIG. 2·20 ACTUATOR – ELEVON SERVO (with dynamic pressure feedback)

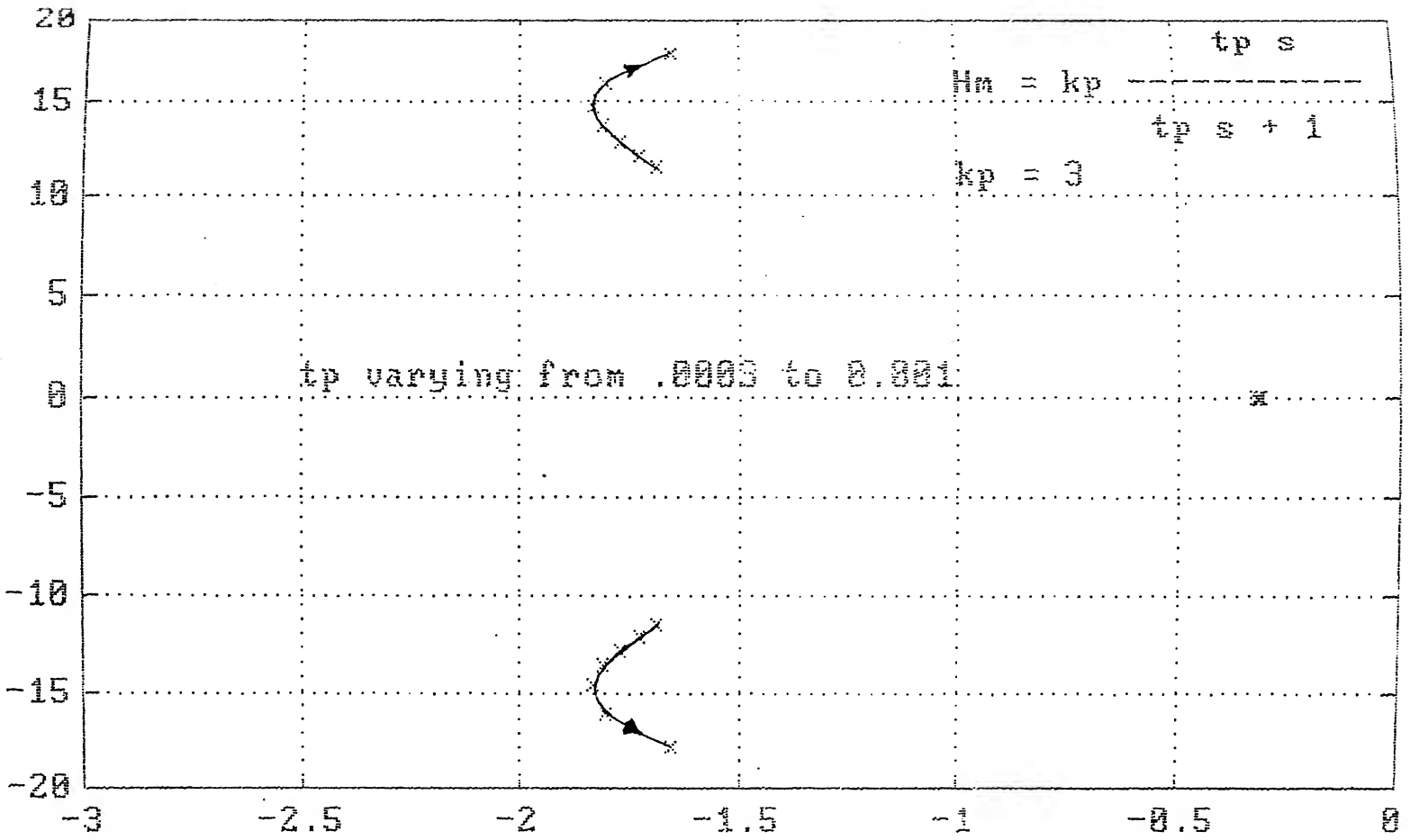

FIG. 2.21 ROOT LOCUS OF ELEVON ACTUATION SYSTEM (DETERMINATION OF DPF)

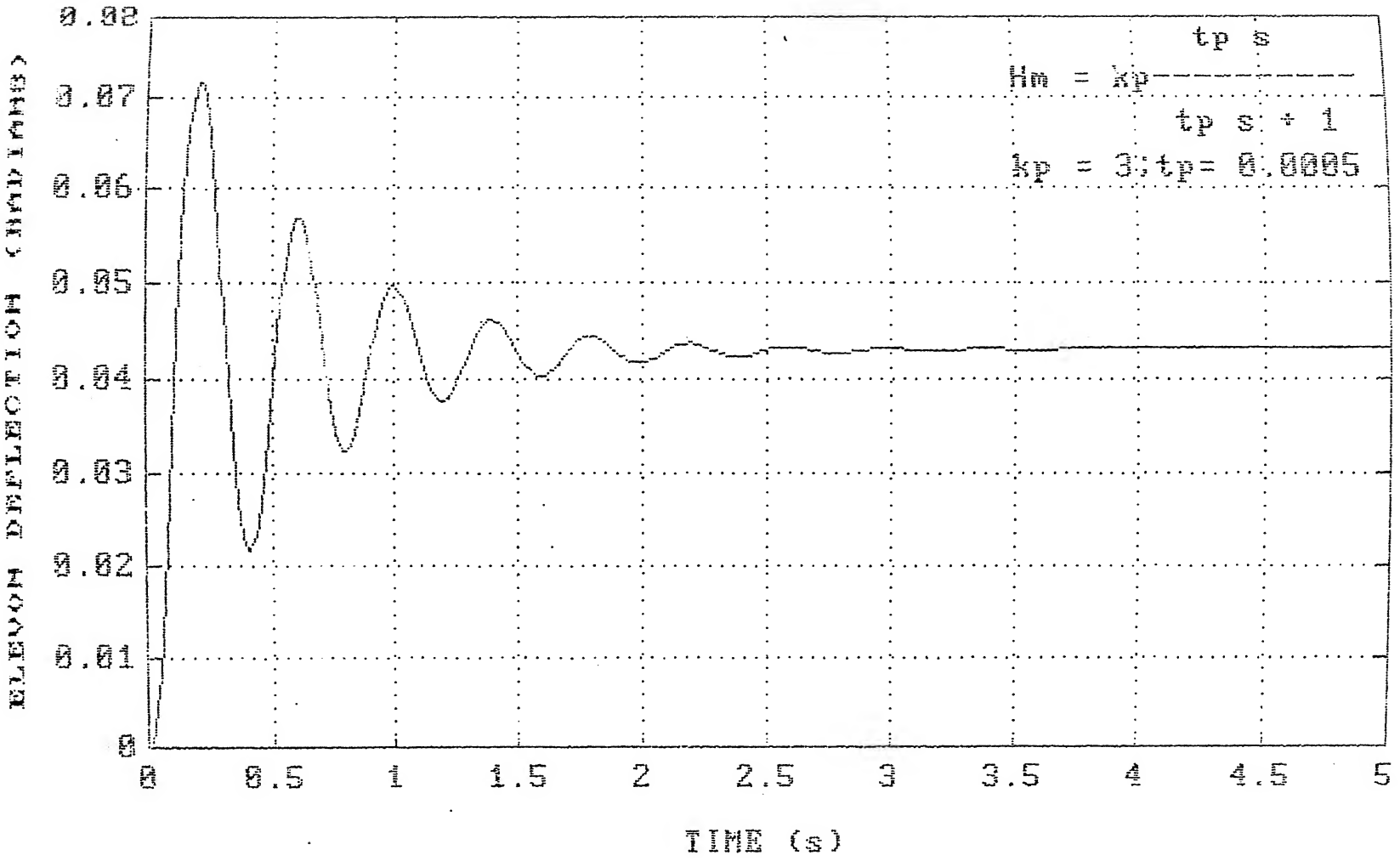

FIG. 2.22a STEP RESPONSE OF ELEVON ACTUATION SYSTEM (WITH DPF)

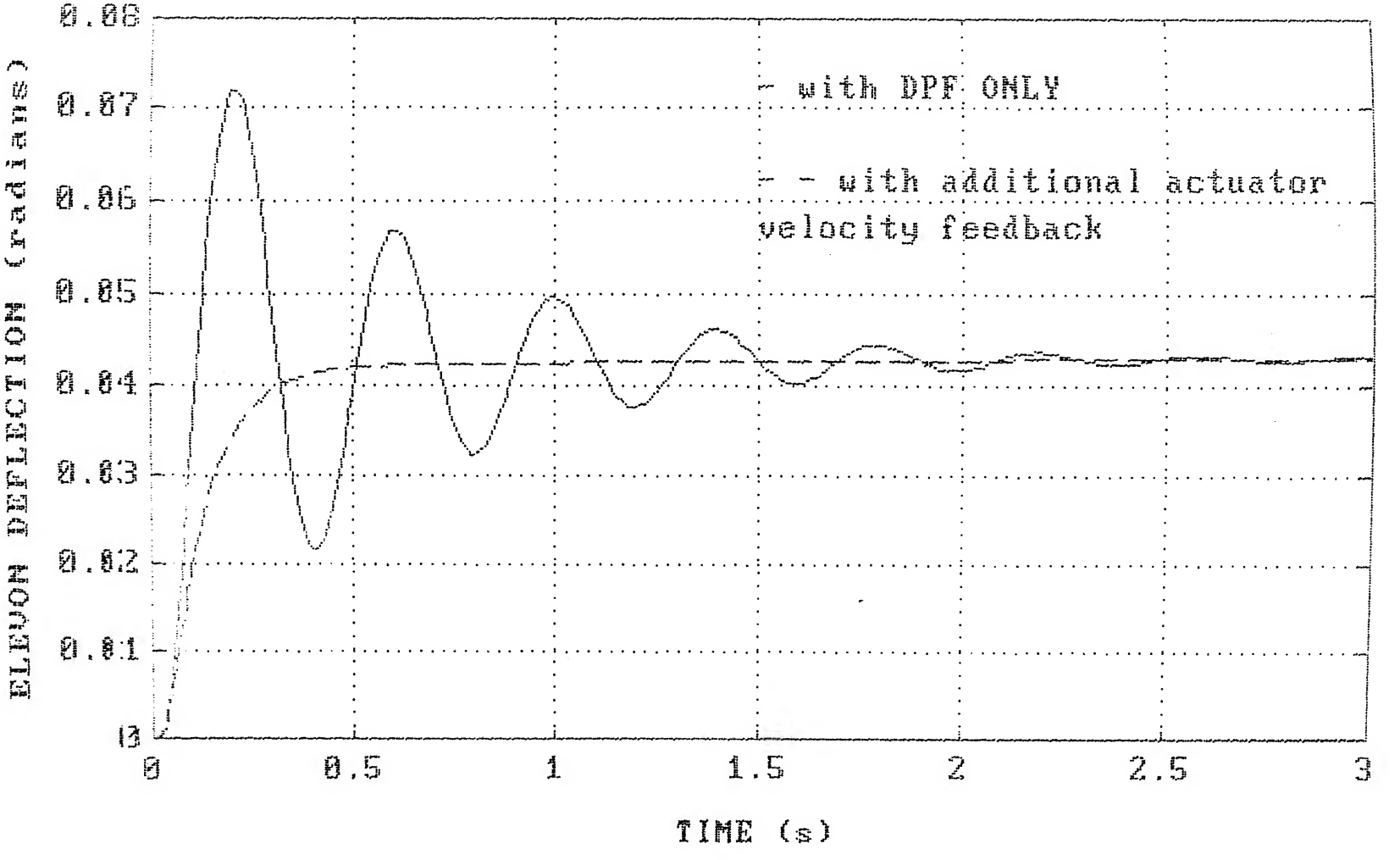

FIG. 2.22b STEP RESPONSE OF ELEVON ACTUATION SYSTEM (WITH VELOCITY FEEDBACK)

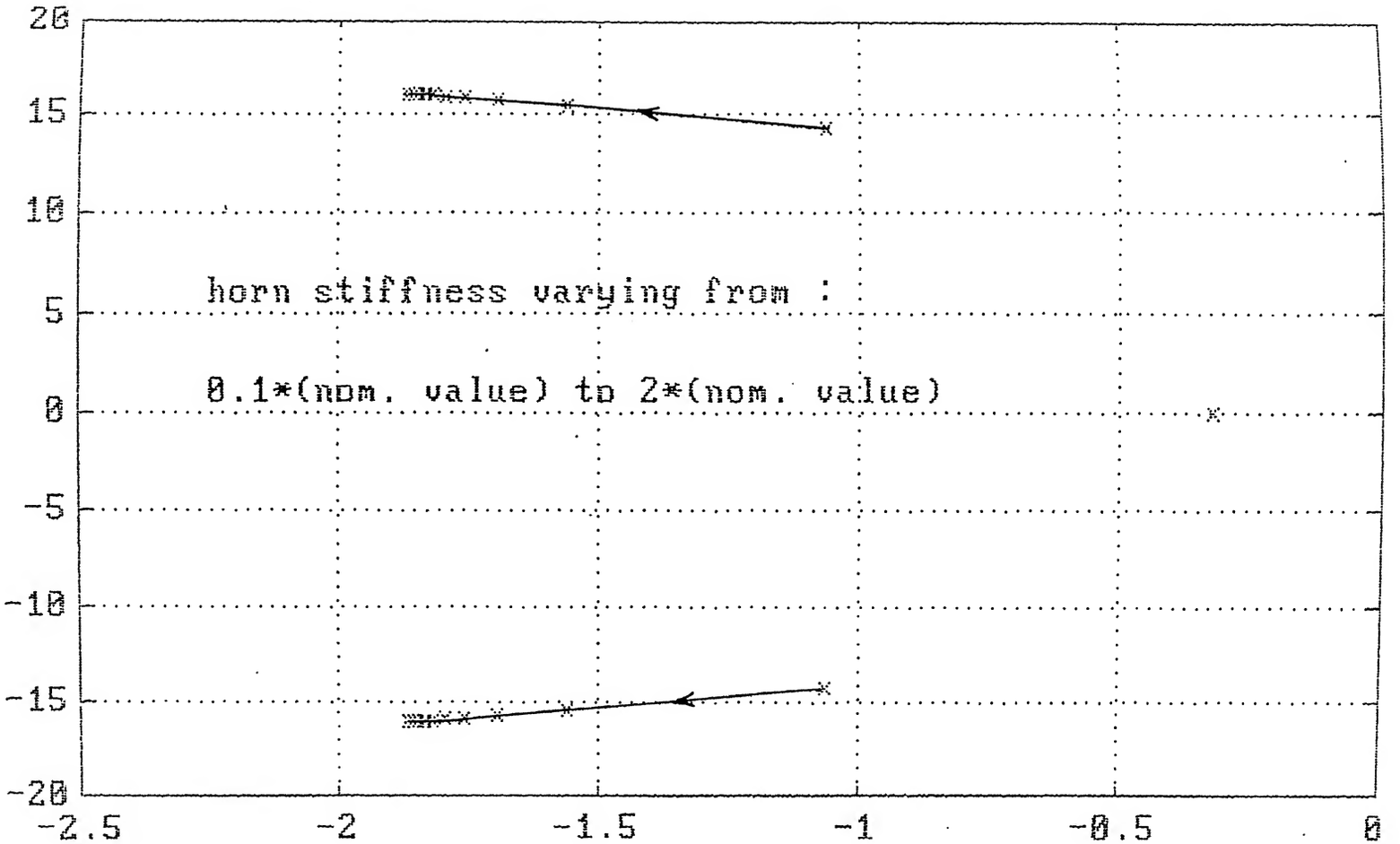

FIG. 2.23A ROOT LOCUS OF ACTUATOR-ELEVON SERVO SYSTEM; PARAMETER : HORN STIFFNESS

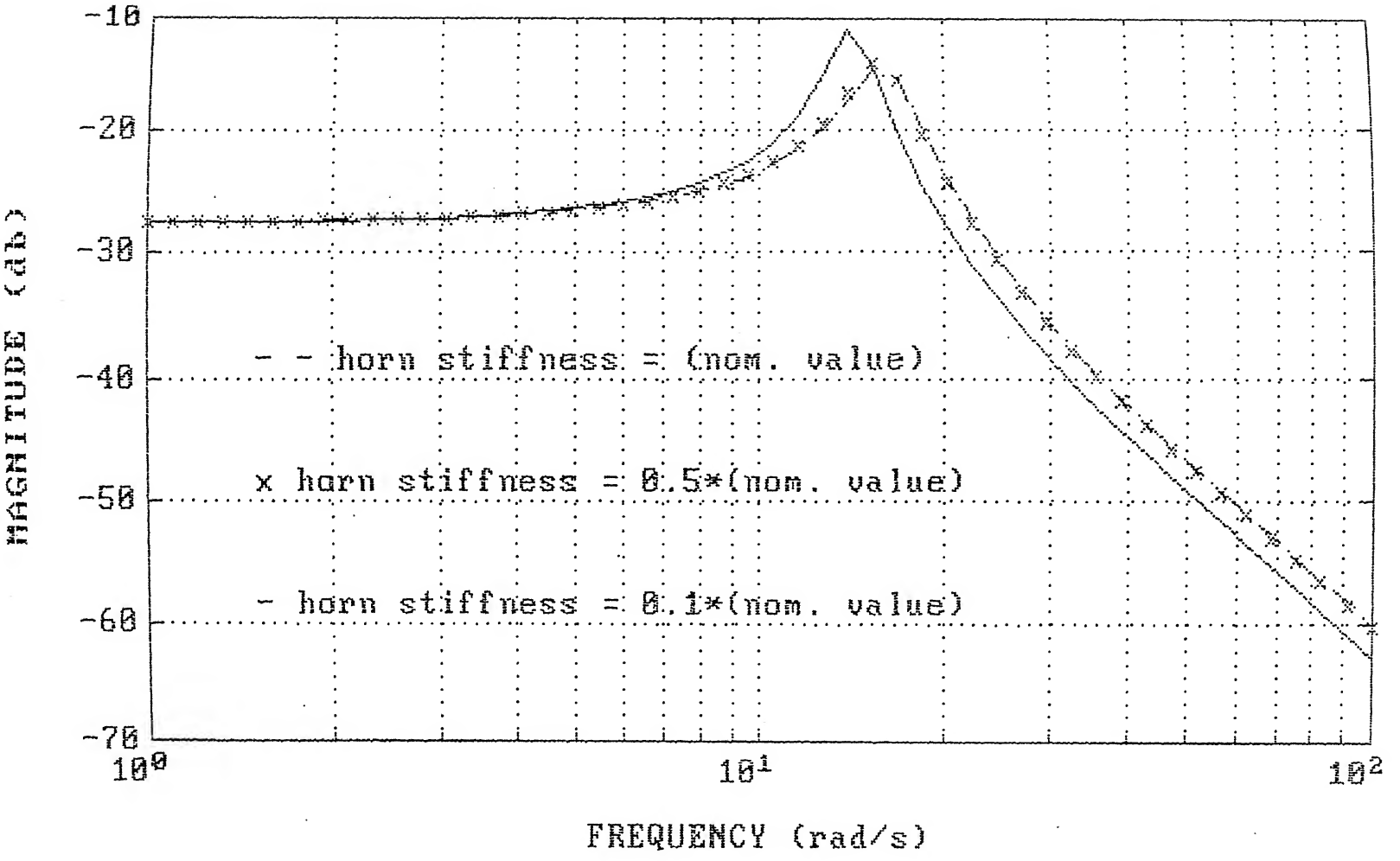

FIG. 2.23B FREQUENCY RESPONSE OF ELEVON ACTUATION SYSTEM; PARAMETER : HORN STIFFNESS

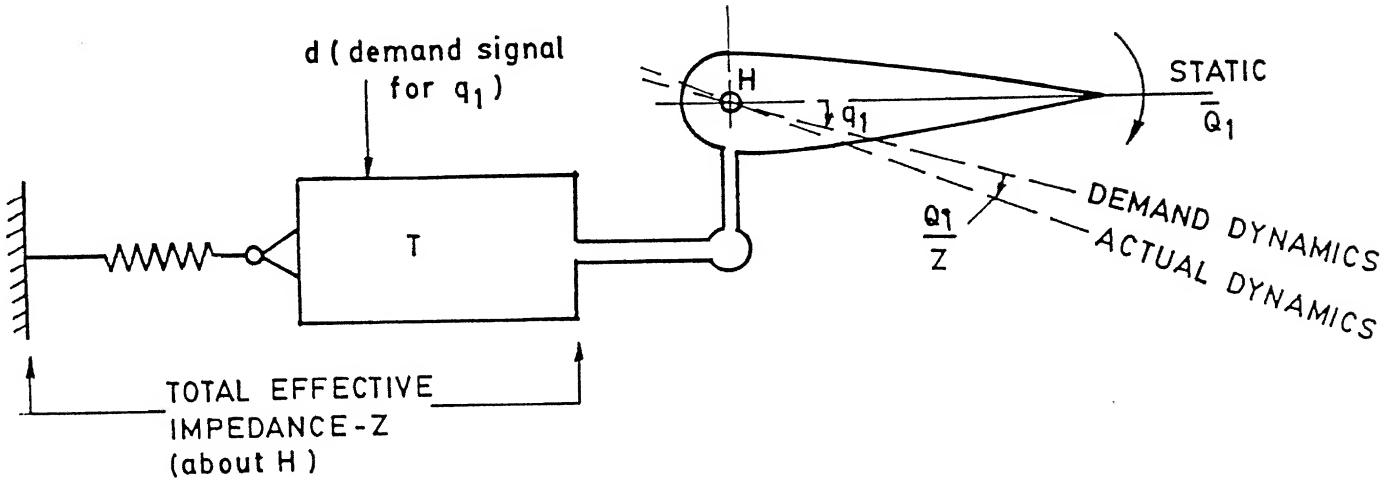

FIG. 3.1 DYNAMIC EFFECT OF ACTUATOR IMPEDANCE

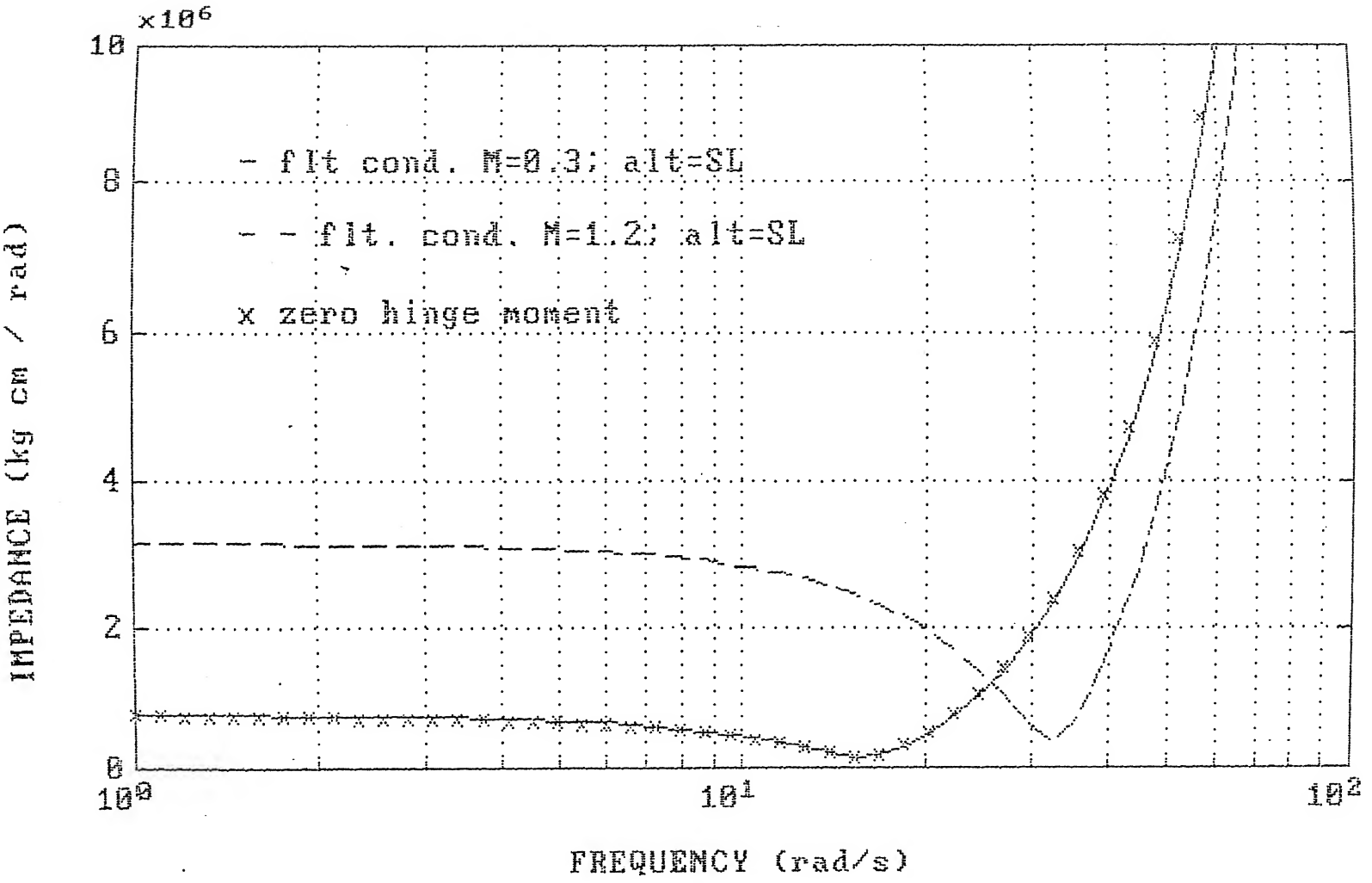

FIG. 3.2 IMPEDANCE CHARACTERISTICS OF ELEVON ACTUATION SYSTEM

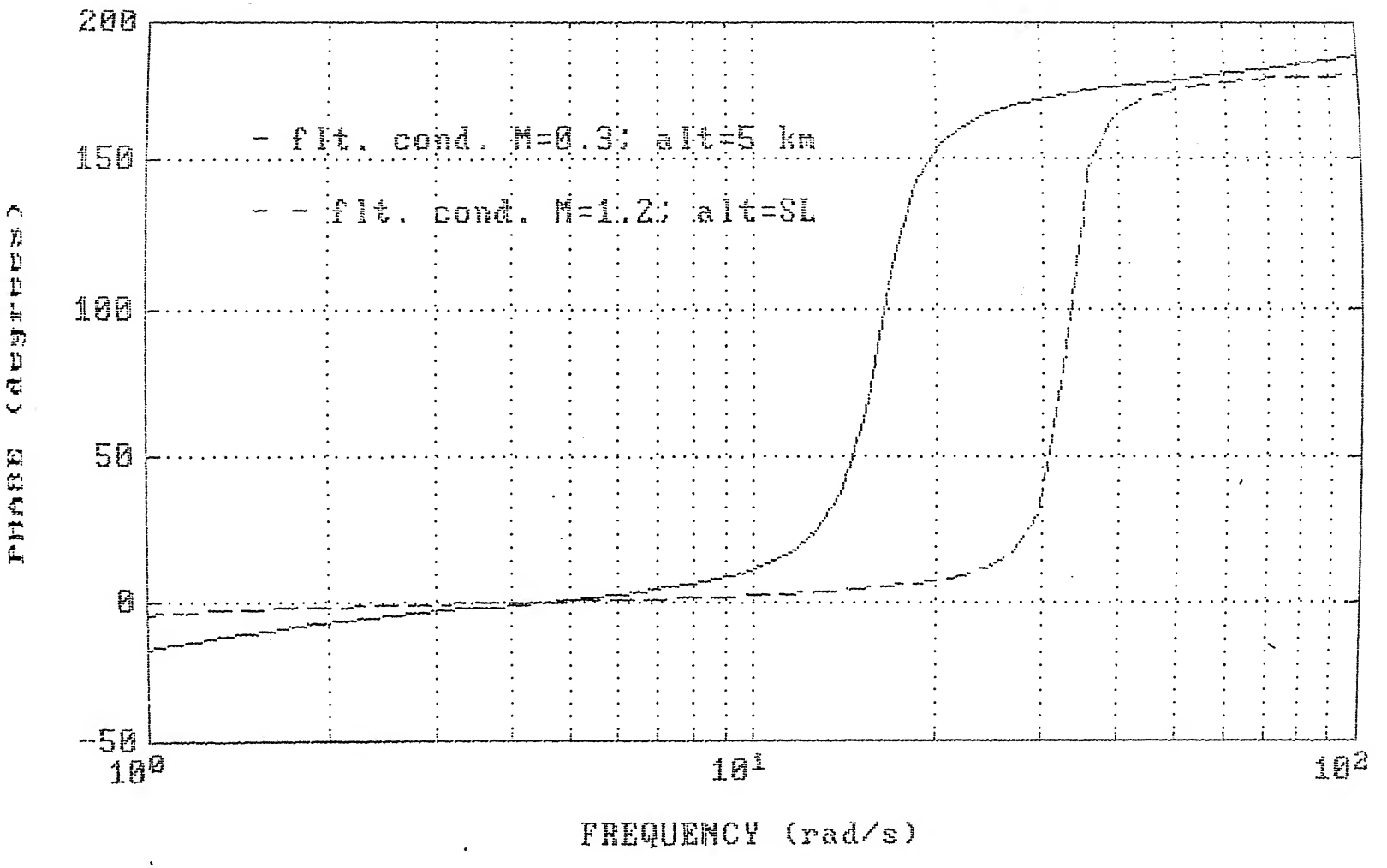

FIG. 3.3 IMPEDANCE CHARACTERISTICS OF ELEVON ACTUATION SYSTEM

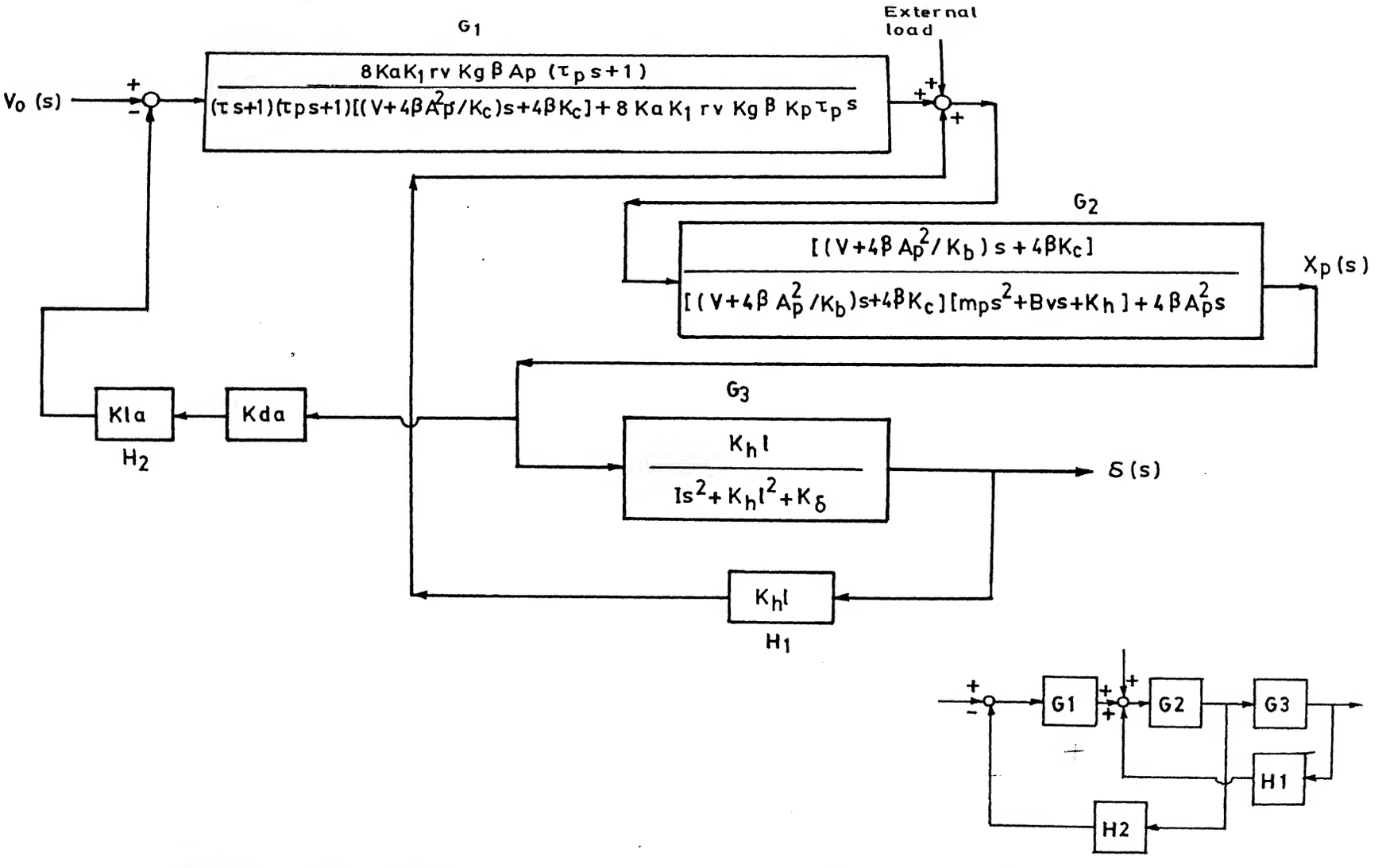

FIG 3.4a. TRANSFER FUNCTION / COMPLIANCE OF ELEVON ACTUATION SYSTEM

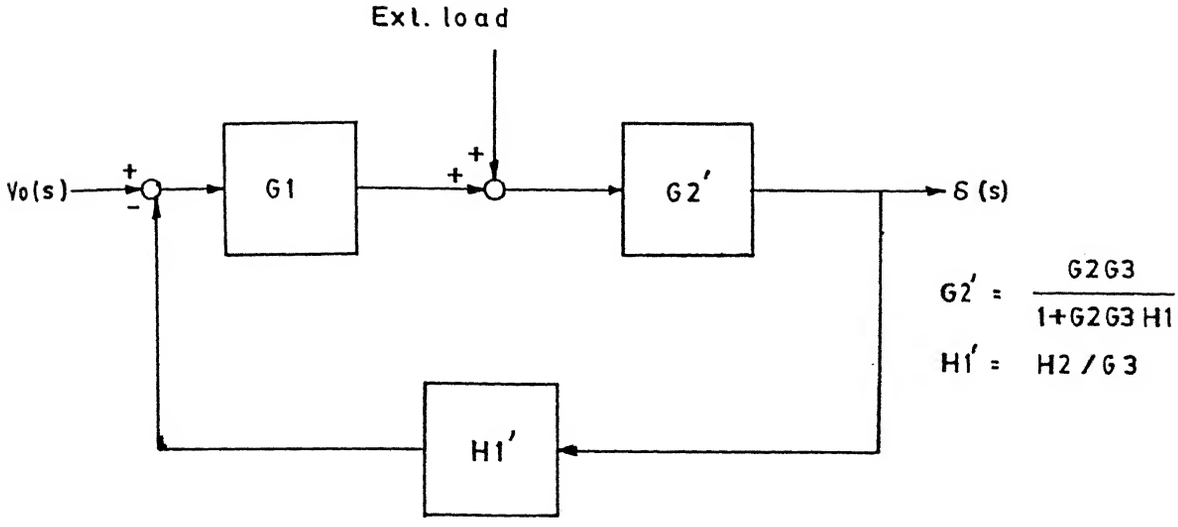

FIG. 3·4b. SIMPLIFIED REPRESENTATION OF TRANSFER FUNCTION / COMPLIANCE OF ELEVON ACTUATION SYSTEM

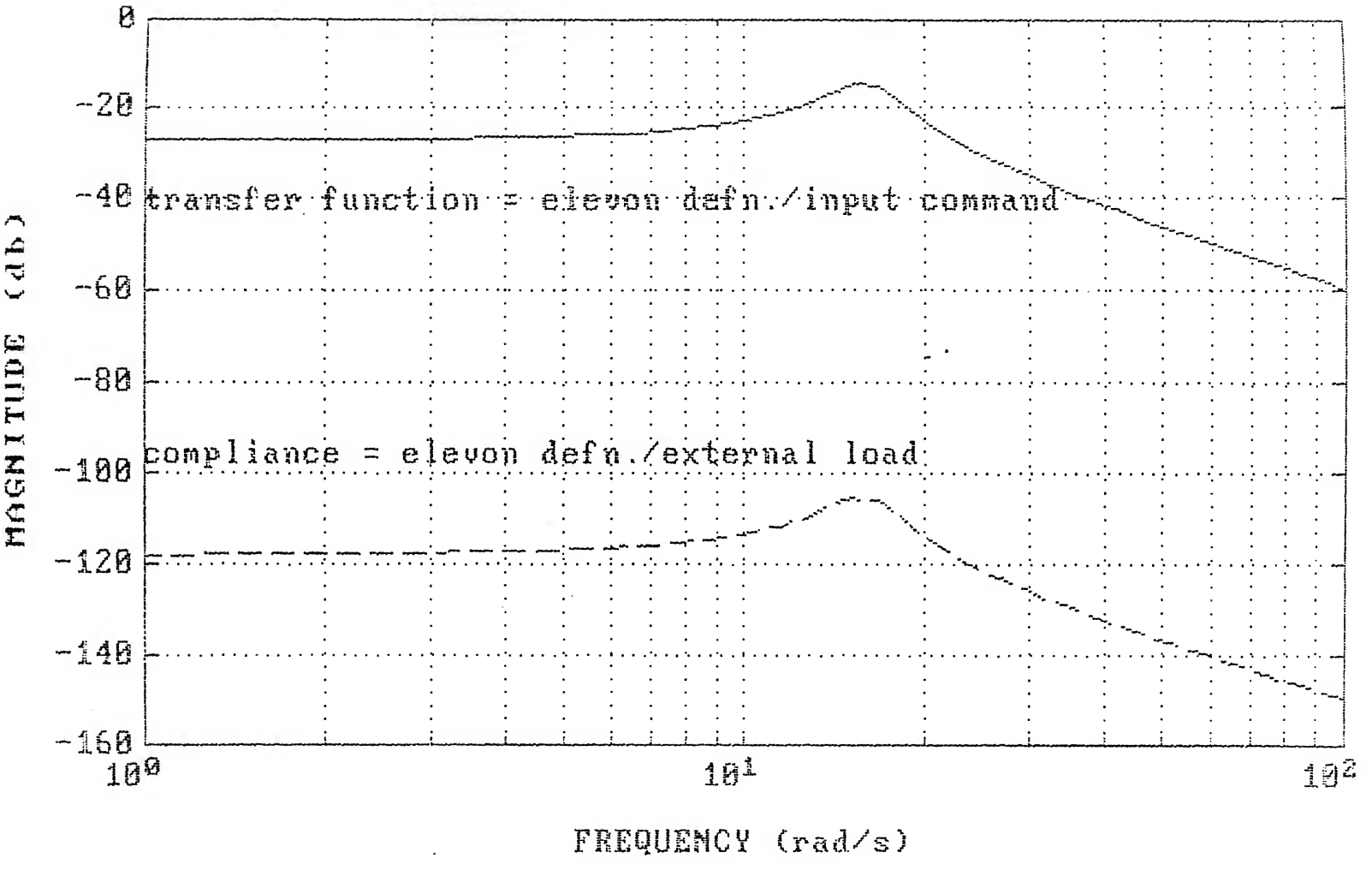

FIG. 3.5 COMPARISON OF TRANSFER FUNCTION AND COMPLIANCE OF ELEVON ACTUATION SYSTEM

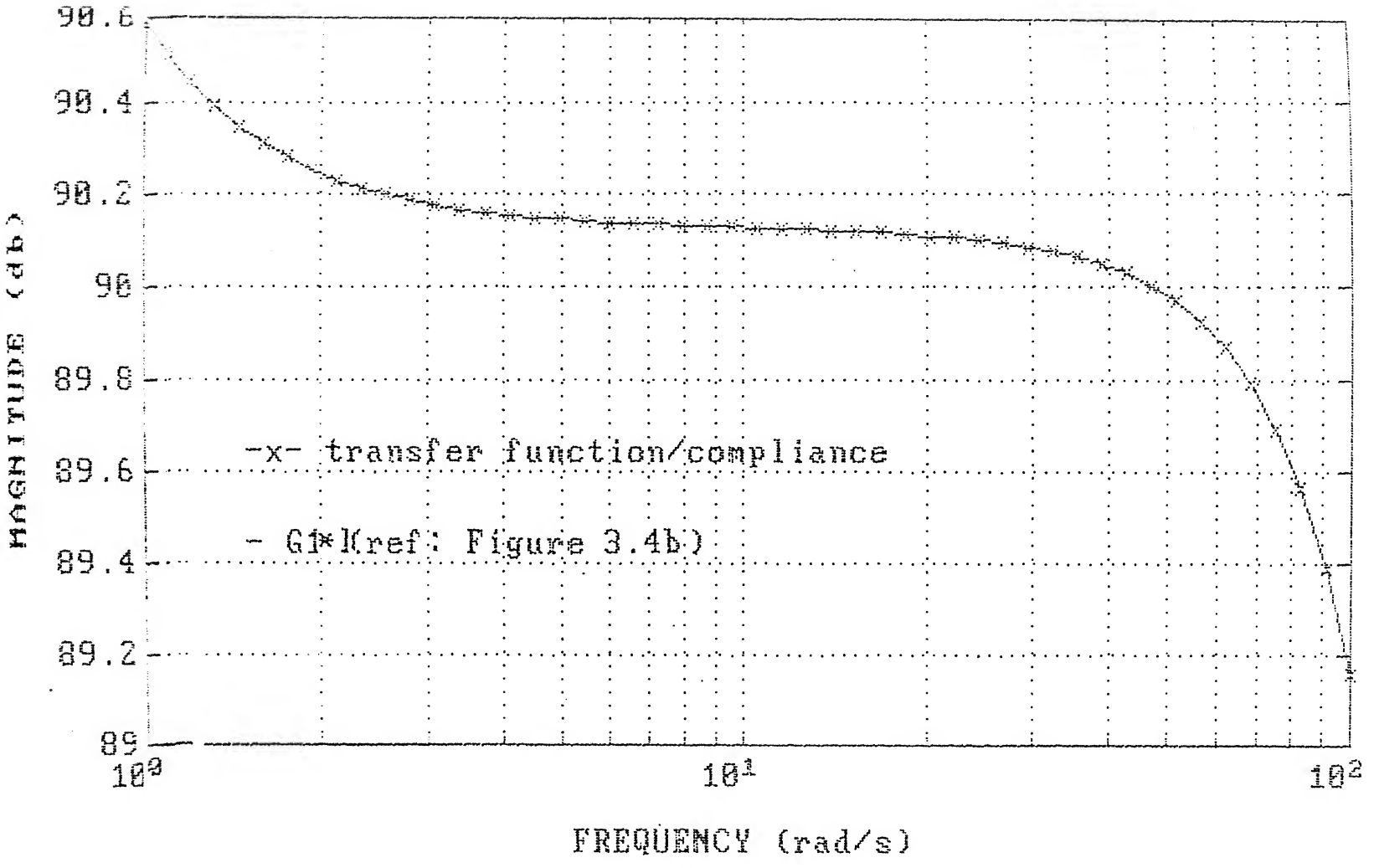

FIG. 3.6 FREQUENCY RESPONSE OF TRANSFER FUNCTION BETWEEN TORQUE AND THE COMMAND INPUT FOR A FIXED ELEVON DEFLECTION

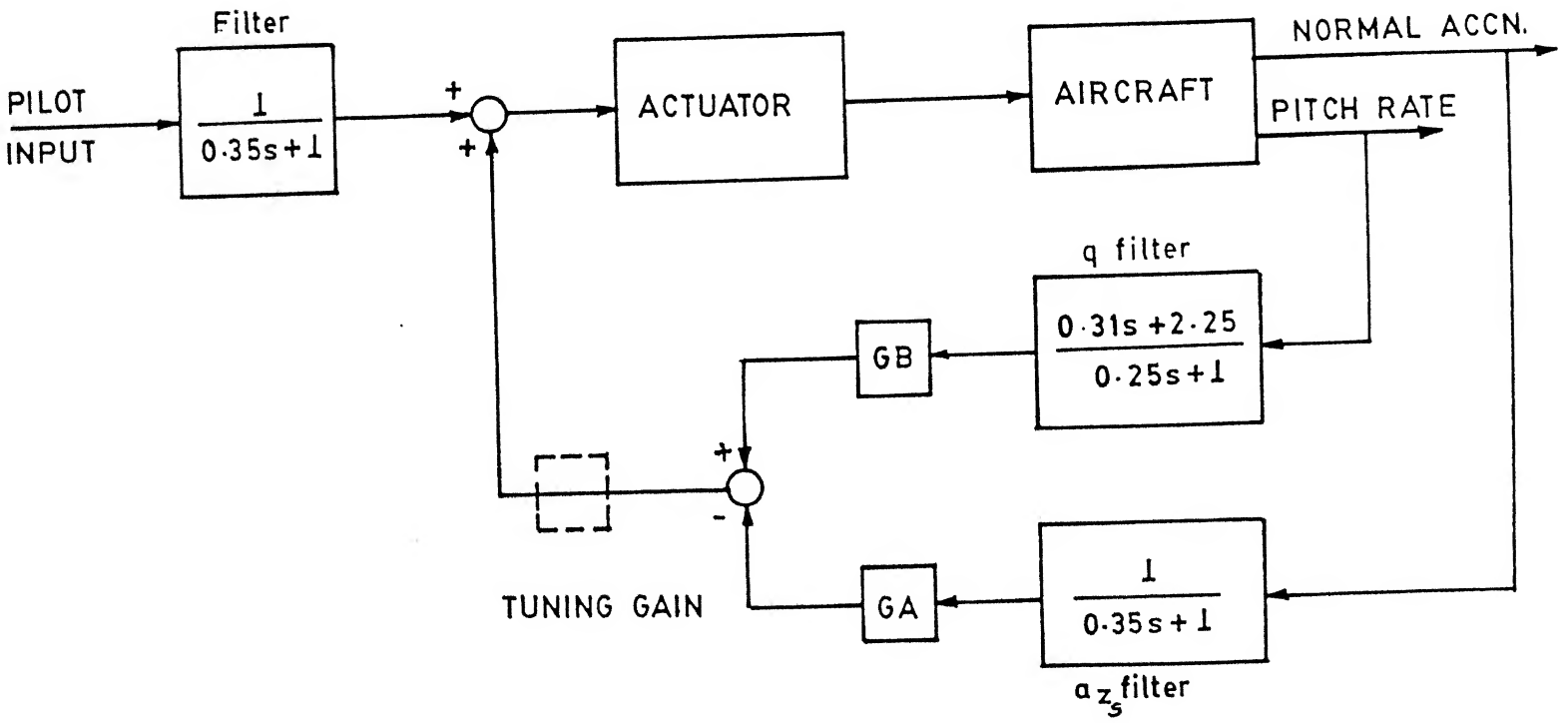

FIG. 4·1 CONTROL LAW SCHEMATIC

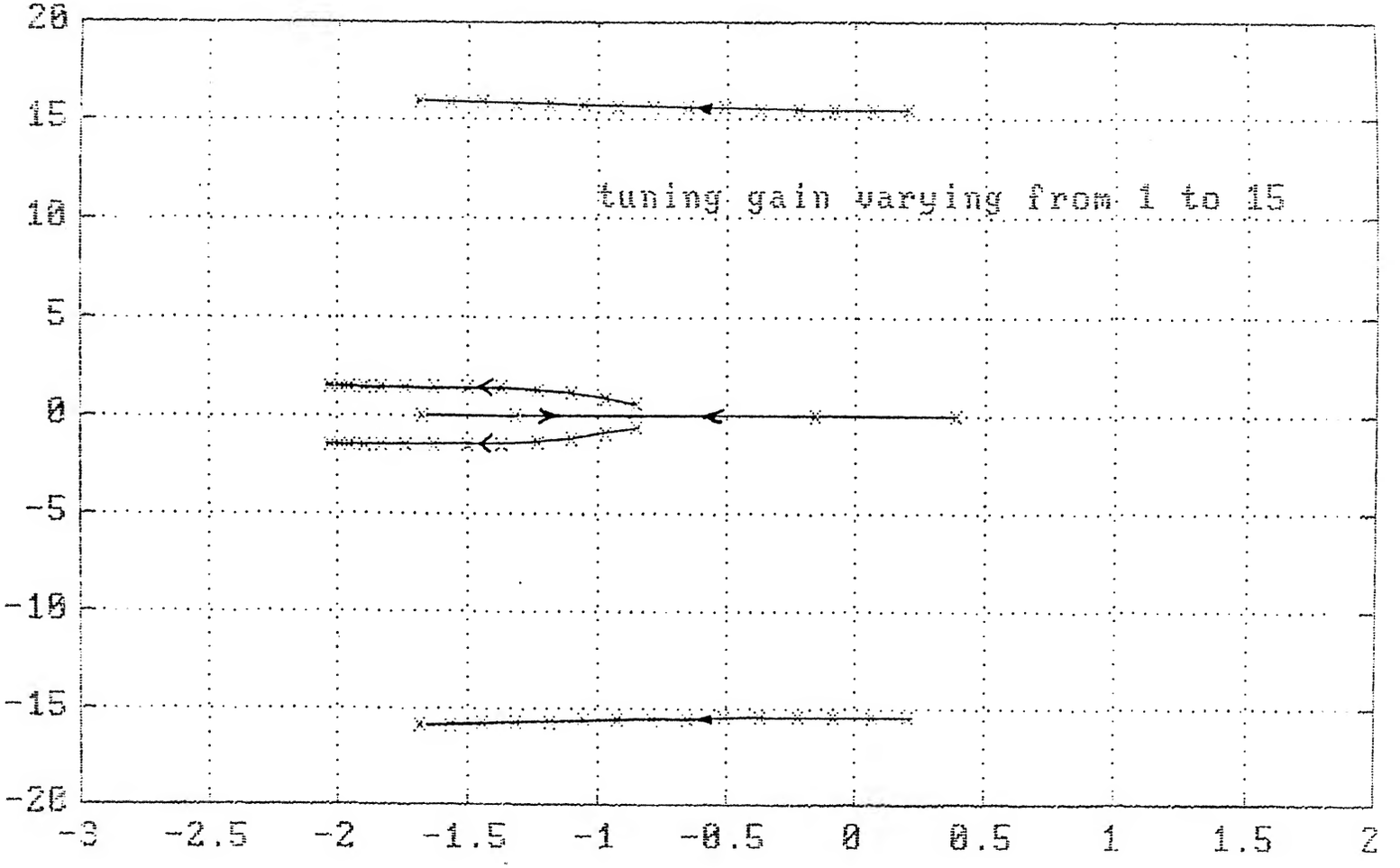

FIG. 4.2 ROOT LOCUS OF AIRPLANE (DETERMINATION OF TUNING GAIN)

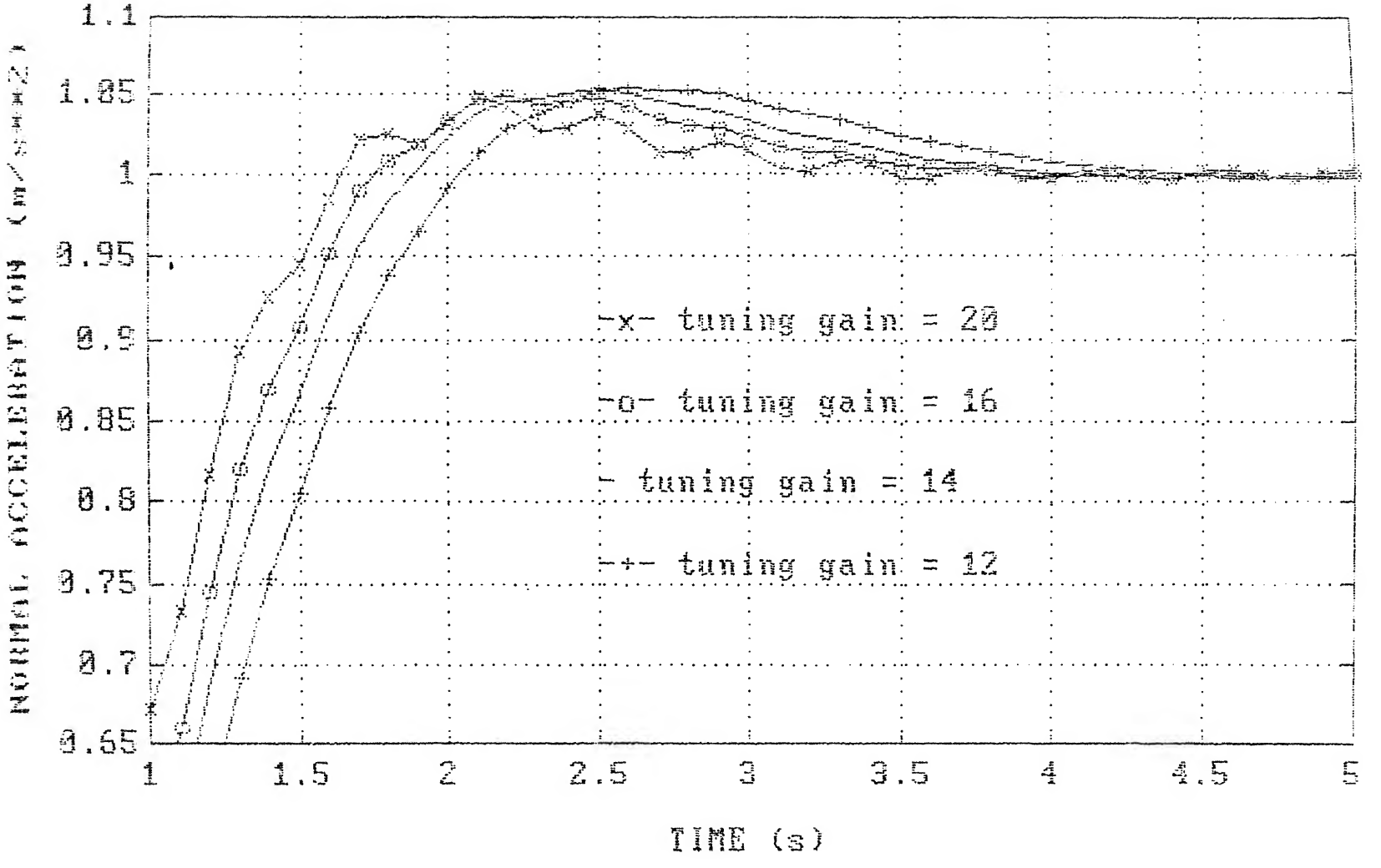

FIG. 4.3A STEP RESPONSE OF AIRPLANE ; PARAMETER : TUNING GAIN

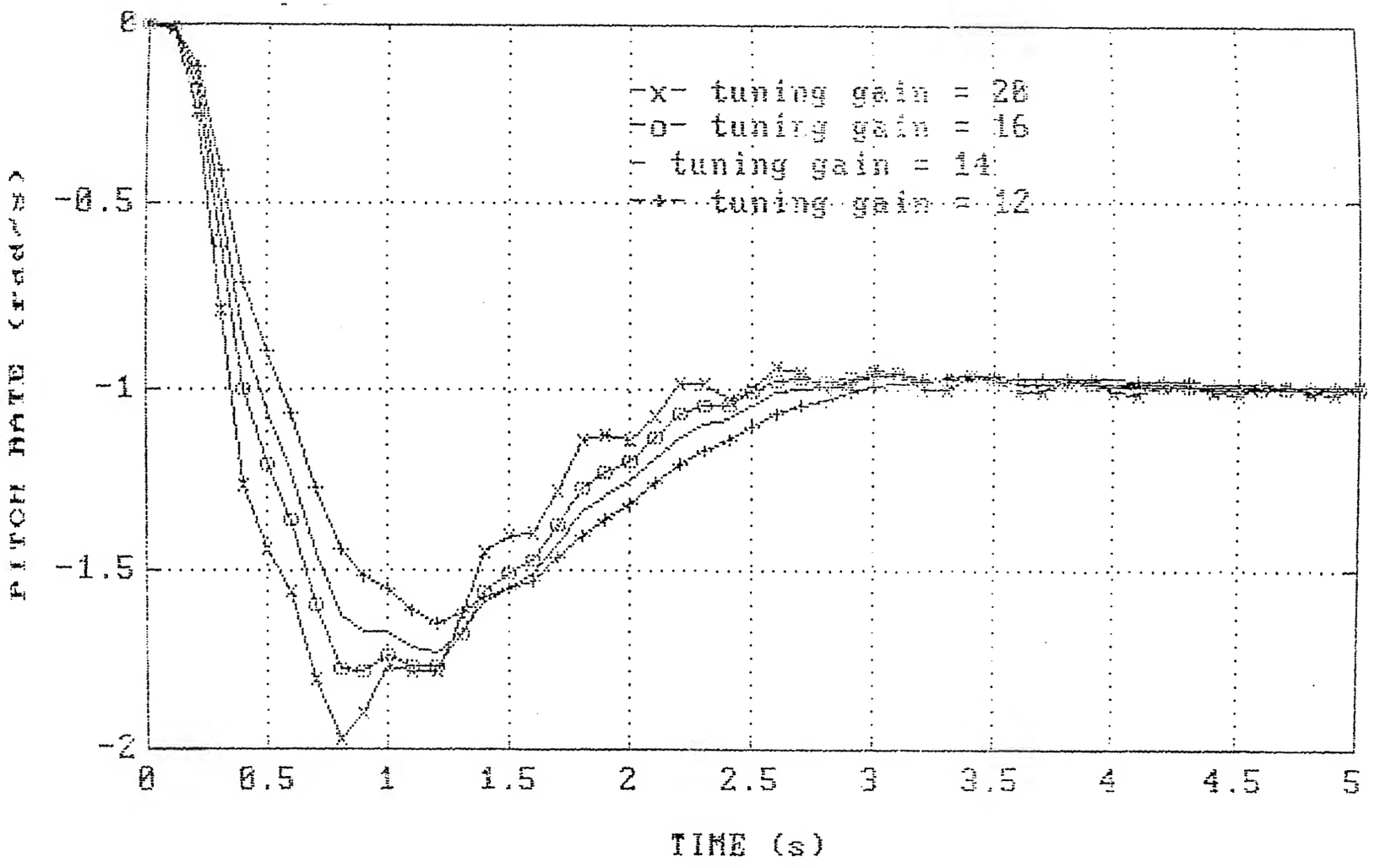

FIG. 4.3B STEP RESPONSE OF AIRPLANE; PARAMETER : TUNING GAIN

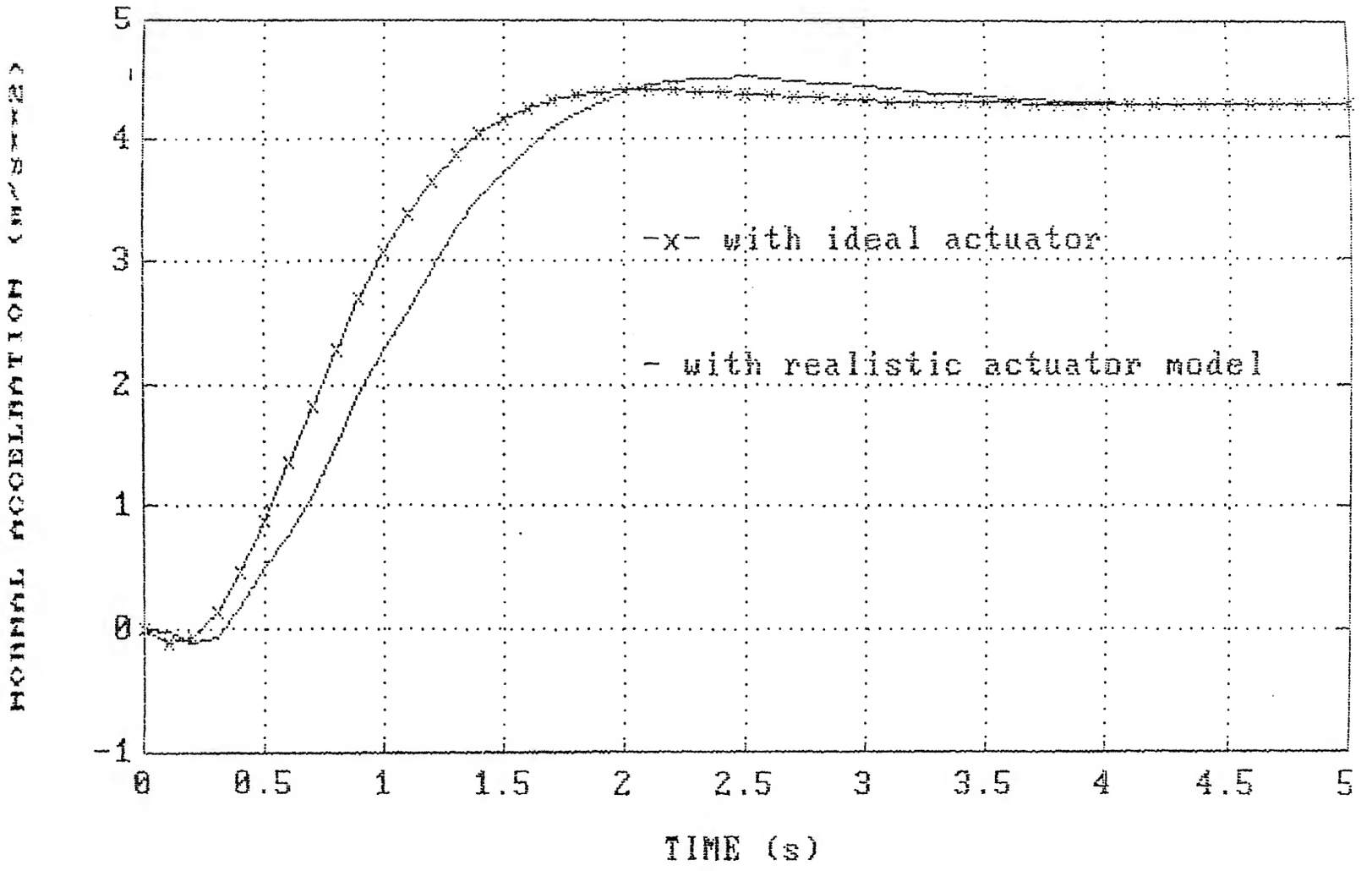

FIG. 4.4A STEP RESPONSE OF AIRPLANE — REALISTIC VS IDEAL ACTUATOR MODEL

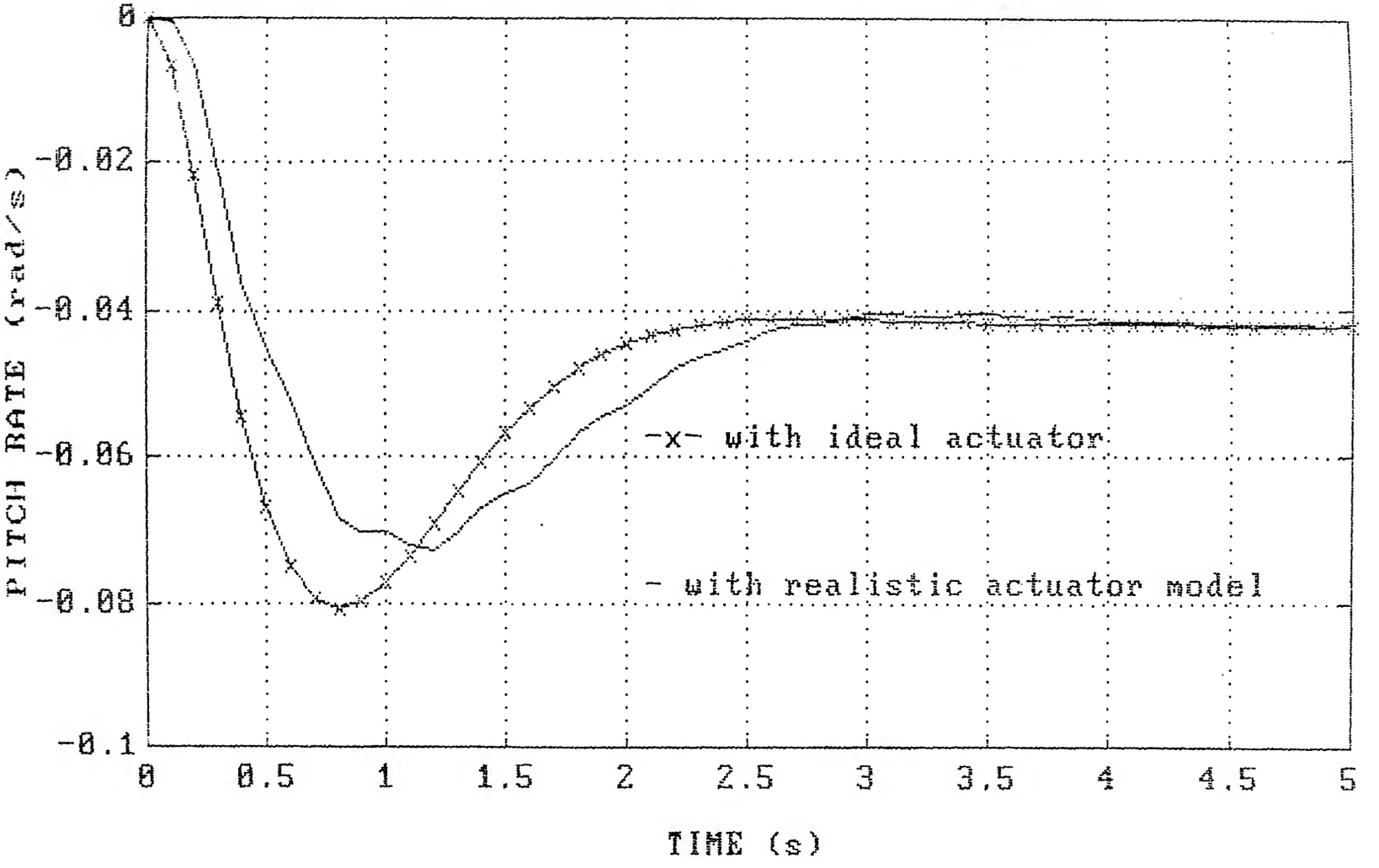

FIG. 4.4B STEP RESPONSE OF AIRPLANE — REALISTIC VS IDEAL ACTUATOR MODEL

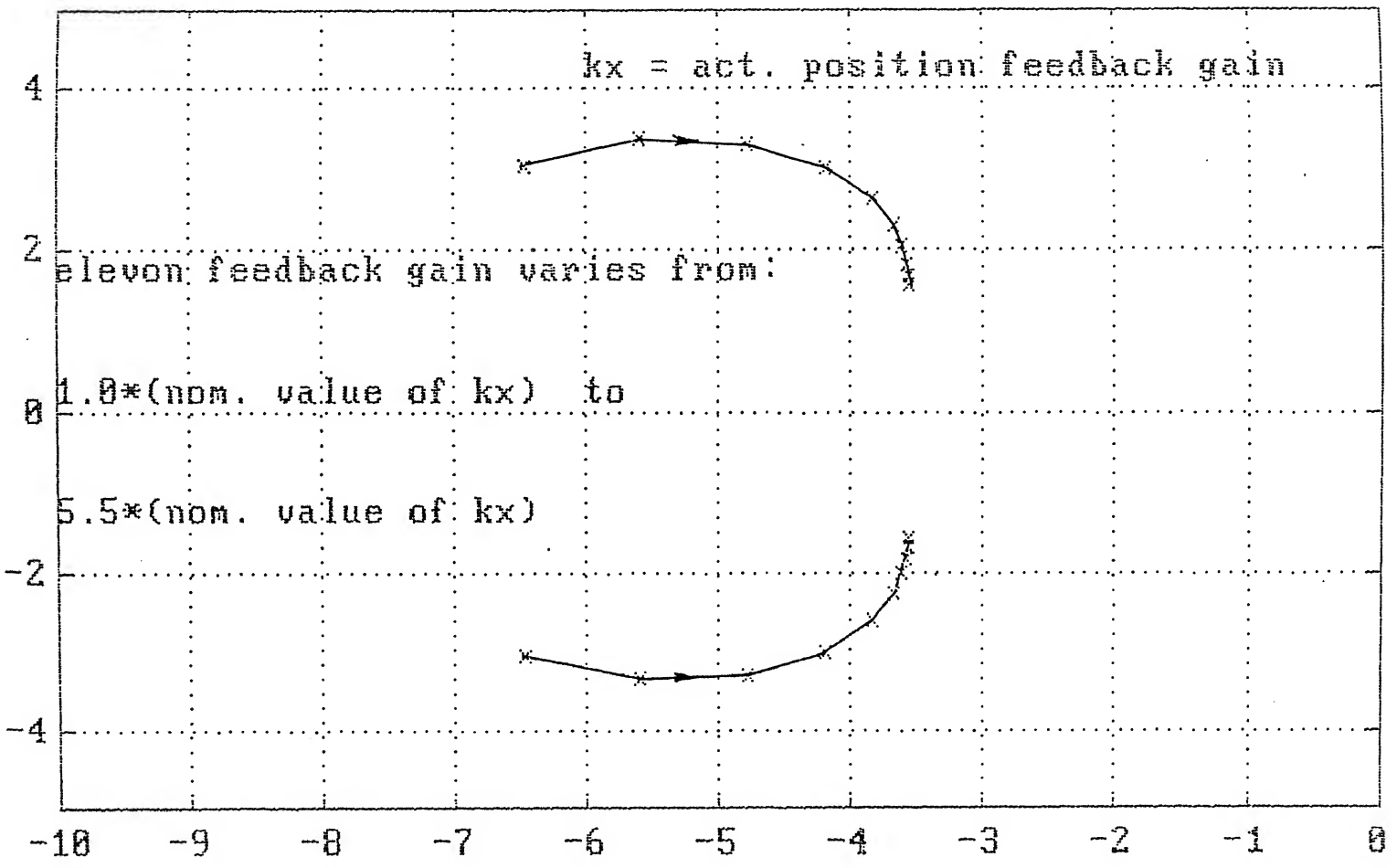

FIG. 4.5A ROOT LOCUS OF AIRPLANE; PARAMETER: ELEVON POSITION FEEDBACK GAIN

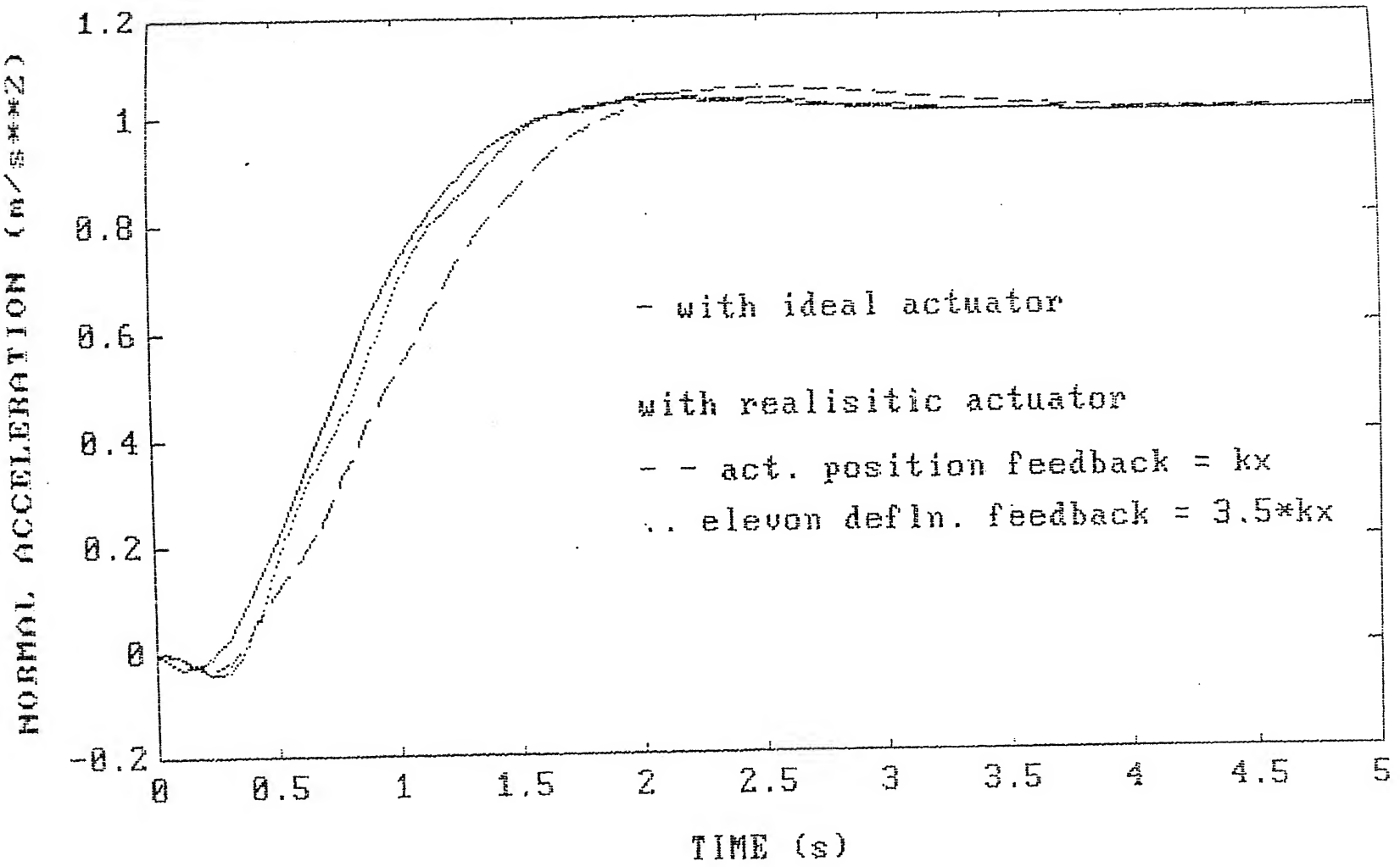

FIG. 4.5B STEP RESPONSE OF AIRPLANE FOR OPTIMAL ELEVON POSITION FEEDBACK GAIN

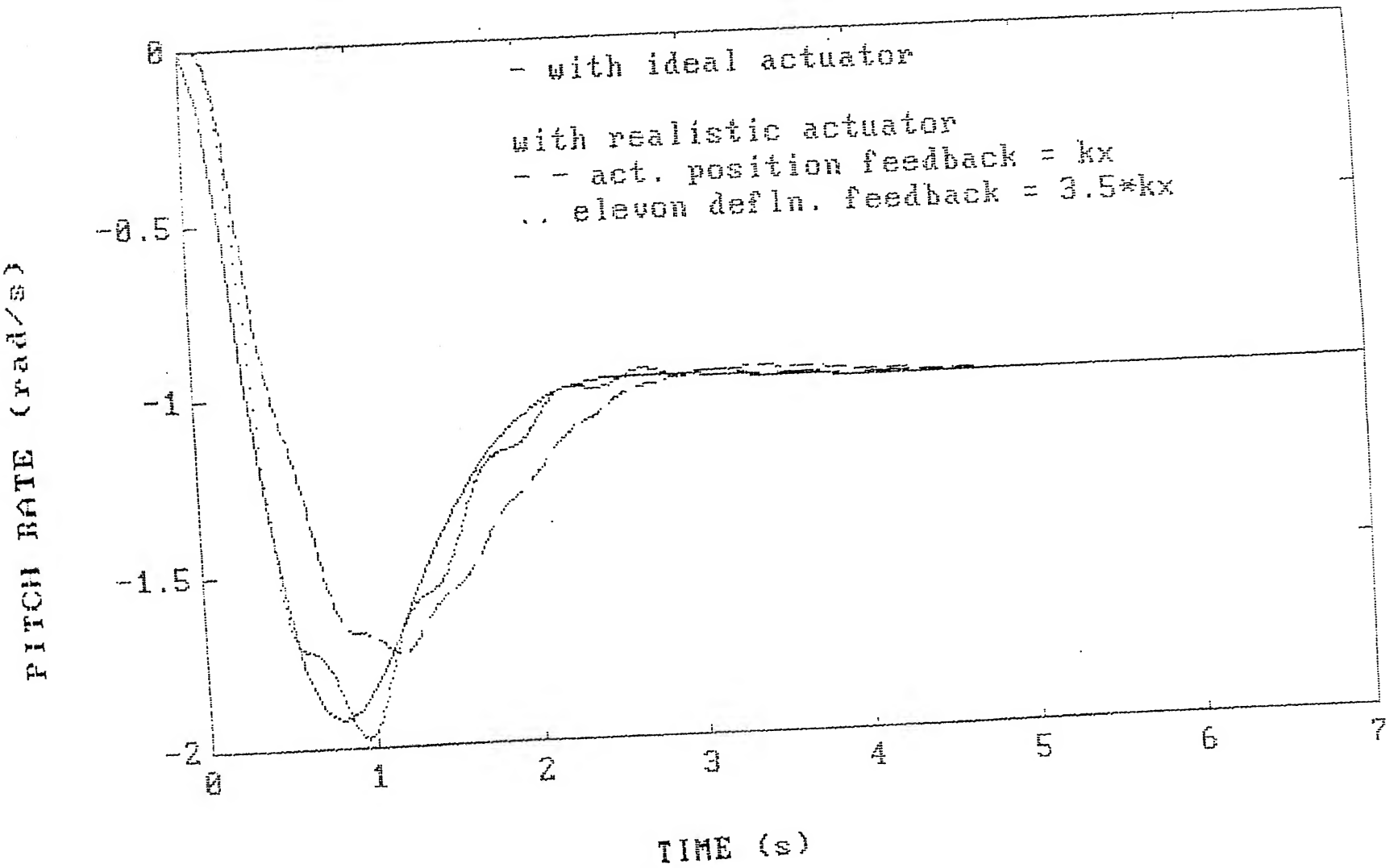

FIG. 4.5C STEP RESPONSE OF AIRPLANE FOR OPTIMAL ELEVON POSITION FEEDBACK GAIN

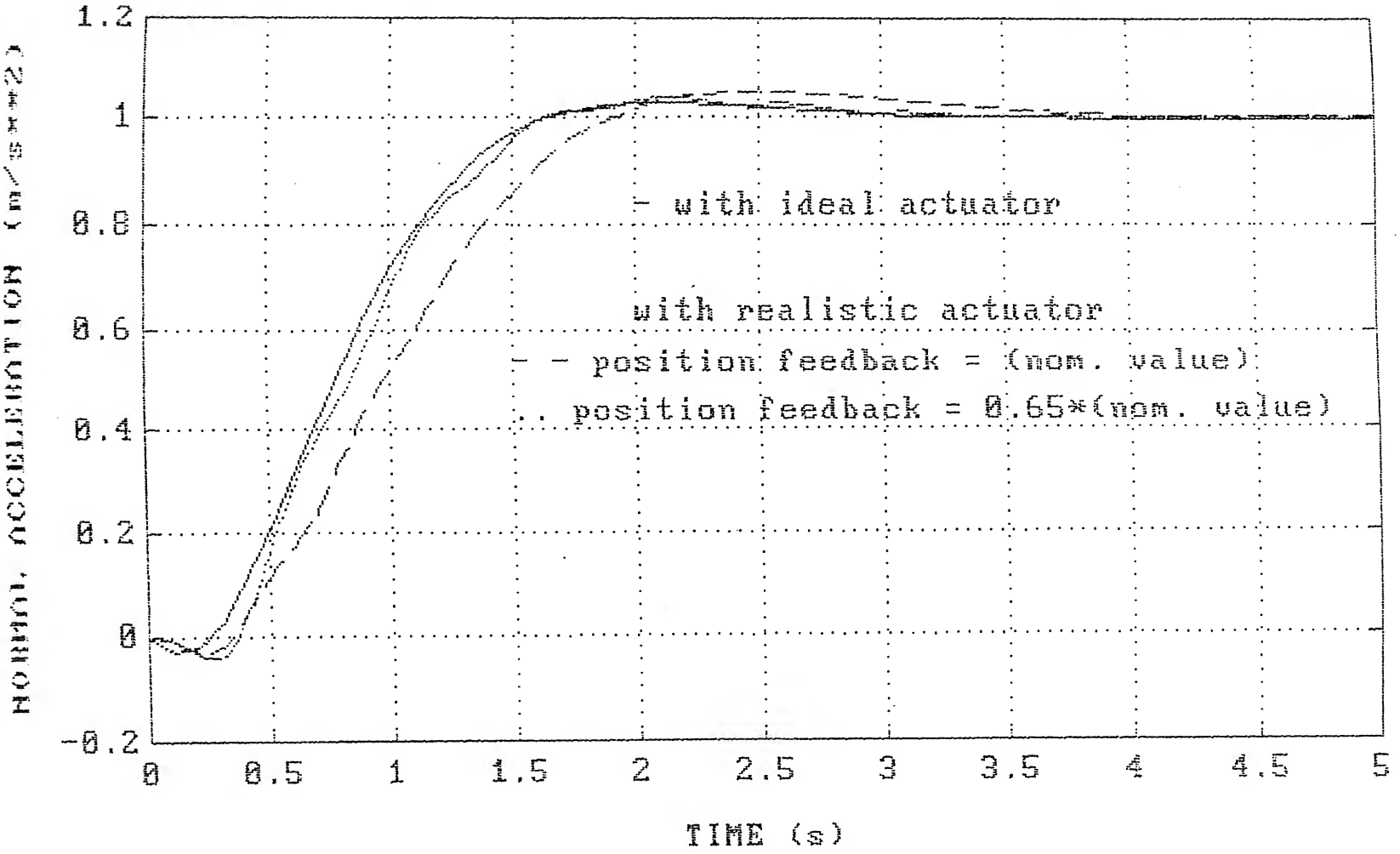

FIG. 4.6A STEP RESPONSE OF AIRPLANE FOR OPTIMAL ACTUATOR POSITION FEEDBACK GAIN

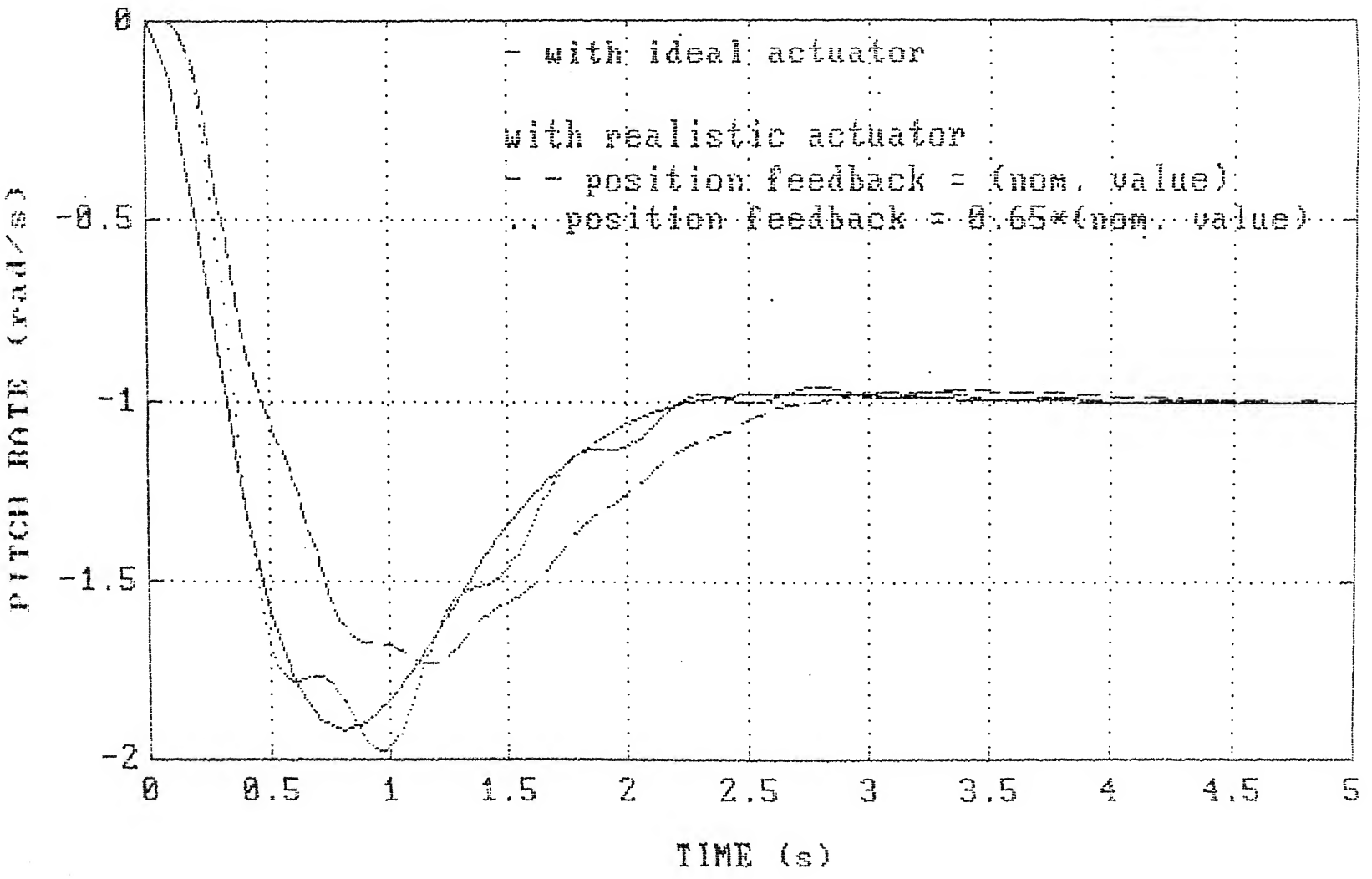

FIG. 4.6B STEP RESPONSE OF AIRPLANE FOR OPTIMAL ACTUATOR POSITION FEEDBACK GAIN

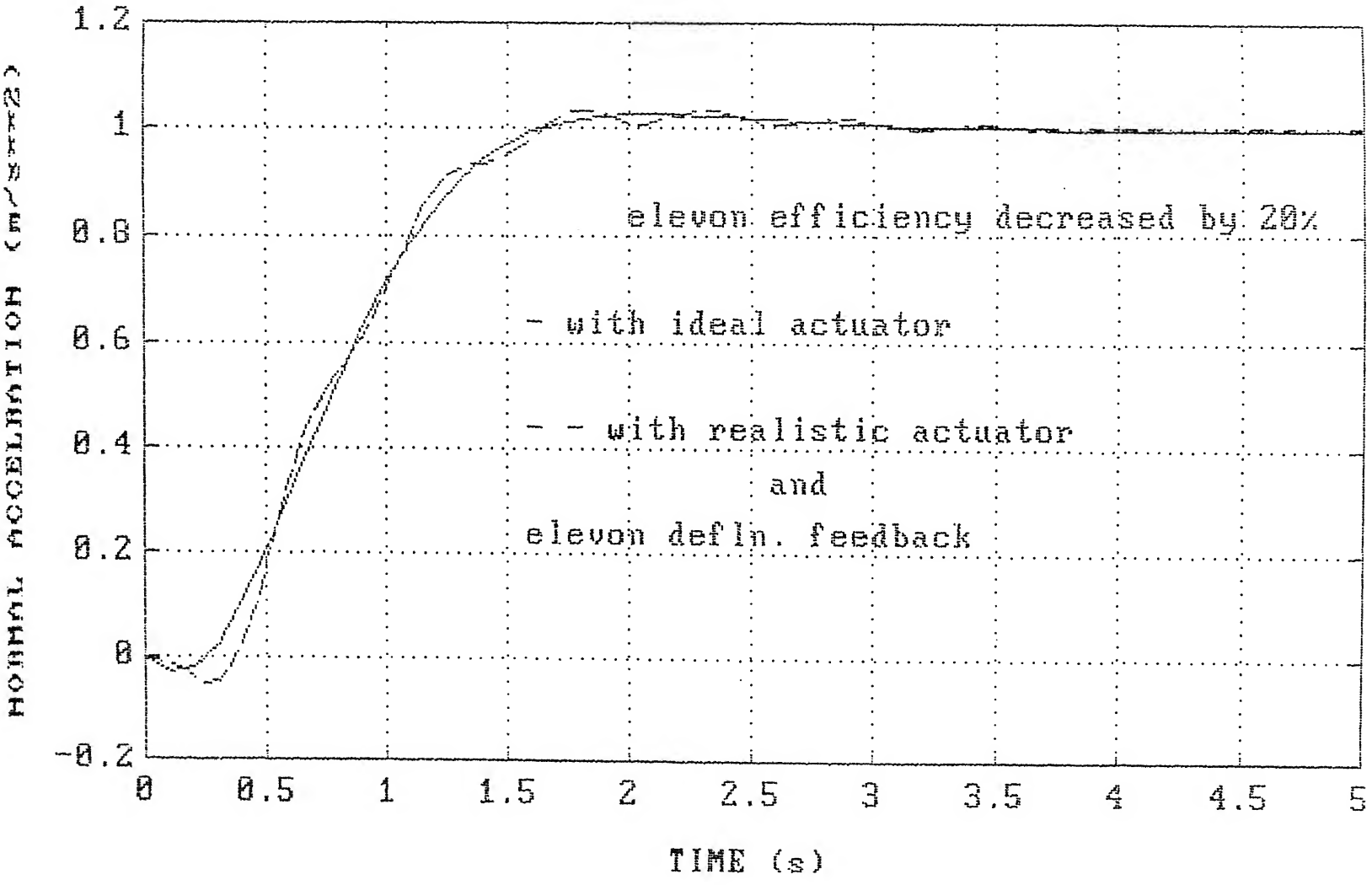

FIG. 4.7A STEP RESPONSE OF AIRPLANE FOR REDUCED EFFICIENCY OF THE ELEVON

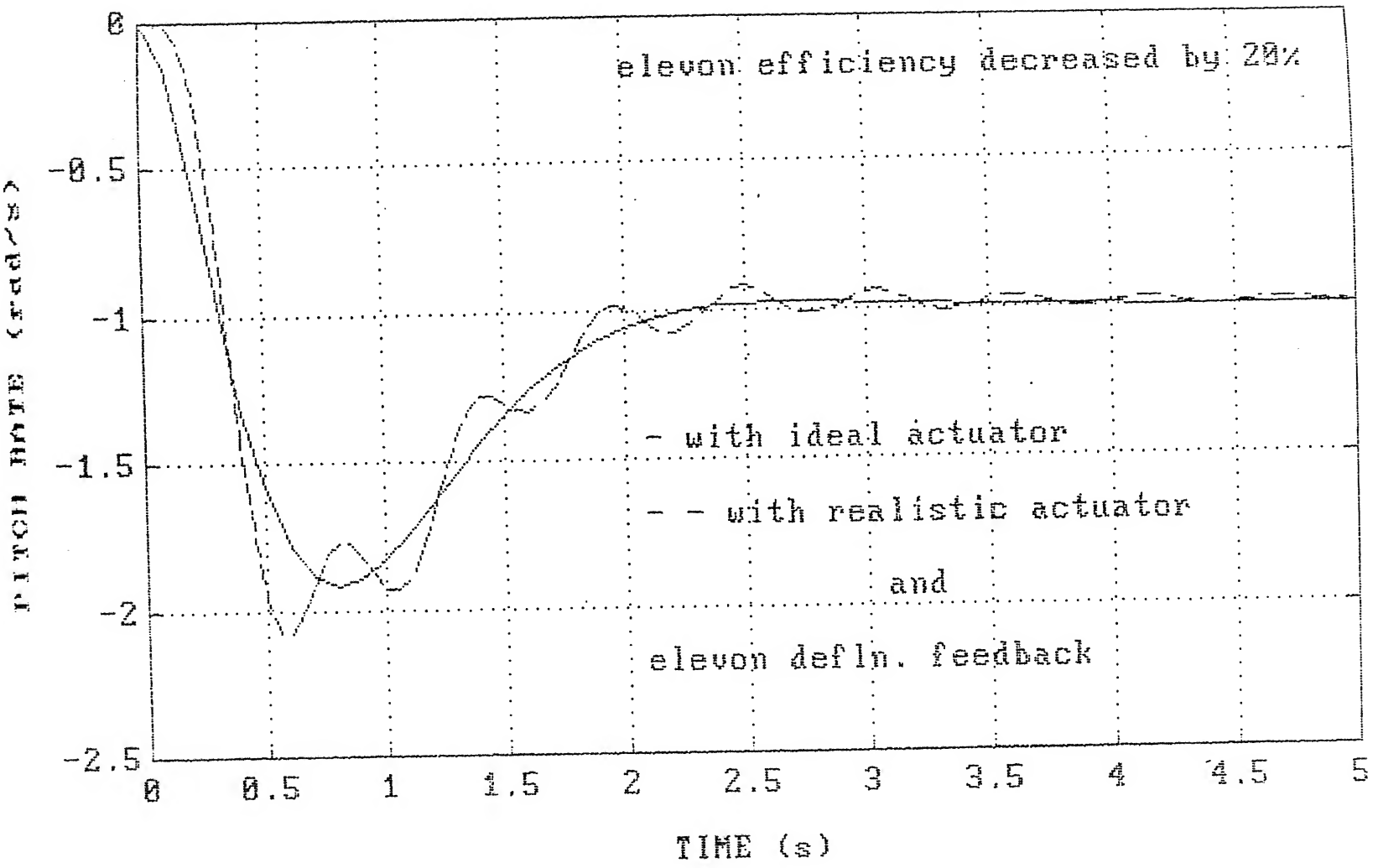

FIG. 4.7B STEP RESPONSE OF AIRPLANE FOR REDUCED EFFICIENCY OF THE ELEVON

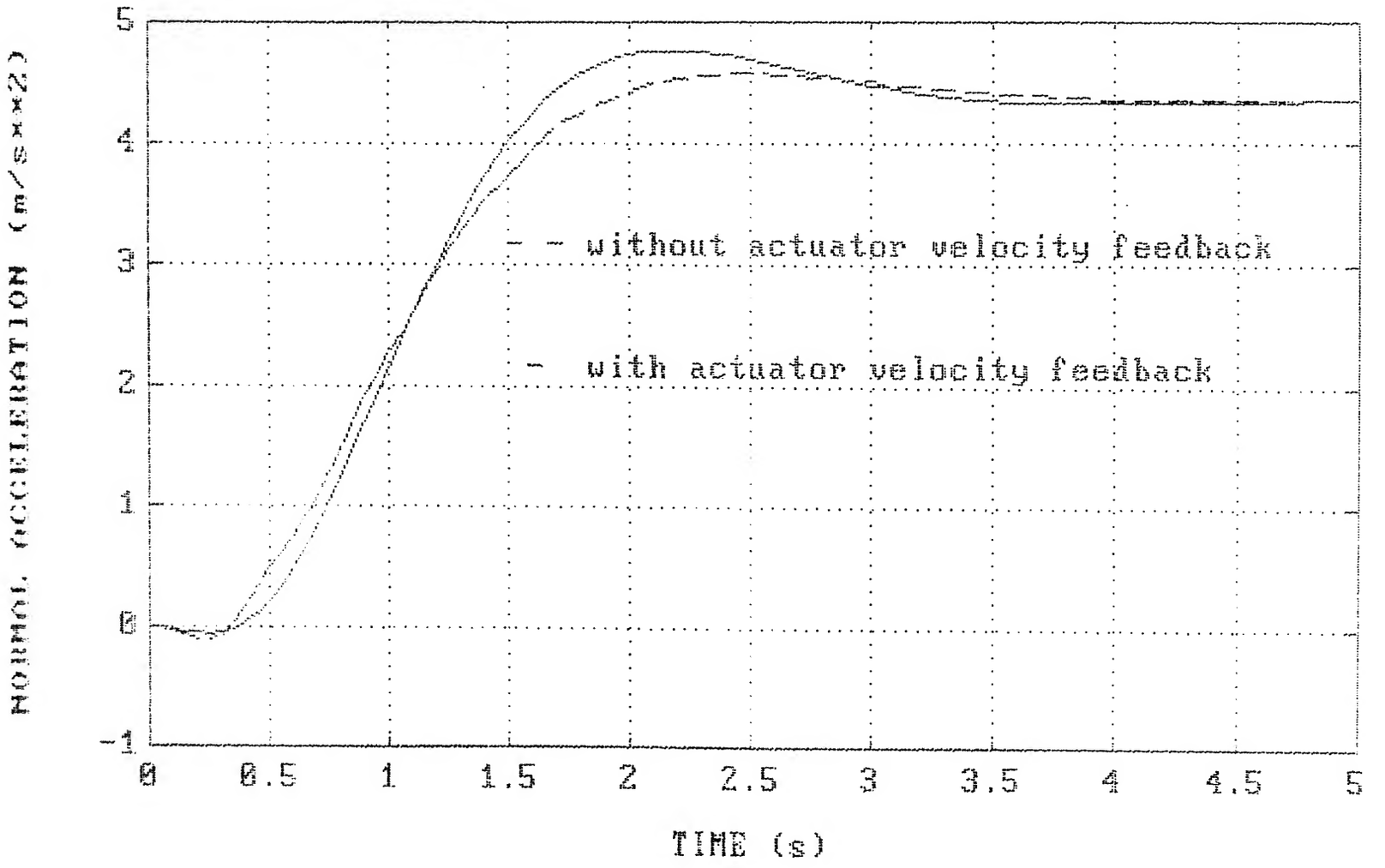

FIG. 4.8a STEP RESPONSE OF AIRPLANE (WITH ACTUATOR VELOCITY FEEDBACK)

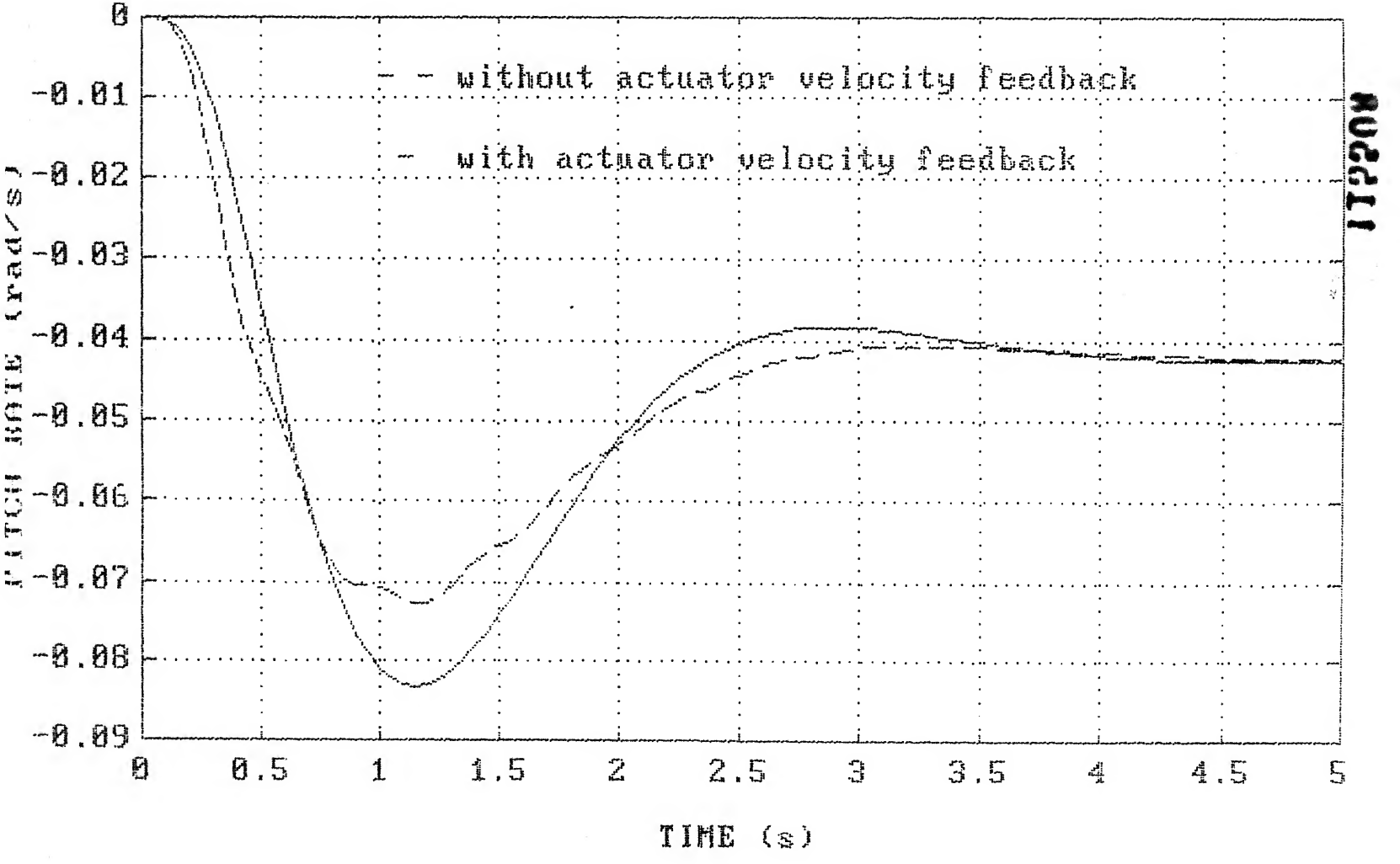

FIG. 4.8b STEP RESPONSE OF AIRPLANE (WITH ACTUATOR VELOCITY FEEDBACK)